

**Investigating the functional consequences of the interaction between engineered ubiquitin variants and the *Salmonella* novel E3 ligase SspH1**

By

Bradley E Dubrule

A thesis submitted in partial fulfillment of the requirements for the degree of

Master of Science

In

Immunology

Department of Medical Microbiology and Immunology

University of Alberta

## Abstract

During infection some pathogenic gram-negative bacteria, such as *Salmonella*, manipulate the host ubiquitination system through the delivery of secreted effectors known as novel E3 ubiquitin ligases (NELs). Despite the presence of NELs amongst these well-studied bacterial species, their unique structure has limited the tools that are available to probe their molecular mechanisms and explore their therapeutic potential. In this work, we report the identification of two engineered ubiquitin variants that can modulate the activity of the *Salmonella enterica* serovar Typhimurium encoded NEL, SspH1. We show that these ubiquitin variants suppress SspH1-mediated toxicity phenotypes in *Saccharomyces cerevisiae*. Additionally, we provide microscopic and flow cytometric evidence that SspH1-mediated toxicity is caused by interference with *S. cerevisiae* cell cycle progression that can be suppressed in the presence of ubiquitin variants. *In vitro* ubiquitination assays revealed that these ubiquitin variants increased the amount of SspH1-mediated ubiquitin chain formation. Interestingly, despite the increase in ubiquitin chains, we observe a relative decrease in the formation of SspH1's preferred K48-linked ubiquitin chains on its substrate, PKN1. Taken together our findings suggest that SspH1 toxicity in *S. cerevisiae* occurs through cell cycle interference and that an engineered ubiquitin variant approach can be used to identify probes that modulate the activity of bacterially encoded ubiquitin ligases.

# Preface

This thesis contains original work performed or substantially contributed to by Bradley Dubrule. It also contains content co-authored by various collaborators. Ashley Wagner (University of Alberta) and Dr. Amit Bhavsar (University of Alberta) were responsible for the cloning of various *S. cerevisiae* and *E. coli* strains as well as the design of the yeast toxicity assays. Additionally, Ashley Wagner (University of Alberta) was responsible for the *S. cerevisiae* western blots confirming protein expression. Adithya Subramanian (University of Alberta) was responsible for the purification of SspH1 used in the *in vitro* ubiquitination assays. Dr. Adam Middleton (University of Otago) was responsible for performing *in silico* AlphaFold predictions of the interaction between SspH1 and ubiquitin. Dr. Wei Zhang (University of Toronto) and Dr. Sachdev Sidhu (University of Toronto) were responsible for the initial identification of Ubv A06 and Ubv D09 from the engineered ubiquitin library. Dr. Gary Eitzen (University of Alberta) provided reagents and aided in the conceptualization of *S. cerevisiae* experiments.

I would also like to extend my deepest thanks to my colleagues within the medical microbiology and immunology department who allowed me access to their instruments and provided helpful feedback and discussion throughout the project.

# Acknowledgements

This work could not have been completed without the mentorship of my supervisor, Dr. Amit Bhavsar. Thank you for sharing your knowledge of bacteriology, biochemistry, and providing a model of the commitment necessary to pursue a career in research. I am immensely grateful for the support I experienced under your tutelage and for the freedom you granted me to pursue what interested me. The opportunity to conceptualize my own experiments, expand my repertoire of techniques, and engage in education beyond the requirements of my degree has been invaluable in my development as a researcher. It has been an honor to be able to travel and present my research as a member of your lab. Beyond science, I am exceptionally appreciative of all the places I was able to experience and the people I was able to meet during my time as a Bhavsar lab member. Your appreciation for flow cytometry along with your reminders of the importance of knowing your amino acids will be remembered fondly.

I would like to thank Dr. Wael Elheneway and Dr. Rob Ingham for serving as members of my supervisory committee. Their willingness to share their expertise, provide feedback on experiments, and encouraging words have been invaluable and I can't thank them enough for the time and effort they have put into my development as a researcher. Additionally, I would like to thank Dr. Oliver Julien for serving as my external examiner and Dr. Troy Baldwin for serving as my exam chair.

It cannot be overstated the amount of gratitude I would like to extend to the current and former members of the Bhavsar lab: Asna Latif, Malcolm Forester, Zahra Zhandi, Jason Lane, Meghan Bunn, Ivan Domingo, Ghazal Bomblalorad, Cole Delyea, Brooke Hatala, Tracy Lee, Ashley Wagner and Chrissy Doung. Throughout all the trials and difficulties, I encountered during the completion of this degree, I always knew that I could look to you for support and levity in any situation. Our numerous whiteboard and blue couch discussions, whether the topic was related to our research or about life in general, were always a highlight of my week and will be sorely missed. I would be remiss to not also extend my gratitude to the friends of the Bhavsar lab, who brought joy, humor and a novel outlook into the lab nearly every day. Additionally, to the graduate students of the department of medical microbiology and immunology, thank you for fostering an environment of support, collaboration, and camaraderie.

None of the work we accomplish in the department would have been possible without the vital work done by the MMI office staff, in particular Tabitha Nguyen, Leanne Van Wyk, Michelle Zanduski and Leandro Solis Aguilar. Furthermore, I would like to extend my thanks to those who I met throughout my role in procurement, in particular Delilah Gerein and Mahmoud Karim, for always ensuring we received the right reagents and for all their wisdom I've enjoyed over the years.

I am eternally grateful for the everlasting love offered by my parents, Remi Dubrule and Susan Kotowich-Dubrule and brother, Dustin Dubrule. Their consistent presence and unwavering support in my academic and scientific pursuits has been and will always be appreciated more than they will ever know. Finally, I would like to express my utmost gratitude to Lucie Laferriere. She has been my biggest supporter and a never-ending source of encouragement, love, and happiness throughout this journey. Whether it has been celebrating my successes or overcoming the inevitable misadventures of research, this degree would not have been possible without her by my side.

This work was supported by operating grants from the Natural Sciences and Engineering Research Council of Canada (RGPIN-2020-04359 to APB) and the Government of Alberta Major Innovation Fund for Antimicrobial Research- One Health Consortium (RCP-19-003-MIF to Amit Bhavsar). This research has also been funded by the Li Ka Shing Institute of Virology (LKSIOV). I was supported by studentships from the University of Alberta Faculty of Medicine & Dentistry and LKSIOV. Amit Bhavsar holds a Canada Research Chair (Tier 2) in Pattern Recognition Receptor Pathophysiology and this research was undertaken, in part, thanks to funding from the 10 Canada Research Chairs Program (231622). Some experiments were performed at the University of Alberta Faculty of Medicine & Dentistry Flow Cytometry Facility, RRID:SCR\_019195, which receives financial support from the Faculty of Medicine & Dentistry and Canada Foundation for Innovation (CFI) awards to contributing investigators. Mass Spectrometry experiments were performed by the Alberta Proteomics and Mass Spectrometry Facility in the Faculty of Medicine and Dentistry at the University of Alberta.

## Table of Contents

|  |            |
|--|------------|
| <b>Abstract</b> .....  | <b>ii</b>  |
| <b>Preface</b> .....   | <b>iii</b> |
| <b>Acknowledgements</b> .....  | <b>iv</b>  |
| List of Figures .....  | viii       |
| List of Tables.....  | ix         |
| List of Abbreviations.....   | x          |
| <b>Chapter 1: Introduction</b> .....   | <b>1</b>   |
| 1.1 Overview of the Ubiquitination Cascade in Eukaryotic Cells .....             | 1          |
| 1.2 Overview of <i>Salmonella</i> Epidemiology & Pathogenesis .....              | 7          |
| 1.3 Structure & Function of Type III Secretion Systems .....                     | 16         |
| 1.4 The Role of Novel E3 Ligases in Pathogenic Ubiquitination .....              | 20         |
| 1.5 Introduction to <i>Salmonella</i> Secreted Protein H1 (SspH1) .....          | 23         |
| 1.6 Structure & Function of PKN1 .....   | 24         |
| 1.7.1 Inhibition of the Ubiquitination Cascade .....                             | 31         |
| 1.7.2 Engineered Ubiquitin Variants as Ubiquitination Inhibitors .....           | 31         |
| 1.8 <i>Saccharomyces cerevisiae</i> as a Versatile Eukaryotic Model System ..... | 37         |
| 1.9 Rationale .....  | 40         |
| 1.10 Hypothesis.....   | 40         |
| <b>Chapter 2: Methods</b> .....  | <b>41</b>  |
| Chapter 2.1: SspH1 Toxicity in <i>S. cerevisiae</i> .....                        | 41         |
| 2.1.1 Cloning & Transformation.....  | 41         |
| 2.1.2 <i>Saccharomyces cerevisiae</i> growth on solid media .....                | 45         |
| 2.1.3 <i>Saccharomyces cerevisiae</i> growth in liquid media .....               | 45         |
| 2.1.4 Flow Cytometry .....   | 45         |
| 2.1.5 Microscopy .....   | 46         |
| 2.1.6 Statistical Analysis .....   | 47         |
| Chapter 2.2: Assessing SspH1 activity <i>in vitro</i> .....                      | 47         |
| 2.2.1 Structure Preparation Using Homology Modelling .....                       | 47         |
| 2.2.2 <i>In silico</i> Protein-Protein Interaction Predictions .....             | 48         |
| 2.2.3 Cloning.....   | 48         |
| 2.2.4 Protein Purification .....   | 50         |
| 2.2.5 Mass Spectrometry.....   | 51         |
| 2.2.6 SspH1 Ubiquitination Assays.....   | 52         |

|   |            |
|---|------------|
| 2.2.7 Immunoprecipitation.....  | 52         |
| 2.2.8 Immunoblotting.....   | 53         |
| 2.2.9 Coomassie Brilliant Blue Protein Staining .....                                   | 53         |
| 2.2.10 Statistical Analysis.....  | 54         |
| <b>Chapter 3: Results.....</b>  | <b>55</b>  |
| 3.1 Identifying Ubiquitin Variant Inhibitors of SspH1.....                              | 55         |
| 3.2 Ubv A06 & Ubv D09 Suppress SspH1-Mediated Toxicity in Yeast.....                    | 60         |
| 3.3 Ubv A06 & D09 Suppress SspH1 Mediated Cell Cycle Arrest in Yeast.....               | 66         |
| 3.4 Ubiquitin variants alter SspH1’s E3 ubiquitin ligase activity <i>in vitro</i> ..... | 71         |
| <b>Chapter 4: Discussion.....</b>   | <b>80</b>  |
| 4.1 Summary.....  | 80         |
| 4.2 Identification of High-Affinity Ubv Binders to SspH1.....                           | 80         |
| 4.3 Ubv A06 and Ubv D09 suppress SspH1 dependent toxicity in <i>S. cerevisiae</i> ..... | 81         |
| 4.4 Ubv D09 modulates SspH1 activity <i>in vitro</i> . .....                            | 82         |
| 4.5 Additional Considerations.....  | 82         |
| 4.6 Conclusion and Future Applications.....   | 83         |
| <b>References.....</b>  | <b>85</b>  |
| <b>Appendix I.....</b>  | <b>103</b> |
| <b>Appendix II.....</b>   | <b>107</b> |
| Yeast Actin Cytoskeleton Was Not Affected by SspH1 Expression .....                     | 107        |
| Imaging Flow Cytometry.....   | 109        |
| Imaging Flow Cytometry Did Not Reveal SspH1-mediated Cell Cycle Perturbations .....     | 110        |

## List of Figures

|  |     |
|--|-----|
| Fig. 1.1.1 Simplified Depiction of the Ubiquitination Cascade.....                               | 4   |
| Fig. 1.1.2 Structure of Ubiquitin.....   | 5   |
| Fig. 1.1.3 Function and Structure of Ubiquitin Chains.....                                       | 6   |
| Fig. 1.2.1 Strategies for <i>Salmonella</i> Typhimurium Invasion .....                           | 11  |
| Fig. 1.3.1 Depiction of <i>Salmonella</i> Type III Secretion System Structure.....               | 17  |
| Fig. 1.4.1 Domain Structure of the Novel E3 Ligases Encoded by <i>Salmonella</i> .....           | 22  |
| Fig. 1.6.1 Domain Structure of Protein-Kinase C Related (PRK) Kinases .....                      | 26  |
| Fig. 1.6.2 Activation of PKN1 .....  | 28  |
| Fig. 1.6.3 Different Role of PRK Signaling.....  | 29  |
| Fig. 1.7.1 Identification of High-Affinity Ubiquitin Variants by Phage Display.....              | 35  |
| Fig. 1.7.2 Regions Mutated in the Ubiquitin Variant Phage Display Library.....                   | 36  |
| Fig. 1.8.1 Cell Cycle of <i>Saccharomyces cerevisiae</i> .....                                   | 39  |
| Fig. 3.1.1 Identifying Ubiquitin Variants with a High Binding Affinity for SspH1 .....           | 56  |
| Fig. 3.1.2 Ubiquitin Variants have a Higher Predicted Binding Affinity for SspH1 .....           | 58  |
| Fig. 3.2.1. Ubv A06 & D09 are not Toxic to Yeast when Expressed Alone .....                      | 62  |
| Fig. 3.2.2. Ubv A06 & D09 Suppress SspH1-Mediated Toxicity in Yeast .....                        | 64  |
| Fig. 3.3.1 Ubv A06 & D09 Suppress SspH1-Mediated Arrest at the Large Budded Stage in Yeast ..... | 68  |
| Fig. 3.3.2 Ubv A06 & D09 Suppress SspH1-Mediated Cell Cycle Arrest in Yeast.....                 | 70  |
| Fig. 3.4.1 Purification of $\Delta$ DiGly and Ubv D09 .....                                      | 74  |
| Fig. 3.4.2. Ubvs modulate the ubiquitination activity of SspH1 <i>in vitro</i> .....             | 75  |
| Fig. 3.4.3. Ubvs modulate SspH1-mediated ubiquitination of PKN1 <i>in vitro</i> .....            | 77  |
| Fig. 3.4.4 Ubvs modulate SspH1-mediated ubiquitination of PKN1 <i>in vitro</i> .....             | 79  |
| sFig. 1.1 Mass Spectrometry of Purified Ubv D09.....   | 103 |
| sFig. 2.1 Gating Strategy for Cell Cycle Flow Cytometry Analysis.....                            | 104 |

## List of Tables

|  |     |
|--|-----|
| Table 1.2.1 Size & Function of Conserved <i>Salmonella</i> Pathogenicity Islands.....    | 13  |
| Table 1.2.2 Representative <i>Salmonella</i> Secreted Effector Proteins .....            | 14  |
| Table 1.3.1 Nomenclature of T3SS of <i>Salmonella</i> enterica serovar Typhimurium ..... | 18  |
| Table 1.4.1 Representative Members of the Novel E3 Ligase Family .....                   | 21  |
| Table 1.7.1 Representative Examples of Inhibitors of Ubiquitination.....                 | 33  |
| Table 2.1.1 Strains Used for Cloning in Yeast Expression Studies.....                    | 43  |
| Table 2.1.2 Primers Used In Cloning.....   | 44  |
| Table 3.3.1 Strains Used for Cloning for Protein Purification Studies .....              | 49  |
| sTable 1. Expression Vectors Summary .....   | 105 |
| sTable 2. Flow Cytometry Instrument Settings.....  | 106 |

## List of Abbreviations

|                         |  |
|-------------------------|--|
| <b>14-3-3</b>           | Protein eluted in the 14 <sup>th</sup> fraction of a bovine brain homogenate from a DEAE cellulose column and located at position 3.3 on a starch electrophoresis gel. (1)   |
| <b>Abs</b>              | Absorbance   |
| <b>AGC</b>              | Group of kinases related to PKA  |
| <b>AKT</b>              | A serine/threonine protein kinase encoded by the oncogene in the transforming retrovirus isolated from the thymoma cell line AKT-8, which is derived from the Stock A Strain k AKR mouse originally inbred in the laboratory of Dr. C. P. Rhoads by K. B. Rhoads at the Rockefeller Institute. (2) |
| <b>ANOVA</b>            | Analysis of variance   |
| <b>AR</b>               | Androgen Receptor  |
| <b>ASC</b>              | Apoptosis-associated speck-like protein with a caspase recruitment domain  |
| <b>ATP</b>              | Adenosine triphosphate   |
| <b>AUC</b>              | Area under curve   |
| <b>BCA</b>              | Bicinchoninic acid   |
| <b>BKC</b>              | Bypass of C-kinase   |
| <b>BLI</b>              | Bio-layer interferometry   |
| <b>Co-IP</b>            | Co-immunoprecipitation   |
| <b>CSM</b>              | Complete synthetic media   |
| <b>CV</b>               | Column volume  |
| <b>DAMP</b>             | Damage associated molecular patterns   |
| <b>DAPI</b>             | 4',6-diamidino-2-phenylindole  |
| <b>ddH<sub>2</sub>O</b> | Milli-Q H <sub>2</sub> O (Ultrapure, Double Distilled)   |
| <b>DEAE</b>             | Diethylaminoethyl  |
| <b>DFIRE</b>            | Distance-scaled, finite, ideal-gas reference state   |
| <b>DHT</b>              | Dihydrotestosterone  |
| <b>dsDNA</b>            | Double-strand deoxyribonucleic acid  |
| <b>DTT</b>              | Dithiothreitol   |
| <b>DUB</b>              | Deubiquitinating Enzyme  |
| <b>EBI</b>              | European Bioinformatics institute  |

|                |   |
|----------------|---|
| <b>ELISA</b>   | Enzyme-linked immunosorbent assay                         |
| <b>EMBL</b>    | European molecular biology laboratory                     |
| <b>EtOH</b>    | Ethanol   |
| <b>Ev</b>      | Empty Vector  |
| <b>Gal</b>     | Galactose   |
| <b>GOAP</b>    | Generalized orientation-dependent all-atom potential      |
| <b>GRC</b>     | Growth reduction coefficient                              |
| <b>GST</b>     | Glutathione S-transferase                                 |
| <b>HA</b>      | Hemagglutinin   |
| <b>HECT</b>    | Homologous to E6-associated protein C-terminus            |
| <b>His</b>     | Histidine   |
| <b>HPLC</b>    | High performance liquid chromatography                    |
| <b>HRP</b>     | Horseradish peroxidase                                    |
| <b>IAP</b>     | Inhibitor of apoptosis                                    |
| <b>ICSP</b>    | International Committee on the Systematics of Prokaryotes |
| <b>IL</b>      | Interleukin   |
| <b>Ile</b>     | Isoleucine  |
| <b>iNTS</b>    | Invasive non-typhoidal <i>Salmonella</i>                  |
| <b>Inv</b>     | Invasion  |
| <b>IP</b>      | Immunoprecipitation                                       |
| <b>IpaH</b>    | Invasion plasmid antigen                                  |
| <b>IPTG</b>    | Isopropyl $\beta$ -D-1-thiogalactopyranoside              |
| <b>ITC</b>     | Isothermal calorimetry                                    |
| <b>ITScore</b> | Iterative knowledge-based scoring function                |
| <b>JAMM</b>    | JAB1/MPN+/Mov34 domain metallo-enzyme proteases           |
| <b>LB</b>      | Lysogeny broth  |
| <b>LRR</b>     | Leucine rich repeat                                       |
| <b>LUBAC</b>   | Linear ubiquitin chain assembly complex                   |
| <b>MAPK</b>    | Mitogen-associated pathway kinase                         |

|                                |  |
|--------------------------------|--|
| <b>MeOH</b>                    | Methanol   |
| <b>MINDY</b>                   | Motif interacting with Ub-containing novel DUB family          |
| <b>MKK</b>                     | Mitogen-activated protein kinase-kinase                        |
| <b>MS</b>                      | Mass Spectrometry  |
| <b>MST</b>                     | Microscale thermophoresis                                      |
| <b>MWCO</b>                    | Molecular weight cut off                                       |
| <b>NEL</b>                     | Novel E3 ubiquitin ligase                                      |
| <b>NF-<math>\kappa</math>B</b> | Nuclear factor kappa B   |
| <b>NOD1</b>                    | Nucleotide binding oligomerization domain containing protein 1 |
| <b>Nop</b>                     | Nodulation outer protein                                       |
| <b>NTS</b>                     | Non-typhoidal <i>Salmonella</i>                                |
| <b>OD</b>                      | Optical density  |
| <b>OTU</b>                     | Ovarian tumor protease   |
| <b>PBS</b>                     | Phosphate buffered saline                                      |
| <b>PCR</b>                     | Polymerase chain reaction                                      |
| <b>PDK</b>                     | Phosphoinositide-dependent kinase                              |
| <b>PEG</b>                     | Polyethylene glycol  |
| <b>PFA</b>                     | Paraformaldehyde   |
| <b>PI</b>                      | Propidium Iodide   |
| <b>PIP<sub>2</sub></b>         | Phosphatidylinositol 4,5 biphosphate                           |
| <b>PIP<sub>3</sub></b>         | Phosphatidylinositol 3,4,5 biphosphate                         |
| <b>PKC</b>                     | Protein kinase C   |
| <b>PKN1</b>                    | Serine/Threonine-protein kinase N1                             |
| <b>Prg</b>                     | PhoP-repressed gene  |
| <b>PRK</b>                     | Protein kinase C-related kinase                                |
| <b>PRR</b>                     | Pattern recognition receptors                                  |
| <b>PSI</b>                     | Pounds per square inch   |
| <b>pSLT</b>                    | <i>Salmonella</i> -associated virulence plasmid                |
| <b>PSM</b>                     | Peptide spectral matches                                       |

|                              |  |
|------------------------------|--|
| <b>Ras</b>                   | Rat sarcoma virus protein                          |
| <b>Rec</b>                   | Recombination                                      |
| <b>Rho</b>                   | Ras homologous protein                             |
| <b>RING</b>                  | Really interesting new gene                        |
| <b>Rip</b>                   | <i>Ralstonia</i> protein injected into plant cells |
| <b>RLM1</b>                  | Resistance to lethality of MKK1P386 overexpression |
| <b>RMS</b>                   | Root mean square                                   |
| <b>RPM</b>                   | Rotations per minute                               |
| <b><i>S. Typhimurium</i></b> | <i>Salmonella enterica</i> serovar Typhimurium     |
| <b>SalFos</b>                | <i>Salmonella</i> Foodborne Syst-OMICs             |
| <b>SBF</b>                   | SCB binding factor                                 |
| <b>SCB</b>                   | Swi4/6 cell cycle box                              |
| <b>Sct</b>                   | Secretion and cellular translocation               |
| <b>SEM</b>                   | Standard error of the mean                         |
| <b>Sip</b>                   | <i>Salmonella</i> invasion protein                 |
| <b>SKP2</b>                  | S-phase kinase-associated protein 2                |
| <b>Slr</b>                   | <i>Salmonella</i> leucine-rich protein             |
| <b>SLT</b>                   | Suppressor of lytic phenotype                      |
| <b>SMAC</b>                  | Second mitochondria-derived activator of caspases  |
| <b>SMURF</b>                 | Smad ubiquitin regulatory factors                  |
| <b>Spa</b>                   | Surface presentation of antigen                    |
| <b>SPI-1</b>                 | <i>Salmonella</i> pathogenicity island-1           |
| <b>SPI-2</b>                 | <i>Salmonella</i> pathogenicity island-2           |
| <b>Ssa</b>                   | Secretion system apparatus                         |
| <b>SSDNA</b>                 | Salmon Sperm DNA                                   |
| <b>Sse</b>                   | Secretion system effector                          |
| <b>SspH1</b>                 | <i>Salmonella</i> secreted protein H1              |
| <b>SspH2</b>                 | <i>Salmonella</i> secreted protein H2              |
| <b>T3SS</b>                  | Type 3 secretion system                            |

|                        |  |
|------------------------|--|
| <b>TBS</b>             | Tris-buffered saline                               |
| <b>TI</b>              | Toxicity index                                     |
| <b>TMB</b>             | 3,3',5'5-tetramethylbenzidine                      |
| <b>Tween</b>           | Polysorbate 20                                     |
| <b>TXA<sub>2</sub></b> | Thromboxane A <sub>2</sub>                         |
| <b>UAP</b>             | Ubiquitin associated protien                       |
| <b>Ub</b>              | Human Ubiquitin                                    |
| <b>UBD</b>             | Ubiquitin binding domain                           |
| <b>Ubv</b>             | Ubiquitin variants                                 |
| <b>UCH</b>             | Ubiquitin C-terminal hydrolases                    |
| <b>UCSF</b>            | University of California, San Francisco            |
| <b>Uev</b>             | Ubiquitin-cojugating enzyme variant                |
| <b>UIM</b>             | Ubiquitin interacting motif                        |
| <b>USP</b>             | Ubiquitin specific proteases                       |
| <b>vDUB</b>            | Viral deubiquitianting enzyme                      |
| <b>WWP1</b>            | WW domain-containing E3 ubiquitin protein ligase 1 |
| <b>ZUP</b>             | Zinc finger-containing ubiquitin peptidase         |

# Chapter 1: Introduction

## 1.1 Overview of the Ubiquitination Cascade in Eukaryotic Cells

Ubiquitin is a small, 76 amino acid (7.8 kDa) protein which has an indispensable role in intracellular signaling within eukaryotic cells. It has remained highly conserved throughout eukaryotic evolution with there being only 3 amino acid (Pro19, Glu24, Ala28 in human are found as Ser19, Asp24, Ser28 in yeast) differences between yeast and human ubiquitin. (3) The covalent attachment of ubiquitin onto its intended target occurs post-translationally and is mediated by the ubiquitin cascade, a sequential enzymatic pathway made up of three families: the E1 ubiquitin activating enzymes, the E2 ubiquitin conjugating enzymes and the E3 ubiquitin ligases. (4) Through this pathway, the C-terminal glycine residue (G76) of ubiquitin forms a covalent bond with the  $\epsilon$ -amino group of a lysine residue on the substrate. (5) Attachment of ubiquitin is also reversible through the activity of deubiquitylating enzymes (DUBs), providing another layer of complexity into how ubiquitin signaling can affect cellular processes. (6)

The ubiquitin cascade begins with the E1 activating enzymes which catalyze an adenylation reaction of the C-terminal -COOH of free ubiquitin that then allows a thioester linkage between the diglycine tail of free ubiquitin and the catalytic cysteine of the E1 enzyme to be formed, creating a conjugate that is abbreviated as E1~Ub. (7–10) Once the first Ub molecule has been transferred to the catalytic cysteine of the E1, a second Ub can be recruited to the open adenylation site to generate a “double loaded” E1 that is preferentially recognized by the E2. (11) The E1~Ub<sub>2</sub> conjugate then interfaces with a free E2 conjugating enzyme where the active site Ub will be transferred onto the catalytic cysteine of an E2, forming a conjugate that is abbreviated as E2~Ub. (12–14) This E2~Ub conjugate can then interact with an E3 ubiquitin ligase to facilitate the transfer of Ub onto the catalytic site of the E3 or directly onto the substrate using the E3 as a scaffold to coordinate the transfer. (15–17) The diversity of these enzymes increases with progression through the cascade with only 2 known eukaryotic E1s, ~30 known E2s and over 600 known E3 ligases. (18) The low diversity of E1 and E2 enzymes is likely owed to the fact that they only interact with the highly conserved ubiquitin or other components of the enzymatic cascade, conversely, the greater diversity of E3 ligases is likely due to their role in

determining the substrate specificity for ubiquitin attachment which requires them to be able to target a variety of host and non-host proteins. Included in this diversity is the existence of two distinct mechanisms of E3-mediated ubiquitin transfer. E3s belonging to the Really Interesting New Gene (RING) family, lack a catalytic residue and do not directly bind to ubiquitin but rather coordinate the transfer from the E2~Ub conjugate directly to the substrate. (19) Conversely, E3s which belong to the Homologous to E6AP C-terminus (HECT) or the RING-between-RING (RBR) family of ligases form direct thioester bonds with ubiquitin providing an intermediate between E2 and substrate. (20,21) (Fig. 1.1.1)

The diversity of ubiquitin signaling is also influenced by the amount and topology of the ubiquitin chains which are conjugated onto the substrate. Chains of multiple ubiquitin residues can be formed through conjugation of the C-terminal glycine residue of an incoming ubiquitin onto one of seven lysine residues (K6, K11, K27, K29, K33, K48, K63) or the N-terminal methionine residue (M1). (22–24) (Fig. 1.1.2) These chains can be homotypic, which contain only a single type of linkage, or heterotypic, which contain a multitude of linkage types, including the possibility of branched ubiquitination. Of the 8 potential ubiquitin linkage sites, K48 and K63 are considered typical and have a much larger body of research behind them. (25) Recent innovations in technology have allowed for the study of the remaining atypical chains (M1, K6, K11, K27, K29, K33) leading to an increased understanding of the role these linkages play in cellular signaling. (18,26) Details of the role of the atypical ubiquitin linkages are found in Fig. 1.1.3. Ubiquitin chains containing K48-linkages have been shown to target substrates for proteasomal degradation and is often considered the canonical ubiquitin linkage. (17,27,28) Conversely, ubiquitin chains containing K63-linkages have been shown to have multiple non-proteolytic properties, including roles in protein trafficking, inflammatory signaling and DNA repair. (22,29) In addition to different linkages, ubiquitin chains can be modified by the presence of ubiquitin-like molecules, such as SUMO or NEDD8, or other post-translational modification such as acetylation, or phosphorylation. (28,30,31) Ultimately, ubiquitin chains are recognized by a variety of proteins which contain ubiquitin binding domains (UBDs) which interpret the chain conformation and convert the ubiquitin signal into cellular activity. (32–35)

In addition to the process of labelling proteins through ubiquitination, it has also been shown that deubiquitination, accomplished by deubiquitinating enzymes (DUBs), plays a necessary role

in controlling intracellular signaling. (36) Accordingly, there are over 100 human encoded DUBs belonging to seven structural families: the ubiquitin specific proteases (USP), the ubiquitin C-terminal hydrolases (UCH), the Josephin domain proteases, the ovarian tumor (OTU) proteases, the JAB1/MPN<sup>+</sup>/Mov34 domain (JAMM) metallo-enzyme proteases, the motif interacting with Ub-containing novel DUB family (MINDY) of proteases and the zinc finger-containing ubiquitin peptidase (ZUP). (6,37–39) The enzymatic activity of these molecules results in the cleavage of the isopeptide bond formed between the C-terminal tail of a ubiquitin molecule and the corresponding lysine residue. Although each family of DUB shares a similar mechanism of action they have unique targets, both in terms of substrate and lysine-linkage specificity. (40) Additionally, dysregulation of DUBs is associated with the development of a variety of diseases further underlying their essential role in maintaining homeostasis. (41) This further underscores the complex and intricate nature of the ubiquitin network that not only regulates cellular homeostasis but also provides an origin for disease biogenesis and a target for pathogens. (15,16,18,40,42)

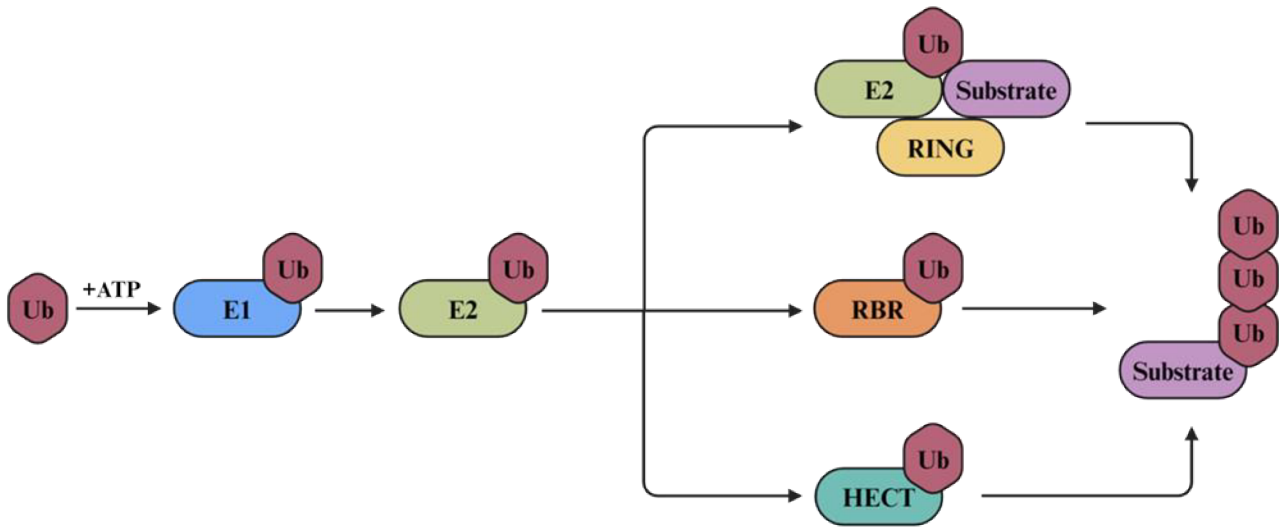


**Fig. 1.1.1 Simplified Depiction of the Ubiquitination Cascade**

The formation of ubiquitin chains occurs through multiple sequential reactions. Free ubiquitin (Ub) is first conjugated onto the E1 activating enzyme forming an E1~Ub conjugate. The E1 enzyme then transfers the activated Ub to the E2 conjugating enzyme forming an E2~Ub conjugate. The E2~Ub conjugate then coordinates with an E3 enzyme to facilitate the transfer of Ub onto the substrate. In the case of the Really Interesting New Gene (RING) E3 ligases, Ub is not directly transferred onto the E3 enzyme which instead coordinates the transfer of the Ub from the E2 directly to the substrate. Conversely, in the case of RING-between-RING (RBR) or homologous to E6AP C-terminus (HECT) the Ub is directly conjugated to a catalytic residue which is then transferred directly from the E3 to the substrate. Created with Biorender.com.

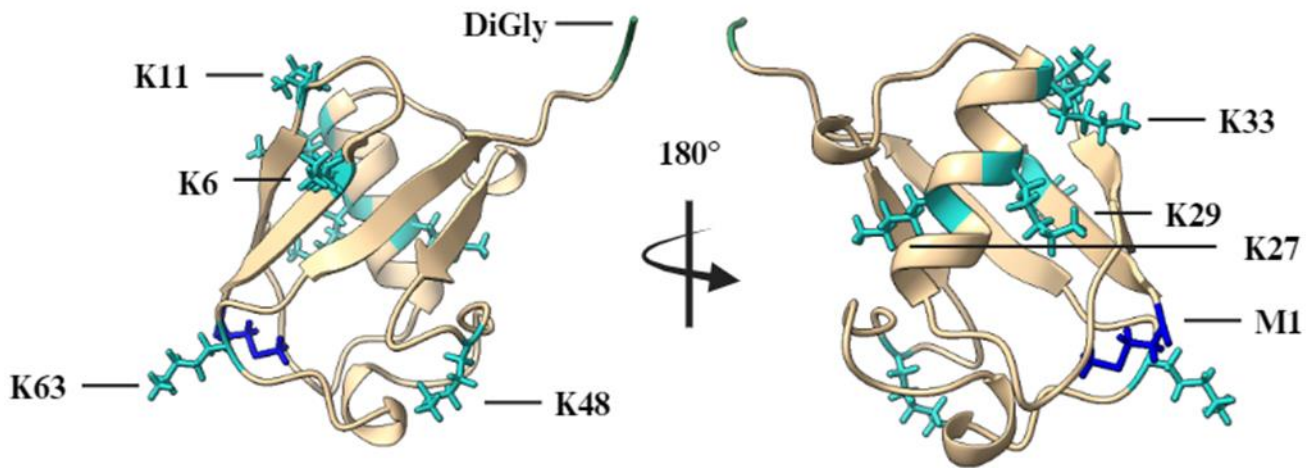


**Fig. 1.1.2 Structure of Ubiquitin**

Human ubiquitin visualized in ChimeraX V1.2.5 (PDB: 1UBQ) Lysine residues (K6, K11, K27, K29, K33, K48, K63) are highlighted in teal. Methionine (M1) is highlighted in blue. C-terminal diglycine (DiGly) is highlighted in green.

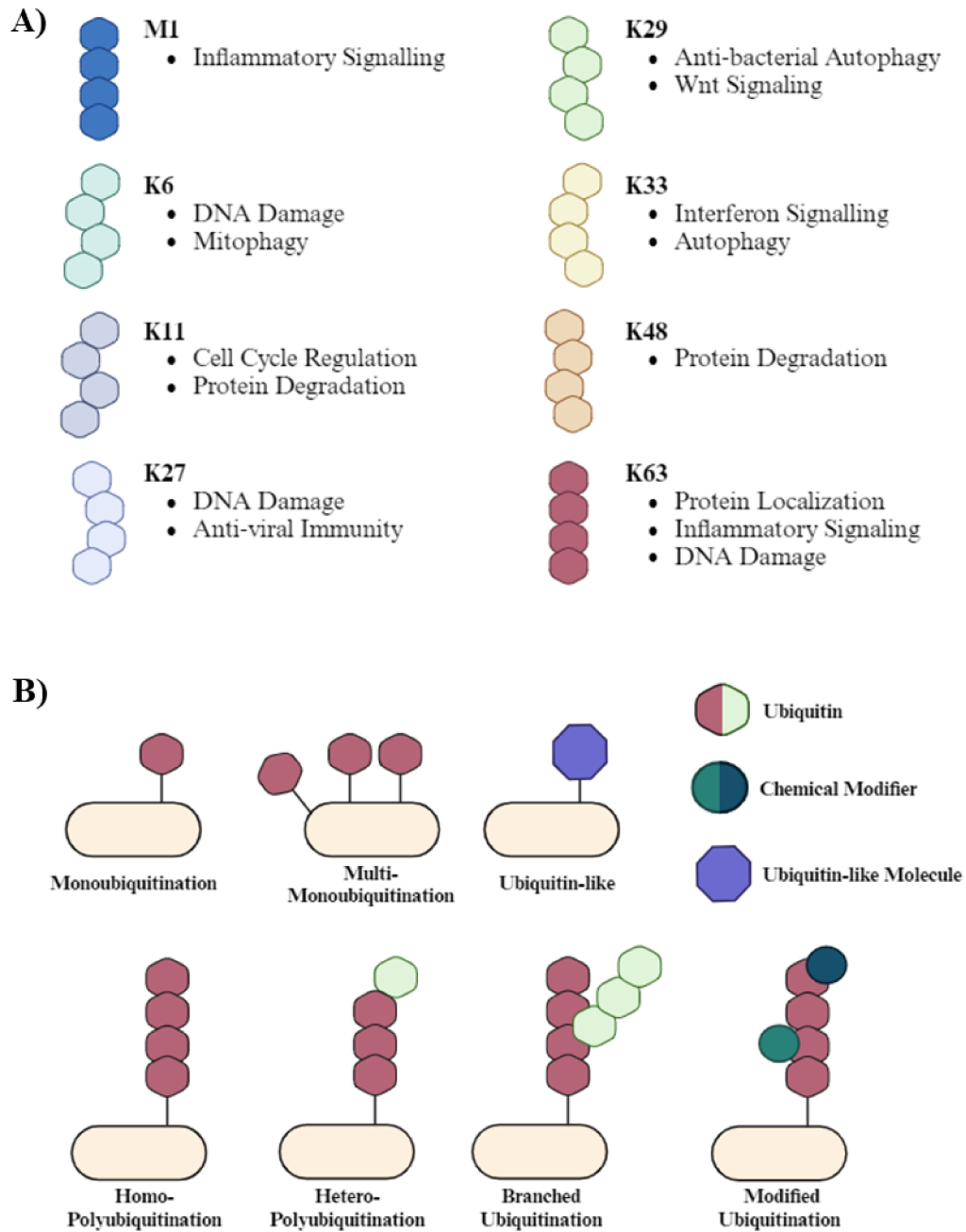


**Fig. 1.1.3 Function and Structure of Ubiquitin Chains**

(A) Description of the function of ubiquitin chains linked through M1 or the 7 internal lysines.

(B) Overview of the different potential composition of ubiquitin chains. Adapted from (43).

Created with Biorender.com

## 1.2 Overview of *Salmonella* Epidemiology & Pathogenesis

*Salmonella* is a genus of facultatively anaerobic, rod-shaped, Gram-negative bacteria composed of a diverse array of serotypes. It was first identified and cultured by Daniel Salmon and Theobald Smith in 1885, who named the bacterium “*Salmonella*” in honor of Dr. Salmon. (44) The specifics of *Salmonella* nomenclature were long an issue of debate before a ruling by the Judicial Commission of the International Committee on the Systematics of Prokaryotes (ICSP) divided the genus into two species, *S. bongori* and *S. enterica*. (45) *S. bongori* is mainly associated with infection of cold-blooded animals, although some human infections have been previously reported. (46,47) Conversely, *S. enterica* is mainly associated with the infection warm-blooded animals, including humans, and is currently comprised of 6 subspecies (*enterica*, *salamae*, *arizonae*, *diarizonae*, *houtenae*, *indica*), however, with the rise of whole genome sequence availability, 5 additional subspecies have been postulated (*londinensis*, *brasiliensis*, *hibernicus*, *essexiensis*, *reptilium*) as well as the elevation of *S. enterica* subsp. *arizonae* to being its own species. (48–50) *S. enterica* subsp. *enterica*, contributes to approximately 99% of all *Salmonella* infections in warm-blooded animals, leading to it being the most well studied of the *Salmonella* subspecies. (51)

*S. enterica* serovars are further divided into typhoidal or non-typhoidal, depending on the type of disease they cause. (52) Typhoidal serovars, including *S. Typhi* and *S. Paratyphi*, are adapted specifically to the human host where invasive infection leads to development of life-threatening enteric fever. (53,54) In 2019 there were 13 million reported cases of typhoid fever worldwide which resulted in 133 000 deaths; India and the surrounding regions were particularly affected by a high typhoidal *Salmonella* disease burden. (55) In contrast to the invasive, human-restricted nature of typhoidal *Salmonella*, Non-typhoidal *Salmonella* (NTS), such as *S. Typhimurium*, *S. Enteritidis*, *S. Heidelberg* or *S. Newport*, are found in a broad range of hosts and primarily cause self-limiting gastroenteritis. (52) In 2010 it was estimated that 93.8 million cases of gastroenteritis linked to NTS infection occur annually worldwide, leading to an estimated 155 000 deaths. (56) Notably, within Canada, the United States and Europe, where NTS infections are consistently reported, *Salmonella* is a leading cause of foodborne illness. (57,58) Transmission of NTS occurs through the fecal-oral route, with many infections stemming from the consumption of contaminated animal products, fresh produce, or water. (57)

Asymptomatic infections in domesticated animals are also relatively common, providing a reservoir for *Salmonella* and contributing to zoonotic transmission through contamination or direct host-host transmission. (58,59) Additionally, certain serovars of NTS, such as *S.* Typhimurium, *S.* Enteritidis or *S.* Dublin, possess the ability to enter the bloodstream leading to an invasive NTS disease (iNTS). (60) iNTS disease presents with similar clinical outcomes to typhoid fever, including febrile illness alongside respiratory symptoms, and possesses a much higher fatality rate than NTS. (61) An estimated 535 000 incidences of iNTS occurred in 2017 leading to 77 000 deaths amongst all infected individuals. (62) The burden of iNTS has been on the rise in recent years leading to an increase in the pressure to develop novel treatments or vaccines as many of the iNTS-associated strains are multi-drug resistant. (63–65)

Regardless of the origin, the most common route of entry into the human host is through the gastrointestinal tract where *Salmonella* must cross the intestinal epithelium to colonize the host since it is a facultative intracellular pathogen. (66) *Salmonella* accomplishes this goal by exploiting phagocytic intestinal cells, such as microfold (M) cells or dendritic cells (DC), or by inducing non-phagocytic cells to uptake the bacterium. (67,68) Additionally, *Salmonella* outcompetes the host commensal microbiota using a variety of virulence factors. (69) (Fig. 1.2.1)

M-cells are a specialized antigen sampling cell type found within the Peyer's patch, where they are a component of the follicle-associated epithelium (FAE). (70) These cells play an important role in the mucosal immune response by establishing a close connection to the underlying lymphocytes which allows them to easily present mucosal antigens. This close connection to the immune system makes M-cells an attractive target for bacterial pathogens. (71) *Salmonella* interaction with M-cells induces significant cytoskeletal rearrangements leading to micropinocytosis which prompts an increase in internalization of both bacteria and antigens as well as increased M-cell maturation. (70–73) These cytoskeletal rearrangements are detrimental to the integrity of M-cells causing a breakdown in the architecture of the FAE, further increasing *Salmonella* invasion. (72) CX3CR1<sup>+</sup> DCs, which can form trans-epithelial dendrites allowing for direct access to luminal antigens, are also exploited for *Salmonella* invasion. (74) These trans-epithelial protrusions can be targeted by *Salmonella* in a manner that leads to bacterial uptake into the DC thereby crossing the epithelial barrier. (74)

Uptake into non-phagocytic cells is mediated by virulence factors which are encoded on pathogenicity islands (PAIs). PAIs are cluster of genes, 10-100kb in length, found on the chromosome, plasmids or bacteriophages which can be acquired through horizontal gene transfer and are found exclusively in pathogenic strains of bacteria. (75) 24 *Salmonella*-encoded pathogenicity islands (SPIs) have been described with SPIs 1-5 existing in all serovars of *Salmonella enterica*. (76) (Table 1.2.1) SPI-1 and SPI-2 are unique because they each encode the necessary structural and regulatory components of a type III secretion system (T3SS) known as T3SS-1 and T3SS-2, respectively. SPI-1 contains the necessary virulence factors to facilitate *Salmonella* uptake into non-phagocytic cells, whereas SPI-2 contains important factors which facilitate intracellular survival. (77,78) (Table 1.2.2) Expression of SPI-1 encoded genes occurs prior to host cell invasion and is triggered by environmental cues which relay when *Salmonella* adhesion to the host cell has occurred. This leads to the assembly of the T3SS-1 and the release of its associated effectors into the host cell. (79) It is important to note that not all effectors secreted by the T3SS-1 are encoded within the corresponding SPI. Effectors may be encoded on a different SPI or other mobile genetic elements such as prophages or *Salmonella*-associated virulence plasmids (pSLT). (80) The combinatorial activity of T3SS-1 secreted effectors alters the host cytoskeletal prompting the formation of membrane extensions, known as ruffles, which engulf the bacteria. (81)

Following internalization, *Salmonella* will express the SPI-2 encoded T3SS and its associated effectors leading to the establishment of an intracellular compartment known as the *Salmonella*-containing vacuole (SCV). (82,83) SCVs in epithelial cells are translocated to the basolateral membrane where bacteria can be released into the submucosal layer of the gastrointestinal tract. They also act as sites for bacterial replication. (84) Once *Salmonella* has crossed the epithelial barrier, either through the exploitation of a phagocytic cell or inducing uptake and passage through non-phagocytic cells, they are engulfed by phagocytes, notably macrophages, through a macropinocytotic process that utilizes both SPI-1 dependent and independent endocytic pathways. (85) Upon entering a macrophage, *Salmonella* will again establish an SCV, which provides a niche for bacterial survival and replication. (86,87) One consequence of this invasion is the production of IL-8 alongside other pro-inflammatory cytokines, generating an environment that conveys a growth advantage to *Salmonella* when compared to other members of the host microbiota. (88)

*Salmonella* is a thoroughly researched pathogen with a vastly more complicated pathogenic repertoire than I have presented here, these details have been discussed at great length elsewhere and the reader is referred to these reviews. (49,51,80,89–92)

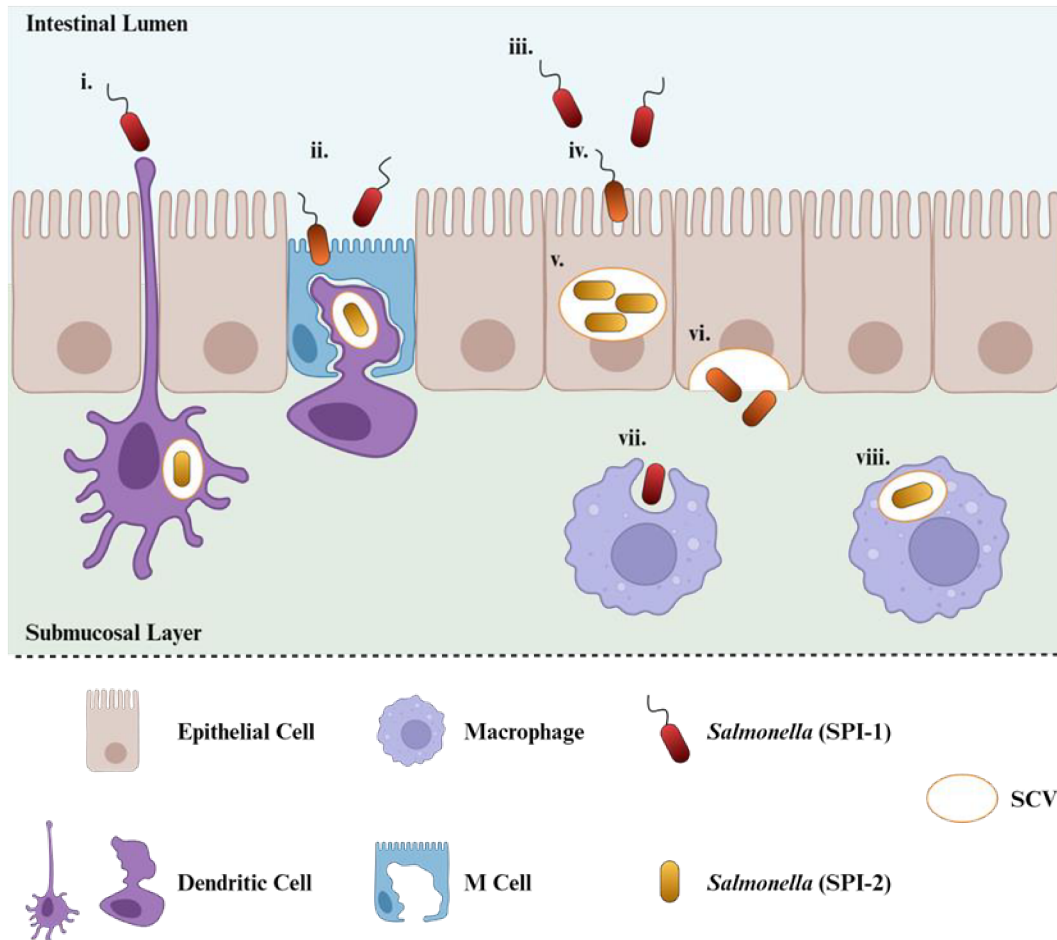


**Fig. 1.2.1 Strategies for *Salmonella* Typhimurium Invasion**

**i.** *Salmonella* can be directly phagocytosed by transepithelial CX3CR1+ dendritic cells, directly bypassing the epithelial barrier **ii.** *Salmonella* adhere to the surface of M cells and induce cytoskeletal rearrangements leading to micropinocytosis. Micropinocytosed *Salmonella* are then able to invade the underlying M cell-associated phagocytes where they can establish a *Salmonella*-containing vacuole (SCV) and begin replicating. **iii.** *Salmonella* adhere to non-phagocytic epithelial cells within the lumen. Attachment to the epithelial cell induces the expression of the SPI-1 encoded genes, including T3SS-1. **iv.** T3SS-1 associated effectors are secreted into the epithelial cell, inducing cytoskeletal rearrangement leading to membrane ruffling and *Salmonella* engulfment. **v.** *Salmonella* which have been engulfed began to express SPI-2 encoded genes, including T3SS-2 and the associated effectors, to establish an SCV. **vi.** The SCV translocates to the basolateral membrane where *Salmonella* are released into the

submucosal layer. **vii.** *Salmonella* adhere to macrophages in the submucosal layer and are phagocytosed. **viii.** Phagocytosed *Salmonella* express SPI-2 encoded genes, including T3SS-2 and the associated effectors, leading to the establishment of an SCV. Adapted from (80) Created with Biorender.com.

**Table 1.2.1 Size & Function of Conserved *Salmonella* Pathogenicity Islands**

| <b>SPI</b> | <b>Size (kb)</b> | <b>Function</b>                                      |
|------------|------------------|--|
| SPI-1      | 39.8             | Invasion, Encodes T3SS-1                             |
| SPI-2      | 39.7             | Intracellular survival & replication, Encodes T3SS-2 |
| SPI-3      | 34               | Survival in macrophages during low Mg <sup>2+</sup>  |
| SPI-4      | 27               | Adhesion to epithelial cells, Encodes T1SS           |
| SPI-5      | 7.6              | Stimulate pro-inflammatory cytokines                 |

Adapted from (76). Overview of conserved *Salmonella* pathogenicity islands (SPI). Size is provided in kilobases (kb). Function indicates role of associated effectors during infection.

**Table 1.2.2 Representative *Salmonella* Secreted Effector Proteins**

| <b>Effector</b>         | <b>Encoded on</b> | <b>T3SS</b> | <b>Function</b>   | <b>Reference</b> |
|-------------------------|-------------------|-------------|---|------------------|
| <b>SPI-1 Associated</b> |                   |             |   |                  |
| AvrA                    | SPI-1             | 1           | Inhibit inflammation & apoptosis                                      | (93–95)          |
| SptP                    | SPI-1             | 1           | Reset host cytoskeleton, Dampen proinflammatory response              | (93–95)          |
| SipA                    | SPI-1             | 1           | Increase internalization efficiency                                   | (93–95)          |
| SipB                    | SPI-1             | 1           | Phagocytotic apoptosis  | (93–95)          |
| SipC                    | SPI-1             | 1           | Induce membrane ruffling  | (93–95)          |
| SopB                    | SPI-5             | 1           | Promote membrane fission, macropinocytosis & epithelial cell survival | (76,94,95)       |
| SopD                    | Chromosome        | 1/2         | Promote membrane fission & macropinocytosis                           | (94–96)          |
| SopE2                   | Chromosome        | 1           | Promote membrane ruffling & proinflammatory response                  | (94–96)          |
| <b>SPI-2 Associated</b> |                   |             |   |                  |
| SseF                    | SPI-2             | 2           | Formation of microtubule bundles surrounding SCV                      | (93,97)          |
| SseG                    | SPI-2             | 2           | Contribute to filament formation                                      | (93,97)          |
| PipB                    | SPI-5             | 2           | Facilitate interaction of SCV with ER membrane                        | (97,98)          |
| SteA                    | Chromosome        | 1/2         | Formation of tubules & vacuole partitioning                           | (97)             |
| SifA                    | Chromosome        | 2           | Maintain SCV & Filament Formation                                     | (95,97)          |
| SteD                    | Chromosome        | 2           | Prevent T cell activation & antigen presentation                      | (97)             |
| PipB2                   | Chromosome        | 1/2         | Movement of mature SCV within host cell                               | (95,97,99)       |
| SseL                    | Chromosome        | 2           | Prevent autophagy & lipid droplet accumulation                        | (95,97)          |
| SifB                    | Chromosome        | 2           | Stabilize SCV   | (95,97,100)      |
| SopD2                   | Chromosome        | 2           | Necessary for bacterial replication in macrophages                    | (95,97)          |
| SseJ                    | Chromosome        | 2           | Stabilize SCV   | (95,97)          |
| SteB                    | Chromosome        | 1/2         | Unknown   | (97,101)         |
| SteC                    | Chromosome        | 2           | Necessary for vacuole-associated actin polymerization                 | (95,97)          |

|                  |                          |     |   |          |
|------------------|--------------------------|-----|---|----------|
| SlrP             | Chromosome               | 1/2 | Inhibits release of IL-1 $\beta$        | (97)     |
| SseK2            | Chromosome               | 2   | Interfere with NF- $\kappa$ B signaling | (95,97)  |
| <b>Accessory</b> |                          |     |   |          |
| SspH1            | Gifsy-3<br>Bacteriophage | 1/2 | Downregulate proinflammatory response   | (95,97)  |
| SspH2            | SPI-12                   | 2   | Enhance NOD1 signaling                  | (97,102) |

Overview of SPI-1- and SPI-2-associated *Salmonella* secreted effector proteins. Encoded on indicates genetic location of indicated effector. T3SS indicates T3SS responsible for translocation of indicated effector. [1 = T3SS encoded by SPI-1; 2 = T3SS encoded by SPI-2] Function indicates role of indicated effector during infection.

### 1.3 Structure & Function of Type III Secretion Systems

T3SS are a conserved molecular apparatus to facilitate invasion and survival found in many gram-negative bacteria. (103,104) These syringe-like structures cross both the bacterial and host cell membranes and allow the bacterium to inject bacterial-encoded proteins, known as effectors, into the cytosol of host cells in an ATP-dependent manner. (105–107) (Fig. 1.3.1) These effectors contribute to infection by modulating host cell processes such as immune signaling, cytoskeletal rearrangement and membrane transport supporting bacterial invasion and the establishment of infection. (80,108) The T3SS itself is a macromolecular structure comprised of an ATPase complex, cytoplasmic ring, basal body, translocators, and export apparatus. (92,109) *Salmonella* encodes two T3SS, T3SS-1, found on SPI-1, and T3SS-2, found on SPI-2. The proteins that constitute these complexes, and their nomenclature, are detailed in Table 1.3.1. (92) Evolutionary analyses indicate that the molecular machinery responsible for the T3SS originated from the molecular machinery used to transport extracellular components of the flagellum. (110,111) T3SS have been the subject of extensive research and details regarding their structure, assembly and function can be found thoroughly described elsewhere. (92,103,109,112)

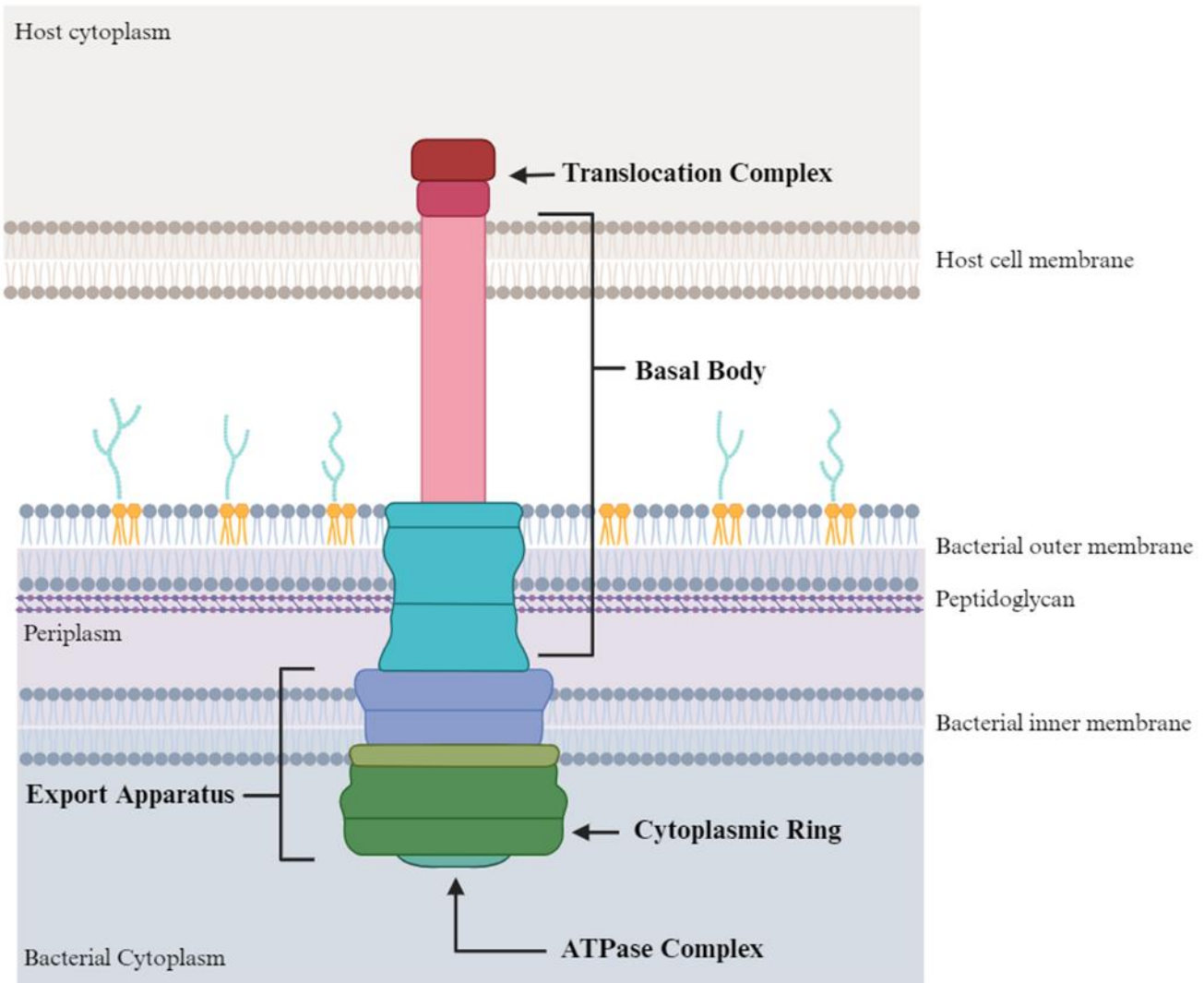


**Fig. 1.3.1 Depiction of *Salmonella* Type III Secretion System Structure**

Graphical depiction of the major structural components of the *Salmonella* T3SS. Adapted from (105,109). Created with Biorender.com.

**Table 1.3.1 Nomenclature of T3SS of *Salmonella enterica* serovar Typhimurium**

| <b>Function</b>              | <b>Unified Nomenclature</b> | <b>T3SS-1</b> | <b>T3SS-2</b> |
|------------------------------|-----------------------------|---------------|---------------|
| <b>Basal Body</b>            |                             |               |               |
| Outer Membrane Ring          | SctC                        | InvG          | SsaC          |
| Secretin                     | -                           | InvH          | -             |
| Inner Membrane Ring          | SctD                        | PrgH          | SsaD          |
| Inner Membrane Ring          | SctJ                        | PrgK          | SsaJ          |
| Needle                       | SctF                        | PrgI          | SsaG          |
| Inner Rod                    | SctI                        | PrgJ          | SsaI          |
| <b>Export Apparatus</b>      |                             |               |               |
| Autoprotease                 | SctU                        | SpaS          | SsaU          |
| Export Gate                  | SctV                        | InvA          | SsaV          |
| Inner Membrane Component I   | SctR                        | SpaP          | SsaR          |
| Inner Membrane Component II  | SctS                        | SpaQ          | SsaS          |
| Inner Membrane Component III | SctT                        | SpaR          | SsaT          |
| <b>Cytoplasmic Ring</b>      | SctQ                        | SpaO          | SsaQ          |
| <b>ATPase Complex</b>        |                             |               |               |
| ATPase                       | SctN                        | InvC          | SsaN          |
| Stator                       | SctL                        | OrgB          | SsaK          |
| <b>Regulators</b>            |                             |               |               |
| Needle-length Regulator      | SctP                        | InvJ          | SsaP          |
| Switch Regulator             | SctW                        | InvE          | SsaL / SpiC   |
| <b>Translocators</b>         |                             |               |               |
| Translocation Pore           | SctB                        | SipC          | SseD          |
| Translocation Pore           | SctE                        | SipB          | SseC          |
| Needle Tip                   | SctA                        | SipD          | SseB          |

Adapted from (92). Overview of the components of the *Salmonella*-encoded T3SSs. Includes specific nomenclature of indicated component for both *Salmonella* T3SS encoded on SPI-1 and SPI-2 as well as the unified nomenclature for bacterial T3SS components.

## 1.4 The Role of Novel E3 Ligases in Pathogenic Ubiquitination

One class of effectors that are secreted through the T3SS of gram-negative bacteria are Novel E3 ubiquitin ligases (NELs). (113) NELs represent a unique architecture of E3 ubiquitin ligase as they do not share any sequence or structural similarity to the previously described eukaryotic E3 ligases, although they are known to form a thioester bond with the C-terminal diglycine motif in a mechanism similar to HECT eukaryotic E3 ligases. (114) Interestingly, they have evolved this architecture in the context of a prokaryotic cell, where there is an absence of ubiquitin encoding genes, indicating their function is uniquely suited to alter the ubiquitome of host cells during infection. (115) These effectors are found in pathogenic bacteria which target a variety of eukaryotic hosts such as *Salmonella enterica*, *Shigella flexneri*, *Sinorhizobium fredii*, *Ralstonia solanacearum*. (Table 1.4.1) (116,117) NELs share a common structural pattern with 2 major domains separated by a flexible linker to facilitate different spatial conformations as well as a short signaling sequence. The signaling domain is a variable sequence found at the N-terminal of the protein which is indispensable for secretion by the T3SS. (114,118) The N-terminal leucine rich repeat (LRR; LxxLPxxLxxLxxxxxVxLxxNPL) domain mediates substrate recognition and plays a role in controlling NEL activity by preventing access to the catalytic cysteine through the adoption of an autoinhibitory conformation. (119,120) The C-terminal globular NEL domain harbors a catalytic cysteine and mediates the interaction with the incoming E2~Ub conjugate. (113) Structural comparison of the four *Salmonella* encoded NELs are depicted in fig. 1.4.1. (116) Interaction of the LRR domain with a substrate leads to a conformational change that exposes the catalytic NEL domain and promotes ubiquitin transfer. The ability to undergo conformational changes is essential in mediating ubiquitin transfer to a substrate, mutations which affect the flexibility between the N-terminal and C-terminal domains abrogate ubiquitination activity. (121,122) NELs have been previously described to preferentially interact with E2s from the promiscuous UBE2D family of conjugating enzymes which are used by all families of eukaryotic E3s. (123) However, due to their differential architecture relative to eukaryotic E3 ligases, the interaction between NELs and E2~Ub conjugates occurs through unique interfaces. (124)

**Table 1.4.1 Representative Members of the Novel E3 Ligase Family**

| <b>Effector</b>                      | <b>Domains</b> | <b>Catalytic Residue</b> | <b># of LRR</b> | <b>Ref</b> |
|--------------------------------------|----------------|--------------------------|-----------------|------------|
| <b><i>Salmonella enterica</i></b>    |                |                          |                 |            |
| SlrP                                 | LRR + NEL      | C546                     | 11              | (125–127)  |
| SspH1                                | LRR + NEL      | C492                     | 8               | (120)      |
| SspH2                                | LRR + NEL      | C580                     | 12              | (118)      |
| SspH3                                | LRR + NEL      | C603                     | 9*              | (128)      |
| <b><i>Shigella flexneri</i></b>      |                |                          |                 |            |
| IpaH 1.4                             | LRR + NEL      | C368                     | 8               | (129)      |
| IpaH 2.5                             | LRR + NEL      | C368                     | 8               | (130)      |
| IpaH 4.5                             | LRR + NEL      | C379                     | 10              | (130)      |
| IpaH 7.8                             | LRR + NEL      | C357                     | 9               | (130)      |
| IpaH 9.8                             | LRR + NEL      | C337                     | 8               | (129)      |
| <b><i>Sinorhizobium fredii</i></b>   |                |                          |                 |            |
| NopM                                 | LRR + NEL      | C338                     | 7               | (131)      |
| <b><i>Ralstonia solanacearum</i></b> |                |                          |                 |            |
| RipAR                                | NEL            | C322                     | 0               | (132)      |
| RipAW                                | NEL            | C177                     | 0               | (132)      |
| RipV1                                | NEL            | C401                     | 0               | (132)      |
| RipV2                                | NEL            | C403                     | 0               | (133)      |

\*Determined using InterPro by EMBL-EBI (134,135).

Adapted from (116). Overview of select members of the novel E3 ligase family of effectors. The presence of a leucine rich repeat (LRR) or novel E3 ligase (NEL) domain is indicated alongside the position of the catalytic cysteine residue and the number of leucine rich repeats.

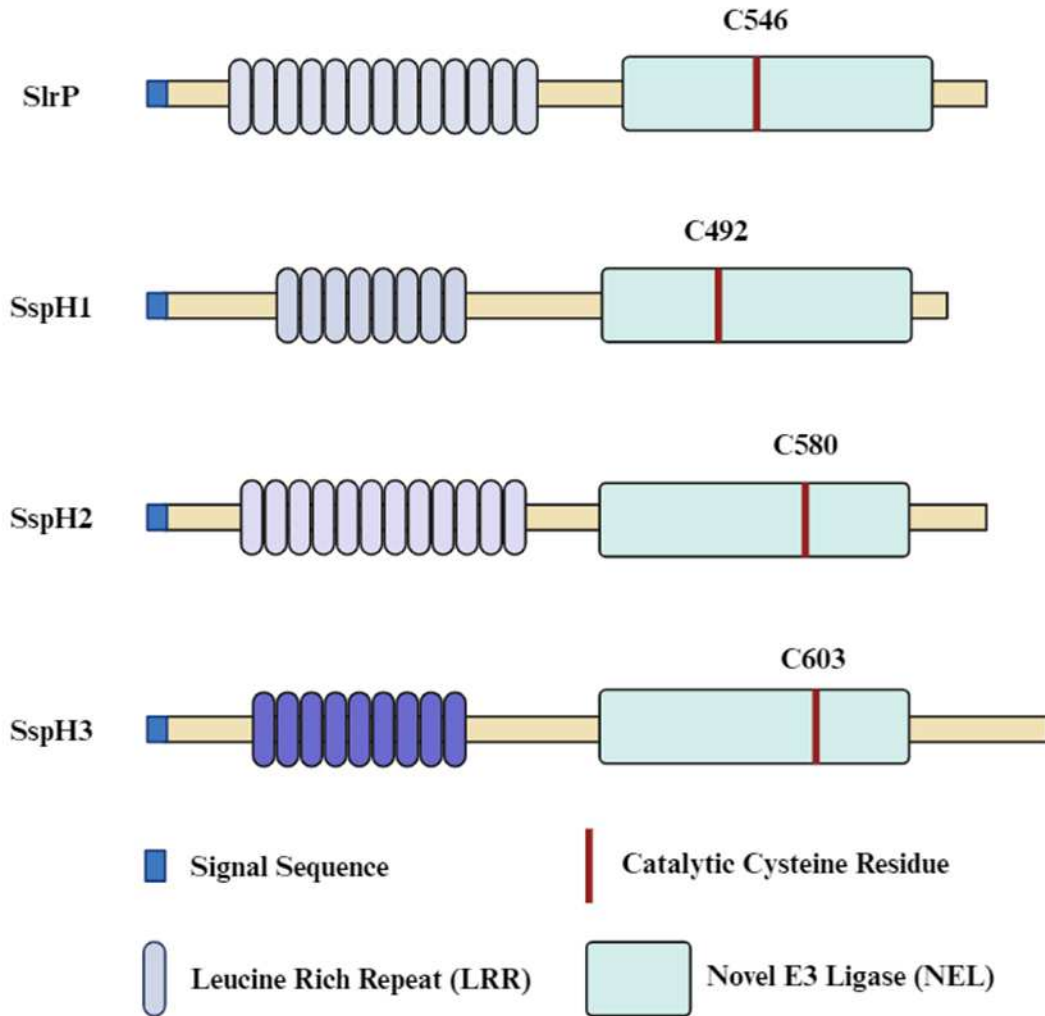


**Fig. 1.4.1 Domain Structure of the Novel E3 Ligases Encoded by *Salmonella***

Graphical comparison of the domains found in *Salmonella* leucine-rich repeat protein (SlrP) and *Salmonella* secreted proteins H1-3 (SspH1-3). Adapted from (116).

## 1.5 Introduction to *Salmonella* Secreted Protein H1 (SspH1)

*Salmonella* secreted protein H1 (SspH1) was identified by Miao et al in 1999 and was one of the first members of the SspH family of NELs. (127) SspH1 is 700 amino acids in length, giving it a molecular weight of ~77 kDa. The catalytic cysteine, C492, is found within the NEL domain; mutation of this cysteine to an alanine (C492A) abrogates SspH1 catalytic activity. (118,129) It has been shown to be encoded on the Gifsy-3 prophage. (136) Recent screening of the *Salmonella* Foodborne Syst-OMICS (SalFos) by Herod et al revealed that SspH1 was present in ~12% of available whole-genome sequences where it is most commonly found in the serovar Typhimurium with ~22% of isolates encoding SspH1. (137) SspH1 is known to be secreted during infection of intestinal epithelial cells as well as macrophages by both the T3SS-1 and T3SS-2. (127,138) After SspH1 is translocated into a host cell it localizes to the nucleus through unknown mechanisms. (139,140) SspH1 has a known role in downregulating NF- $\kappa$ B activity which contributes to lowered pro-inflammatory cytokine secretion. (138,139) Additionally, SspH1 has been shown to interact with the HR1b domain of PKN1 causing it to be ubiquitinated and subsequently degraded. (120) Previous research has indicated that SspH1-mediated degradation of PKN1 can interfere with the androgen receptor potentiating role of PKN1. (120,141) Despite the connection between PKN1 and AKT, work by Herod et al indicates that SspH1-dependent effects on PKN1 levels were insufficient to alter the outcome of AKT signaling likely owed to the complex nature and interconnected activities of the other *Salmonella* secreted effectors. (137) Some research indicates that the ability of SspH1 to lower NF- $\kappa$ B activity is independent of E3 ligase activity which suggests an alternate non-catalytic mechanism of action. (120) Additionally, recent research suggests that SspH1 is responsible for improving *Salmonella* survival during acute gut inflammation, possibly by through the downregulating the NLRC4 inflammasome.(142) Of particular importance for my work, it has been demonstrated that SspH1 expression is detrimental to the growth of yeast in a catalytic activity-dependent manner. (120)

## 1.6 Structure & Function of PKN1

The known substrate of SspH1 is the protein kinase C-related kinase (PRK) family member protein kinase N1 (PKN1). (143) The PRK family is a three-member group of serine/threonine kinases consisting of PKN1 (PRK1/PKN/PKN $\alpha$ ), PKN2 (PRK2/PKN $\gamma$ ) and PKN3 (PRK3/PKN $\beta$ ); all of which are ubiquitously distributed amongst human tissue, although PKN3 is found at very low levels. (144) They all share a common, multi-domain architecture containing three N-terminal homology regions (HR1), a C2-like domain, a kinase domain, which belongs to the AGC kinase superfamily, as well as a C-terminal tail which contains important motifs that mediate protein-protein interactions during PKN activation. (145) Additionally, PKN2 and PKN3 have proline-rich regions found between the C2-like and kinase domains, which are recognized by the SH3 domain of other adaptor proteins. (144) (Fig. 1.6.1) The PRKs are found downstream of the Rho family of GTPases which situate them as important regulators for a diverse number of cellular processes. (146) Despite their importance, our understanding of their structure and function remains incomplete. Given that PKN1 is the known substrate of SspH1, this introduction will mainly focus on the structure, function, and consequences of PKN1 signaling. A comprehensive view of the PRK family as a whole has been described in detail elsewhere. (144)

Prior to the initiation of the signaling cascade PKN1 exists in an autoinhibitory dimer conformation in the cytosol. (147,148) The interaction of lipids, such as arachidonic acid, PIP<sub>2</sub>, or PIP<sub>3</sub>, with the C2-like domain disrupts the dimer, alleviating autoinhibition and leading to membrane recruitment. (149,150) Phosphoinositide-dependent kinase 1 (PDK1) is then recruited to the exposed hydrophobic motif (HM) in the C-terminal tail of PKN1 where it will phosphorylate the T774 residue found in the activation loop. Following T774 phosphorylation, mTOR2 or CDK1 will phosphorylate the S916 residue found in the turn motif of the C-terminal tail leading to the dissociation of PDK1. The HM of the T774/S916 diphosphorylated C-terminal tail interacts with the PDK1-interacting fragment (PIF) pocket leading to a structural change that places the kinase domain in an allosterically active conformation. (144) However, despite the kinase domain being in an active conformation, research indicates that PKN1 itself is not fully active due to what is speculated to be a pseudosubstrate inhibition motif found in the HR1a domain. (151) Regulation by the pseudosubstrate motif is thought to be alleviated through the binding of RhoA to the HR1a domain, which can also contribute to PKN1 activation by

increasing PDK1-mediated phosphorylation. (152) This signaling cascade is depicted in Fig. 1.6.2. In addition to the activation through the phosphorylation cascade described above, PKN1 can also be activated through a proteolytic mechanism as seen during apoptosis where caspase-3 induced cleavage leads to the generation of constitutively active PKN1 fragments. (153) The complexity of PKN1 activation underscores its role as a key mediator in multiple signaling pathways that are induced by a variety of cellular cues.

One prominent role for PKN1 signaling in the context of the immune response is to inhibit pyrin inflammasome formation. (154,155) Under homeostatic conditions, PKN1 is activated through an interaction with RhoA which leads to PKN-mediated phosphorylation of pyrin. Phosphorylated pyrin is then bound by 14-3-3 chaperone proteins to maintain it in an inactive state. When RhoA is inactivated, a common strategy employed during bacterial infection to disrupt the host cytoskeleton, PKN1 activation is abrogated which prevents pyrin phosphorylation and sequestration. Unphosphorylated pyrin can then oligomerize alongside ASC and pro-caspase-1 to form the functional pyrin inflammasome leading to an increase in IL-1 $\beta$  secretion and potentiating the innate immune response. (155) (Fig. 1.6.3)

Another role of PKN1 signaling that has been implicated in the context of *Salmonella* infection, and SspH1 activity in particular, is androgen receptor (AR) signaling. In canonical AR signaling the AR is found associated with chaperones in the cytoplasm in the absence of ligands. In the presence of a ligand, such as the biologically active form of testosterone, dihydrotestosterone (DHT), AR dissociates from its chaperone proteins. (156) PKN1 can bind to the transactivation domain of AR before the PKN1-AR complex is translocated to the nucleus and targeted to the androgen-responsive elements (ARE). (157) After recruitment to the ARE, PKN1 phosphorylates T11 on Histone 3 which recruits a demethylase leading to increased gene transcription. (157) Additionally, activation of the thromboxane receptors TP $\alpha$  and TP $\beta$  by thromboxane A<sub>2</sub> (TXA<sub>2</sub>) can directly induce PKN1 phosphorylation of the T11 residue on Histone 3 to enhance AR recruitment and increase gene transcription. (158) (Fig. 1.6.3)

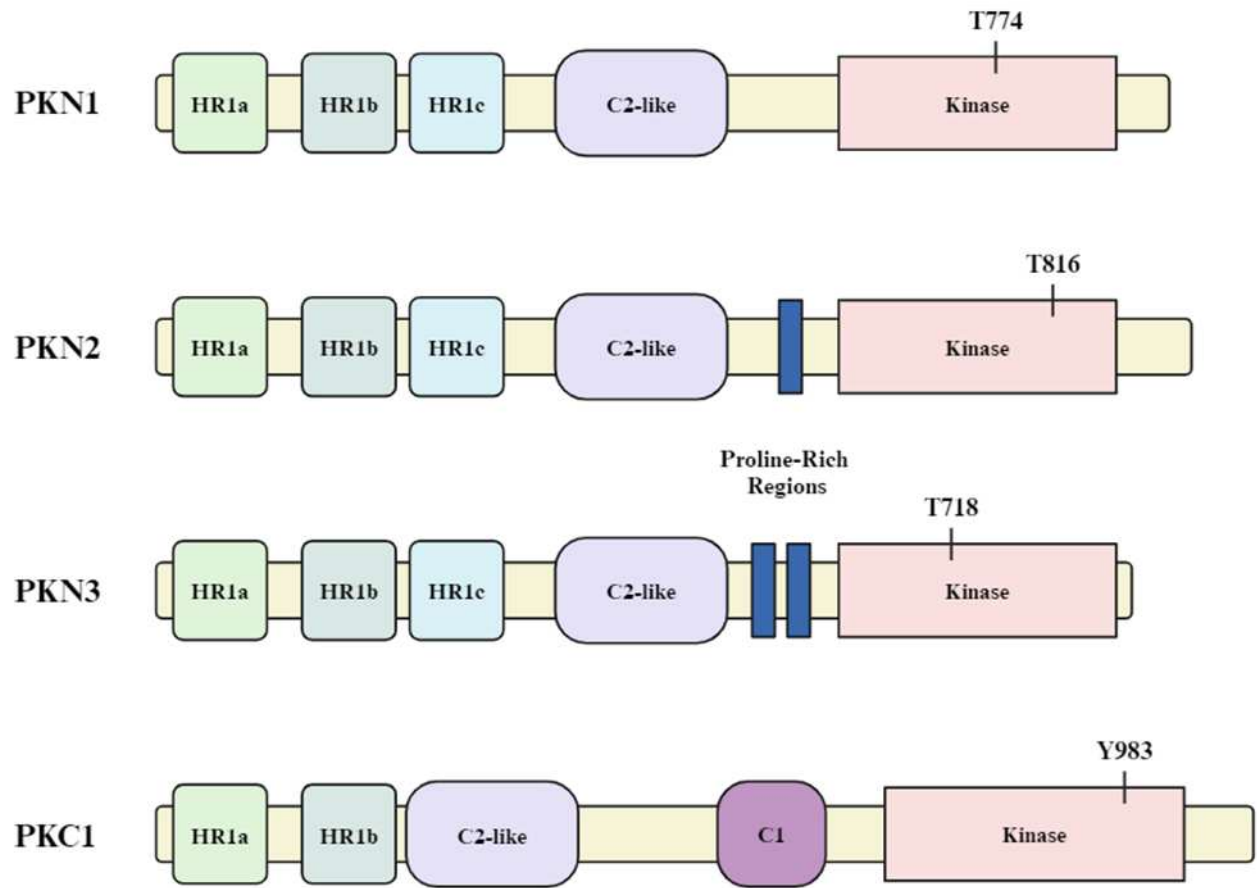


**Fig. 1.6.1 Domain Structure of Protein-Kinase C Related (PRK) Kinases**

Graphical comparison of the PRK family of serine/threonine kinases, PKN1-3, and protein kinase C (PKC), the only PRK family member encoded in *Saccharomyces cerevisiae*.

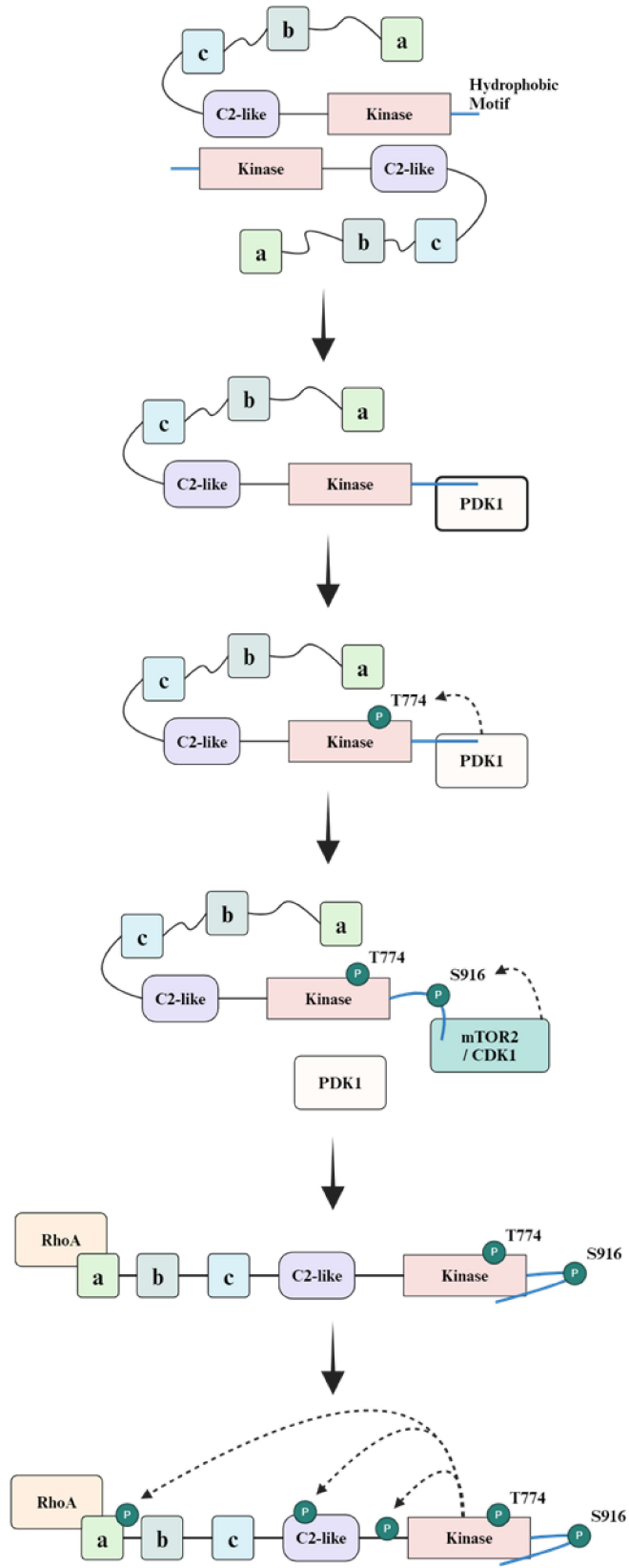


### **Fig. 1.6.2 Activation of PKN1**

**i.** Prior to activation cytosolic PKN1 adopts an autoinhibited dimeric conformation **ii.** Lipid interaction disrupts the PKN1 dimer, leading to membrane localization and allowing PDK1 to be recruited to the C-terminal hydrophobic motif of PKN1. **iii.** PDK1 phosphorylates T774 in the PKN1 activation loop **iv.** mTOR2 or CDK1 are recruited to PKN1 post-T774 phosphorylation leading to the phosphorylation of S916 in the PKN1 turn motif and causing the dissociation of PDK1. **v.** The T774 and S916 diphosphorylated C-terminal tail of PKN1 undergoes a conformational change to interact with the PDK1-interacting fragment (PIF) domain which allosterically activates kinase activity. RhoA is recruited to the HR1a domain of PKN1 to alleviate a speculated pseudosubstrate inhibition motif. **vi.** Complete activation of PKN1 kinase activity allows for self-phosphorylation and phosphorylation of downstream targets. Adapted from (144).

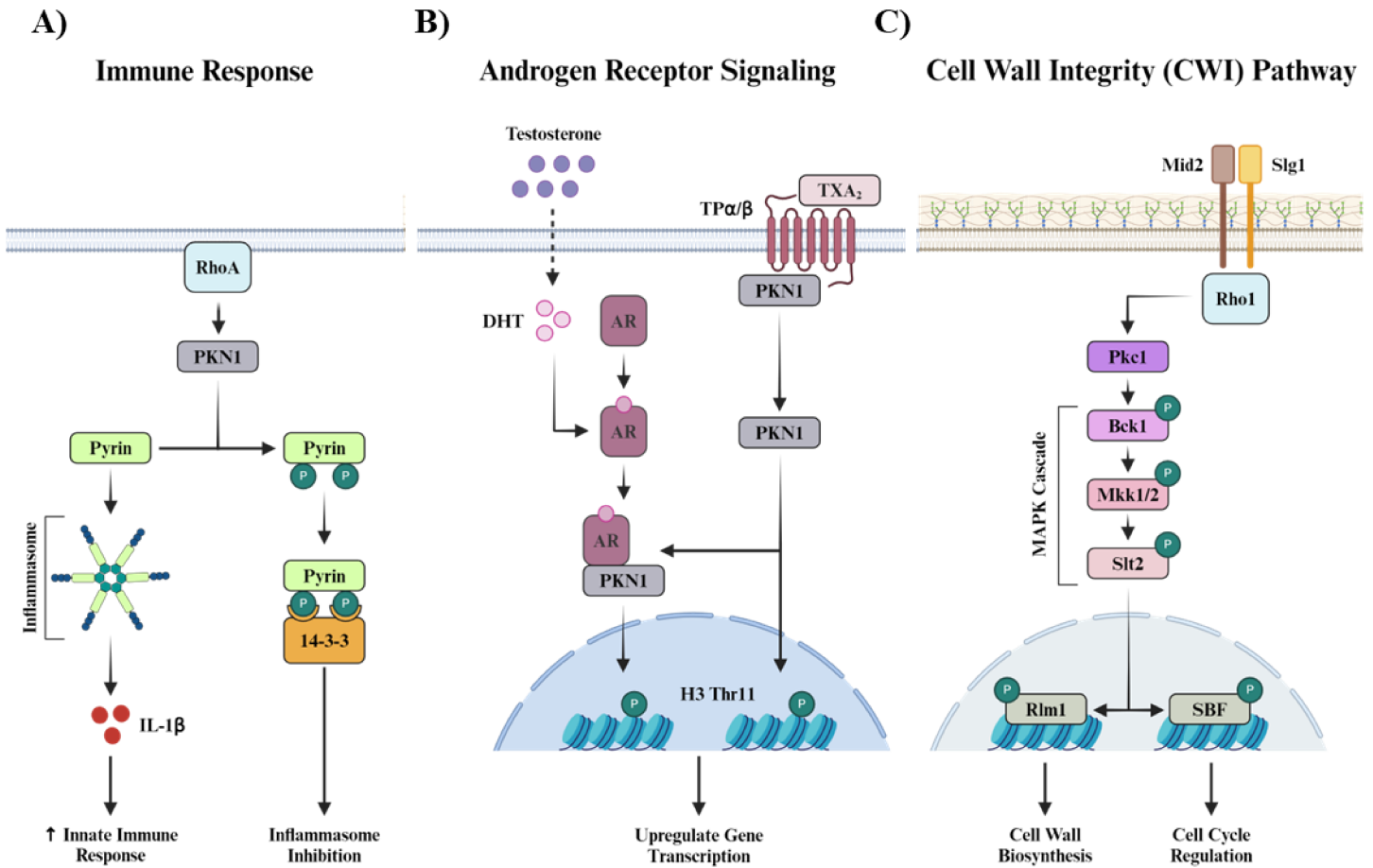


**Fig. 1.6.3 Different Role of PRK Signaling**

(A) PKN1 has a prominent role in regulating the immune response. During homeostatic conditions PKN1 is activated through the interaction with RhoA, activating its kinase activity and allowing it to phosphorylate pyrin. Phosphorylated pyrin is then sequestered by 14-3-3 proteins preventing the formation of inflammasomes. (B) PKN1 plays a role in regulating androgen receptor (AR) signaling. PKN1 interacts with activated AR, which is bound to the activated form of testosterone, to form a PKN1-AR complex. The PKN1-AR complex is then translocated to the nucleus where it targets androgen response elements. PKN1 phosphorylates T11 on Histone 3 which leads to demethylase recruitment and increased gene transcription. Activation of TP $\alpha/\beta$  by Thromboxane A<sub>2</sub> (TXA<sub>2</sub>) can directly induce nuclear localization of PKN1 leading to phosphorylation of T11 on Histone 3 leading to demethylase recruitment and increased gene transcription. (C) PKC1 plays a vital role in maintaining yeast cell wall integrity.

Cell wall stress is detected through the sensor proteins Mid2 and SLG1 which triggers Rho1-dependent activation of Pkc1. Pkc1 phosphorylation induces signaling through the yeast MAPKKK signaling cascade, which consists of Bck1, Mkk1/2, and Slt2. Phosphorylated Slt2 translocates to the nucleus where it will phosphorylate the transcription factor factors Rlm1 or SBF, leading to cell wall synthesis or cell cycle regulation, respectively. (159,160)

### **1.7.1 Inhibition of the Ubiquitination Cascade**

Given the key role ubiquitination plays throughout multiple cellular processes and disease states, it has been an attractive target for the development of novel therapeutics. (161) The sequential nature of the ubiquitin cascade provides multiple, discrete steps which can become the target of inhibitors. During Ub activation there are three interactions which can be biochemically targeted: i) binding of ATP to E1, ii) formation of the covalent bond in the E1~Ub conjugate and iii) binding of E1~Ub to the E2. (161–164) However, since there is a limited number of E1s, their inhibition effects ubiquitination non-specifically which is often detrimental to indispensable cellular processes. (165) The transfer of the ubiquitin molecule from the E2~Ub to the E3 can also be targeted, but this retains the issue of non-specific effects as a single E2 can interact with a diverse array of E3s. (166–168) Finally, the formation of the E3~Ub conjugate and the interaction between the E3 and the substrate are the most specific steps of the cascade and may prove the best target for biochemical inhibition. (161,169) Unfortunately the specific interaction pockets are often shallow and difficult to target using small molecules. (161,170) Nonetheless, many inhibitors of the ubiquitin cascade, primarily cell permeable small molecules, have been developed and their therapeutic potential has been examined in both preclinical and clinical settings. (Table 1.7.1)

### **1.7.2 Engineered Ubiquitin Variants as Ubiquitination Inhibitors**

Despite the structural and mechanistic diversity amongst the enzymes within the ubiquitin signaling network they all share a common substrate in ubiquitin. Interestingly, most of these proteins recognize a common surface on ubiquitin through a low affinity, high specificity interaction. (171,172) This knowledge was leveraged by Dr. Sachdev S. Sidhu to design and construct a phage-displayed ubiquitin variant (Ubv) library that contains over ten billion unique variants (Fig. 1.7.1). (173,174) Ubiquitin-interacting proteins can then be screened against this library using phage display selection to identify Ubv which bind with high-affinity to the protein of interest (Fig. 1.7.2). (175–178) Ubvs can act as competitive inhibitors, preventing the enzyme for which they were selected against from interacting with ubiquitin, or, somewhat surprisingly, act as activators. (169,174) There are many advantages to the Ubv approach; they can be produced rapidly and in a cost-effective manner, they can target unique sites which may not be accessible to other small molecules, they can be optimized on a systematic scale for increased

efficacy, they don't require previous structural knowledge of the interaction between ubiquitin and the protein of interest, they are specific in nature as the sequence found in ubiquitin-binding domains varies between enzymes and they can provide structural details that can be used to steer the design of traditional small molecule inhibitors. (173)

The initial intention of this Ubv library was to identify high-affinity binders for the USP family of DUBs. (174) Not only were efficient Ubv inhibitors identified for three individual USPs, Ernst et al. also identified inhibitors for an OTU and JAMM deubiquitinases as well as an enhancer of NEDD4 E3 ligase activity. (174) Given this success, a Ubv approach has been pursued and employed to identify modulators for all major families of the human encoded E3 ligases. (169,179) While many of the identified Ubvs were inhibitors that bound to the known ubiquitin binding pocket of the E3 ligases some interesting cases existed where ubiquitination was massively increased, or inhibition occurred through binding to a previously undescribed allosteric site. In addition to targeting human E3 ligases, a Ubv approach has also been utilized to identify modulators for some human E2 enzymes as well as proteins containing an ubiquitin-interacting motif (UIM) from both human and yeast. (167,180–183)

Outside of targeting eukaryotic ubiquitin enzymes, Ubvs have also been demonstrated to be effective inhibitors of viral deubiquitinating enzymes (vDUBs). (184) vDUBs play an important role in viral replication and immune suppression for many viruses, including coronaviruses (CoV) and the Crimean-Congo hemorrhagic fever virus (CCHFV), making them attractive pharmacological targets. (185,186) However, their similarity to the human OTU DUB family has complicated the development of selective inhibitors to these viral enzymes. The use of the Ubv platform was able to identify selective inhibitors which were detrimental to viral replication without cross-reacting to human DUBs. (184) This demonstrates the wide-spanning therapeutic potential of a Ubv-based approach that extends beyond the eukaryotic realm of ubiquitin-interacting proteins. Despite the replicable success of inhibiting ubiquitin-interacting proteins with Ubv *in vitro*, it remains a challenge to pursue the therapeutic potential of these molecules due to practical limitations in the efficient delivery of proteins and the immunogenicity of said proteins *in vivo*. (184,187,188)

**Table 1.7.1 Representative Examples of Inhibitors of Ubiquitination**

| <b>Compound</b>              | <b>Target</b>   | <b>Mechanism</b>                                      | <b>Clinical Stage</b> | <b>Reference</b> |
|------------------------------|-----------------|---|-----------------------|------------------|
| <b>Proteasome Inhibitors</b> |                 |   |                       |                  |
| Bortezomib                   | 20S Subunit     | Reversibly binds active site                          | FDA Approved          | (189)            |
| Carfilzomib                  | 20S Subunit     | Irreversibly binds active site                        | FDA Approved          | (190)            |
| Ixazomib                     | 20S Subunit     | Inhibits chymotrypsin-like activity                   | FDA Approved          | (191)            |
| <b>E1 Inhibitors</b>         |                 |   |                       |                  |
| PYR-41                       | Non-Specific E1 | Covalent inhibit active cysteine                      | Preclinical           | (192)            |
| TAK-243                      | Non-Specific E1 | Forms a TAK-243~Ub adduct                             | Preclinical           | (193,194)        |
| Compound I                   | Non-specific E1 | Inhibits E1 ATP activation                            | Preclinical           | (195)            |
| <b>E2 Inhibitors</b>         |                 |   |                       |                  |
| CC0651                       | hCdc34          | Allosteric binding leading to structural displacement | Preclinical           | (196)            |
| NSC697923                    | Ubc-Uev1A       | Impedes Ubc13~Ub conjugation                          | Preclinical           | (197)            |
| Leucettamol A                | Ubc13-Uev1A     | Inhibit Ubc13-Uev1A interaction                       | Preclinical           | (198)            |
| <b>RING E3 Inhibitors</b>    |                 |   |                       |                  |
| Curcumin                     | SKP2            | Downregulates SKP2                                    | Phase 3               | (199)            |
| AT-406                       | IAPs            | SMAC mimetic  | Phase 3               | (200)            |
| <b>RBR E3 Inhibitors</b>     |                 |   |                       |                  |
| BAY 11-7082                  | LUBAC           | Covalently bind active cysteine of Ubc13 and UbcH7    | Preclinical           | (201)            |
| Bendamustine                 | LUBAC           | Inhibits HOIP   | FDA Approved          | (202)            |
| <b>HECT E3 Inhibitors</b>    |                 |   |                       |                  |

|                        |                   |  |             |       |
|------------------------|-------------------|--|-------------|-------|
| HS-152                 | SMURF1            | Reversibly block RHOB ubiquitination   | Preclinical | (203) |
| Heclin                 | Non-specific HECT | Induce inhibitor conformational change | Preclinical | (204) |
| <b>DUBs Inhibitors</b> |                   |  |             |       |
| P50429                 | USP7              | Irreversibly bind catalytic cysteine   | Preclinical | (205) |
| Thiolutin              | Non-specific      | Non-specifically inhibit JAMM          | Preclinical | (206) |
| Pimozide               | USP1/UAP1 Complex | Non-competitive inhibition             | Preclinical | (207) |

Adapted from (164,208). Overview of previously described inhibitors of the ubiquitin cascade. Where available a brief description of the target, mechanism of action and current clinical approval is provided.

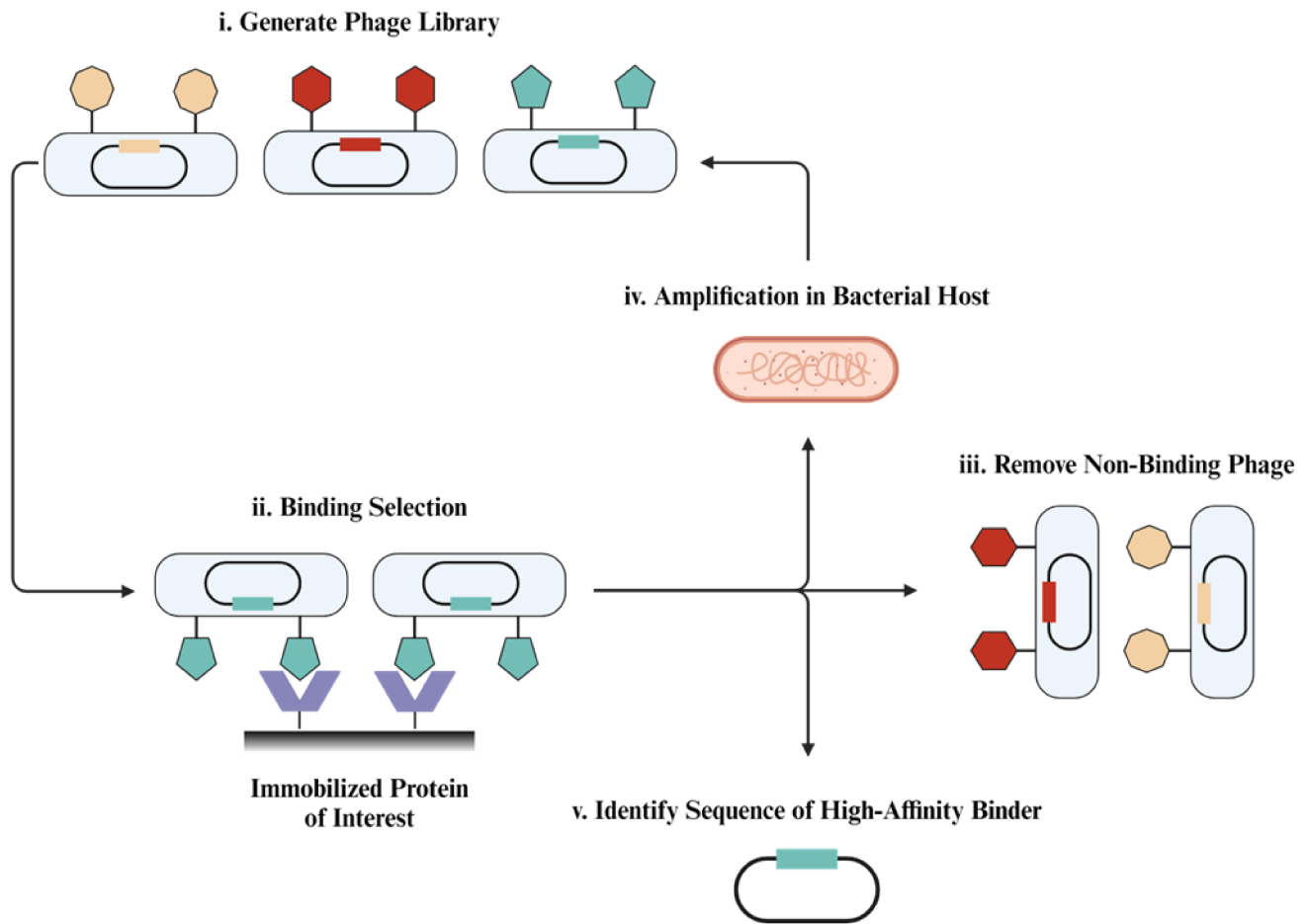


**Fig. 1.7.1 Identification of High-Affinity Ubiquitin Variants by Phage Display**

**i.**  $6.8 \times 10^{10}$  unique ubiquitin variants were generated through soft-randomization of 24 positions within the ubiquitin sequence. These sequences were then fused to the gene encoding the gene-3 mirror coat protein of the M13 bacteriophage to create a stable phage display library. (Leung et al. 2017) **ii.** All Ubv-displaying phages were allowed to attempt to bind to the immobilized protein of interest. **iii.** Non-binding phages are washed away. **iv.** Binding phages are amplified in the host bacteria and steps i-iv are repeated to further enrich for high-affinity Ubv binders to the protein of interest. **v.** Individual clones of high-affinity binders are subjected to DNA sequencing to identify the sequence of the encoded Ubv. Adapted from (173,176).

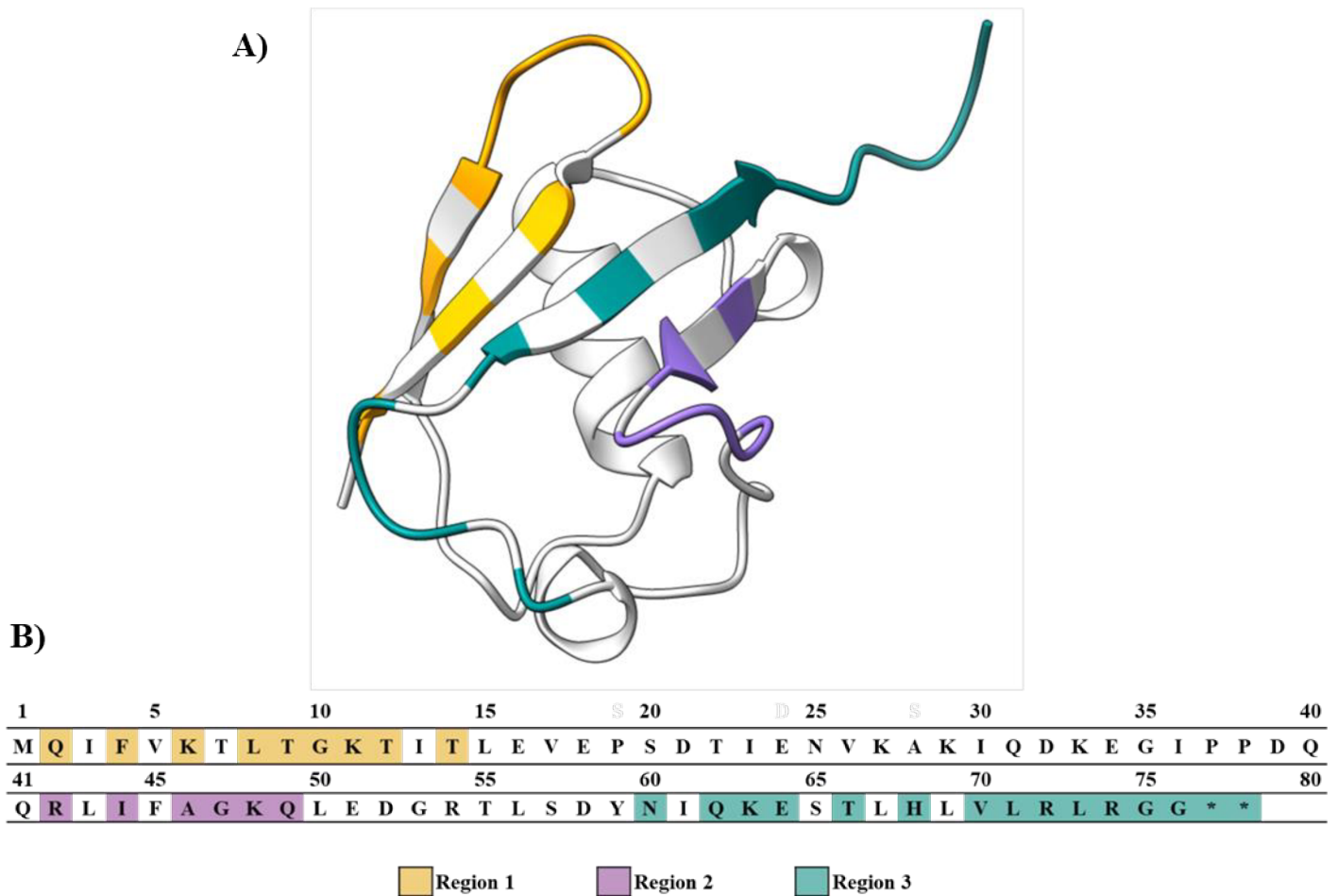


**Fig. 1.7.2 Regions Mutated in the Ubiquitin Variant Phage Display Library**

(A) Structure of human ubiquitin (PDB Entry: 1UBQ) is shown in grey with the three distinct mutation regions colored as followed: Region 1 – Yellow, Region 2 – Purple, Region 3 – Green.

(B) Sequence of human ubiquitin with the residues that were subjected to mutation colored according to mutation region: Region 1 – Yellow, Region 2 – Purple, Region 3 – Green.

## 1.8 *Saccharomyces cerevisiae* as a Versatile Eukaryotic Model System

*Saccharomyces cerevisiae*, also known as budding yeast or baker's yeast, is a single-celled eukaryote belonging to the fungi kingdom of microorganisms. It is one of the best studied eukaryotic organisms on a molecular and genetic level and has a long history of being successfully implemented as a model research organism owing to its short doubling time, ease of culturing and relatively uncomplicated genome architecture while still containing the complex internal structures and conserved cellular processes that are found in many higher-level eukaryotes. (209,210) Additionally, *S. cerevisiae* maintains the ability to be transformed by homologous recombination allowing for facile heterologous gene expression, such as T3SS effectors, through plasmid transformation. (211) Expression of T3SS effectors introduced by transformation is often driven by the *GALI/10* promoter in yeast, this promoter system is induced in the presence of galactose and repressed in the presence of glucose. (212,213) The inducible nature of this promoter provides valuable control over when the potentially toxic effectors are expressed and allows phenotypic comparisons to be made between the non-induced and induced conditions to elucidate the effect of effector expression. *S. cerevisiae* has been employed as a heterologous model organism for the study of bacterial effectors for nearly 20 years, aiding in the study a variety of invasive or adherent pathogens such as *Shigella flexneri*, *Yersinia pestis*, and *Salmonella enterica*. (214,215)

An advantage of *S. cerevisiae* as a model system is the easily monitored cell cycle, as they undergo distinct morphological changes that are coupled with readily assessable fluctuations in genetic content. (216–218) In short, yeast first undergo the G1 phase of the cell cycle where cells grow and prepare for cell division if the environmental conditions are appropriate. Since *S. cerevisiae* are diploid in nutrient-rich conditions, cells within the G1 phase contain a 1N chromosomal count. If the environmental conditions are deemed favorable by the yeast they will progress into the synthesis (S) phase where new genetic material is synthesized, leaving the yeast with a 2N chromosomal count, and a daughter cell will begin to bud out from the mother cell. After the genetic material has been doubled, *S. cerevisiae* enter the G2 phase where the emergence of the daughter cell will continue and nuclear migration towards the bud neck occurs. Once the daughter cell has reached a sufficient size the yeast will enter Mitosis (M), which is comprised of metaphase, anaphase, telophase, and cytokinesis. During this phase the nuclear

content is divided between the mother and daughter cells by microtubular contraction followed by complete separation of the cytoplasm leaving two distinct cells, each with a 1N chromosomal count, thereby completing a single trip through the cell cycle. (216,217) (Fig. 1.8.1)

*S. cerevisiae* encodes a single isoform of a serine/threonine kinase of the PKC super-family, PKC1. (124,219) Much like the previously described PKN1, PKC1 contains multiple domains including two N-terminal HR1 domains (HR1a and HR1b), a C2 domain, a C1 domain, and a C-terminal kinase domain. (Fig. 1.6.1) (220) PKC1 has been demonstrated to play a vital role in the cell wall integrity (CWI) pathway which controls cell wall synthesis and cell cycle progression. (159,221) This pathway is initiated at the cell surface through stress detection by the SLG1 and Mid2 sensor proteins, triggering Rho1-dependent activation of PKC1. (222) Activated PKC1 prompts signaling through a conserved MAPK cascade. The cascade begins with PKC1-mediated phosphorylation of Bck1, which is followed by Bck1-mediated phosphorylation of the Mkk1 or Mkk2, a redundant pair of MAPKKs, then Mkk1/Mkk2-mediated phosphorylation of Slt2. (222,223) Phosphorylated Slt2 will then translocate to the nucleus where it phosphorylates the transcription factors Rlm1, which induces the transcription of genes responsible for cell wall synthesis, or the transcription factor complex SBF, which is a heterodimeric complex consisting of Swi4 and Swi6 that regulates the expression of genes involved in cell cycle control. (224,225) (Fig. 1.6.3) Since SspH1 has been previously shown to interact with PKN1 it is possible the effect of SspH1 expression may be mediated through the disruption of PKC1 signaling in *S. cerevisiae*. (120,138)

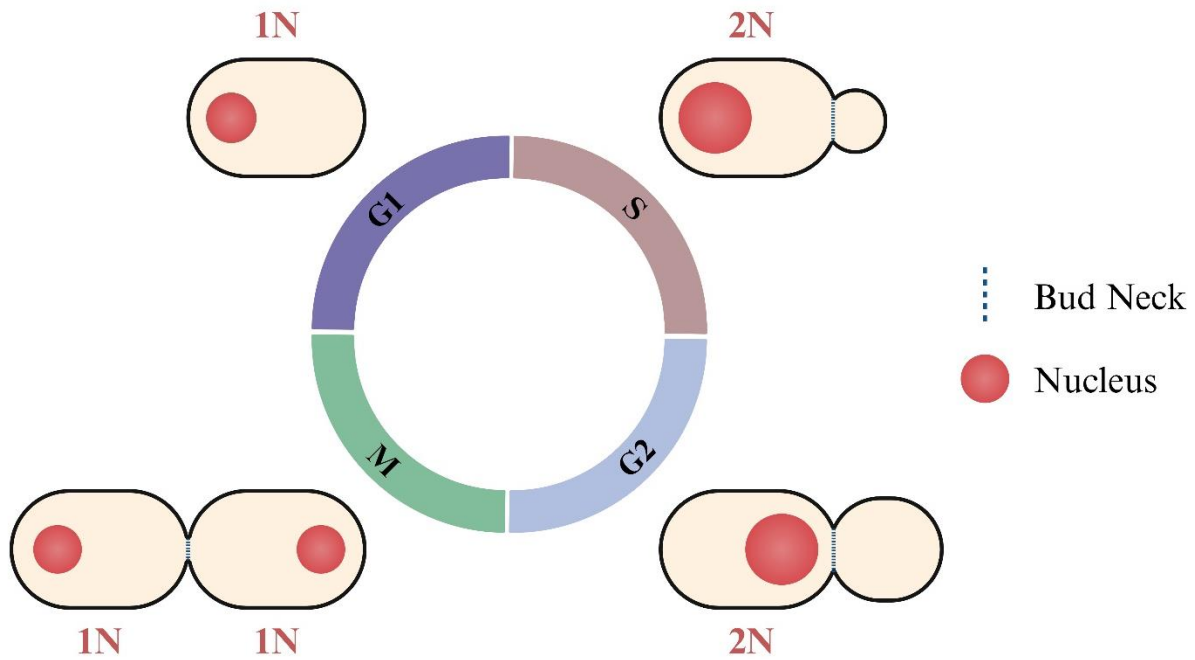


**Fig. 1.8.1 Cell Cycle of *Saccharomyces cerevisiae***

*S. cerevisiae* begin their cell cycle in the first gap (G1) phase where they exist as diploids with a 1N genomic content. They will then progress into the synthesis (S) phase where DNA replication occurs leaving the yeast with a 2N genomic content. Yeast then enter the second gap phase (G2) where daughter cell budding occurs and the nucleus moves towards the bud neck. Finally, the mitosis (M) phase occurs which separates the single 2N nucleus into two 1N nuclei and the mother and daughter cell separate along the bud neck.

## 1.9 Rationale

This thesis investigates whether a ubiquitin variant inhibitor approach can be used to mitigate the function of the bacterially encoded Novel E3 Ligase, SspH1. Despite the prevalence of NELs in pathogenic bacteria there has been little research demonstrating effective ways of targeting these proteins for inhibition. This lack of inhibitors expands to E3 ligases as a whole with there being only a single class of FDA-approved drugs which target an E3 ligase. (169) In an effort to address the absence of inhibitors, a protein-based modulation approach was pursued by Dr. Sachdev Sidhu, who developed a ubiquitin variant phage library and screening strategy to identify Ubvs with enhanced affinity to a target protein. (161,176,179) While this Ubv-based approach has led to effective modulation of the activity of HECT, RBR, RING, and Viral E3 ligases as well as DUB enzymes, it has not yet been successfully implemented in the modulation of NEL ligases.

## 1.10 Hypothesis

Given the success of a Ubv-based modulation strategy with other classes of ubiquitin interacting proteins, I hypothesized that Ubvs with an increased affinity for SspH1, a bacterially encoded E3 ligase, would be effective inhibitors both *in vitro* and *in vivo*. This hypothesis was tested by assessing the growth of yeast co-expressing SspH1 and Ubv on both liquid and solid media. Additionally, the effect of SspH1 on the yeast cell cycle was assessed by both microscopy and flow cytometry. Finally, the effect of Ubvs on SspH1 activity was assessed *in vitro* through ubiquitination assays, including probing substrate-specific ubiquitin chain formation and potential changes to the ubiquitin chain linkage conformations.

# Chapter 2: Methods

## Chapter 2.1: SspH1 Toxicity in *S. cerevisiae*

### 2.1.1 Cloning & Transformation

**Yeast Transformation:** *Saccharomyces cerevisiae* (BY4742  $\alpha$ ; APB 60) were grown overnight in a shaker at 200 rpm and 30°C in complete supplement mixture (CSM) liquid media containing 6.7 g/L complete supplement media with appropriate auxotrophic selection, 50 g/L ammonium sulfate, 17 g/L yeast nitrogen and 1% Glucose. Overnight liquid cultures were then spun down at 900 x g for 3 minutes to collect pellets. The pellets were washed with sterile ddH<sub>2</sub>O followed by 1 mL of 100 mM lithium acetate (LiAc), prior to being suspended in 400  $\mu$ L of 100 mM LiAc. Each transformation requires 50  $\mu$ L of *S. cerevisiae* cell suspension. LiAc was then removed, and reagents were added stepwise in the following order: 240  $\mu$ L of 50% (W/V) PEG 3500 (or a final W/V of 40% PEG 3500), 36  $\mu$ L of 1 M LiAc (or 120 mM), 25  $\mu$ L of boiled Salmon Sperm DNA (SSDNA), then 1  $\mu$ g (or 20 ng/ $\mu$ L) of SspH1, Ubv, PCR product or EV plasmid DNA. Reagents and cell suspension were mixed vigorously to ensure homogenization and incubated at 30°C for 30 minutes, then heat shocked at 42°C for 20 minutes. The cells were then pelleted at 900 x g for 1 minute and resuspended in 100  $\mu$ L of sterile ddH<sub>2</sub>O. Transformed cells were then plated on CSM plates lacking the appropriate amino acids for auxotrophic selection and incubated at 30°C for 48 hours. Through this process the BY4742  $\alpha$  strains APB 51, 52, 53, 173, 174, 175, 176, 185 were generated. (Table 2.1.1)

**Ubv Drag & Drop Cloning:** Yeast expression clones of  $\Delta$ DiGly, Ubv A06 and Ubv D09 were generated as described in Jansen et al. (226) In short, pGREG515 (APB 4) was digested with *SalI*, which removes the HIS3 stuffer fragment and exposes the *rec1* and *rec2* sites. *Rec1* and *rec2* overhangs were added flanking the gene of interest using PCR amplification with pDONR::Ubv A06 (APB 1), pDONR::Ubv D09 (APB 2), pDONR:: $\Delta$ DiGly (APB 3) serving as templates. Primer sequences can be found in Table 2.2. Both the digested pGREG515 vector and PCR product were co-transformed into *S. cerevisiae* for homologous recombination of the PCR fragment into the open pGREG515 backbone.

**Mutagenesis of SspH1<sup>C492A</sup>:** The active site (C492A) mutation of SspH1 was generated in the pcDNA3::2xHA-SspH1 (AB 63) background using the Quikchange II site-directed mutagenesis kit according to the manufacturer's protocol (Agilent). Briefly, primers to mutate the cysteine to alanine were generated using the Quikchange Primer Design tool (Agilent, <https://www.agilent.com/store/primerDesignProgram.jsp>). Mutagenic primers were then mixed with the pcDNA3::2xHA-SspH1 template and amplified by PCR using cycling conditions suggested by the manufacturer. Completed amplification reactions were subjected to digestion with *Dpn* I to remove parental dsDNA. All PCR products were sequence verified. The construct was then propagated into DH10B *E. coli* using standard methods. Through this process the DH10B strains AB 240 and 242 were generated. (Table 1.1.1)

**SspH1 Restriction Cloning:** Yeast expression clones of SspH1 and SspH1<sup>C492A</sup> were generated by digesting pcDNA3::2xHA-SspH1 or pcDNA::2xHA-SspH1<sup>C492A</sup> and p426GALL with *Hind*III and *Xho*I. The inserts were ligated into the digested vector and transformed into DH10B *E. coli* using standard methods. Plasmid was purified from overnight cultures of single colony inoculations and mapped by *Pst*I-digestion. Through this process the DH10B strains AB 63 and 175 were generated. (Table 1.1.1)

**Table 2.1.1 Strains Used for Cloning in Yeast Expression Studies**

| <b>Stock Name</b>  | <b>Organism</b> | <b>Strain #</b> | <b>Description or Source</b>                                    |
|--|-----------------|-----------------|---|
| pcDNA3::2xHA-SspH1   | DH10B           | <b>AB 63</b>    | (227)   |
| p426GALL::2xHA-SspH1   | DH10B           | <b>AB 175</b>   | This work – Amit Bhavsar  |
| pcDNA3::2xHA-SspH1 <sup>C492A</sup>  | DH10B           | <b>AB 240</b>   | This work – Amit Bhavsar  |
| P426GALL::2xHA-SspH1 <sup>C492A</sup>  | DH10B           | <b>AB 242</b>   | This work - Amit Bhavsar  |
| pDONR::Ubv A06   | DH5 $\alpha$    | <b>APB 1</b>    | (174,176)   |
| pDONR::Ubv D09   | DH5 $\alpha$    | <b>APB 2</b>    | (174,176)   |
| pDONR:: $\Delta$ DiGly   | DH5 $\alpha$    | <b>APB 3</b>    | (174,176)   |
| pGREG515   | DH5 $\alpha$    | <b>APB 4</b>    | (226)   |
| pGREG515:: $\Delta$ DiGly  | BY4742 $\alpha$ | <b>APB 51</b>   | This work – Ashley Wagner                                       |
| pGREG515::Ubv A06  | BY4742 $\alpha$ | <b>APB 52</b>   | This work - Ashley Wagner                                       |
| pGREG515::Ubv D09  | BY4742 $\alpha$ | <b>APB 53</b>   | This work - Ashley Wagner                                       |
| <i>Saccharomyces cerevisiae</i><br>[MAT $\alpha$ his3 $\Delta$ 1 leu2 $\Delta$ 0<br>lys2 $\Delta$ 0 ura3 $\Delta$ 0] | BY4742 $\alpha$ | <b>APB 60</b>   | Wild type BY4742 $\alpha$ yeast<br>provided by Dr. Gary Eitzen. |
| pAG426GALL::SspH1<br>+pGREG515:: $\Delta$ DiGly  | BY4742 $\alpha$ | <b>APB 173</b>  | This work - Ashley Wagner                                       |
| pAG426GALL::SspH1<br>+pGREG515::Ubv A06  | BY4742 $\alpha$ | <b>APB 174</b>  | This work - Ashley Wagner                                       |
| pAG426GALL::SspH1<br>+pGREG515::Ubv D09  | BY4742 $\alpha$ | <b>APB 175</b>  | This work - Ashley Wagner                                       |
| pAG426GALL::SspH1 <sup>C429A</sup><br>+pGREG515:: $\Delta$ DiGly   | BY4742 $\alpha$ | <b>APB 176</b>  | This work - Ashley Wagner                                       |
| pAG426GALL::SspH1<br>+pGREG515   | BY4742 $\alpha$ | <b>APB 185</b>  | This work - Ashley Wagner                                       |

**Table 2.1.2 Primers Used In Cloning**

| <b>Primer Name</b> | <b>Nucleotide Sequence</b>                                       |
|--------------------|--|
| pGREG515UbvFor     | 5'-gcgtgacataactaattacatgactcgaggctgaccaactttgtacaagaaagctggg-3' |
| pGREG515UbvRev     | 5'-gcgtgacataactaattacatgactcgaggctgaccaactttgtacaagaaagctggg-3' |
| SspH1C492AFor      | 5'-gcaacagaggcaacatcaactgcagaggaccgggtcacacatgc-3'               |
| SspH1C492ARev      | 5'-gcattgtgaccggctcctctgcagttgatgtgcctctgttc-3'                  |

### 2.1.2 *Saccharomyces cerevisiae* growth on solid media

Co-transformed yeast were grown overnight in a shaker at 200 rpm and 30°C in CSM-LEU-URA + 1% Glucose liquid media. 1 mL of liquid culture for both the inducing and non-inducing conditions was centrifuged at 17 000 x g for 2 min and then washed 3x with 500 µL sterile ddH<sub>2</sub>O. Washed cells were then resuspended in 1 mL of CSM-LEU-URA supplemented with either 1% Glucose (Non-inducing condition) or 1% Galactose (Inducing condition). Cell suspension was diluted with sterile ddH<sub>2</sub>O to obtain 1 mL of an OD<sub>600</sub> of 1. A 1:10 dilution series was then created for each sample encompassing concentrations from 10<sup>0</sup> to 10<sup>-7</sup>. Dilutions were then spotted on plates containing CSM-LEU-URA + 1% Glucose solid media or CSM-LEU-URA + 1% Galactose solid media and incubated at 30°C for 48 hours. After the 48 hour incubation period the number of yeast was enumerated at the lowest concentration where growth was seen and a toxicity index was generated using the following equation  $TI = \frac{CFU (1\% Glucose)}{CFU (1\% Galactose)}$

### 2.1.3 *Saccharomyces cerevisiae* growth in liquid media

Co-transformed yeast were grown overnight in a shaker at 200 rpm and 30°C in CSM-LEU-URA + 1% Glucose liquid media. 1 mL of liquid culture for both the inducing and non-inducing conditions was centrifuged at 17 000 x g for 2 min and then washed 3x with 500 µL sterile ddH<sub>2</sub>O. Washed cells were then resuspended in 1 mL of CSM-LEU-URA supplemented with either 1% Glucose (Non-inducing condition) or 1% Galactose (Inducing condition). Cell suspension was diluted with sterile ddH<sub>2</sub>O to obtain 1 mL of an OD<sub>600</sub> of 1. This cell suspension was then further diluted by adding 900 µl of the appropriate media with 100 µl of cell suspension to achieve a final culture of 1 mL with an OD<sub>600</sub> of 0.1. 200µl of each sample was then aliquoted in triplet into a 96-well clear, flat-bottomed plate. The samples were incubated at 30°C and the OD<sub>600</sub> of each sample was measured every 10 minutes over a period of 48 hours using a Spectramax i3x Microplate Reader. Relative growth was calculated using the following equation:

$$Relative\ Growth = \frac{AUC\ (Gal) / AUC\ (Ctrl\ Gal)}{AUC\ (Glu) / AUC\ (Ctrl\ Glu)} - 1.$$

### 2.1.4 Flow Cytometry

Co-transformed yeast was grown overnight in a shaker at 200 rpm and 30°C in CSM-LEU-URA + 1% Glucose liquid media. 2 mL subcultures were made by diluting overnight cultures to 6 x

10<sup>6</sup> cells per mL in CSM-LEU-URA + 1% Glucose liquid media. Subcultures were washed 3x in 500 µL sterile ddH<sub>2</sub>O before being resuspended in CSM-LEU-URA + 1% Galactose liquid media with 15 µg per mL of nocodazole (Biotechne; Cat # 1228), which induces G2/M arrest through microtubule depolymerization. Cultures were returned to the incubator and grown in a shaker at 200 rpm and at 30°C for 2 hours before being washed 3x in 500 µL sterile ddH<sub>2</sub>O to remove nocodazole. Washed pellets were resuspended in 2 mL CSM-LEU-URA + 1% Galactose liquid media and a 400 µL sample was taken at 0 min. Cultures were returned to the incubator and grown in a shaker at 200 rpm and 30°C for 8 hour post-nocodazole wash. 400 µL samples were centrifuged at 17 000 x g for 2 min., the supernatant was removed, and the pellet was resuspended in 500 µL cold 70% EtOH. Cells suspended in 70% EtOH were stored at 4°C. To process these cells 1.5 mL of 50 mM sodium citrate was added to the 0.5 mL 70% EtOH cell suspension then centrifuged at 400 x g for 5 min before removing 1 mL of supernatant and centrifuging again at 17 000 x g for 2 min. and removing the rest of the supernatant. Pellets were then resuspended in 0.5 mL sodium citrate containing 0.1 mg per mL RNase A and incubated at 37°C for 2 hours. Following RNase A incubation, 0.5 mL of 50mM sodium citrate containing 8 µg per mL of propidium iodide (ThermoFisher Scientific; Cat # P3566) was added to achieve a final concentration of 4 µg per mL of propidium iodide. Cells were processed by Attune NxT which recorded 100 000 events per sample. Data was analyzed with FlowJo V10.6.0. Relative amount of 2N yeast was calculated using the following equation:  $\Delta\%2N = \left( \frac{AUC_{2N} 8 Hour}{AUC_{2N} 0 Hour} - \frac{AUC_{2N} 0 Hour}{AUC_{2N} 0 Hour} \right) \times 100$ .

### 2.1.5 Microscopy

Co-transformed yeast was grown overnight in a shaker at 200 rpm and 30°C in CSM-LEU-URA + 1% Glucose liquid media. Subcultures were made by taking 1.5 mL of overnight culture, centrifuging at 17 000 x g for 2 min and then resuspended in CSM-LEU-URA supplemented with either 1% Glucose (Non-inducing) or 1% Galactose (Inducing). Subcultures with fresh media were returned to the incubator and grown for 8 hours at 30°C while shaking at 200 rpm. After 8 hours 400 µl of culture was fixed with 600 µl of 4% Paraformaldehyde (PFA) for 30-45 minutes at room temperature. The fixed culture was centrifuged at 17 000 x g for 1 min before 500 µl was removed and centrifuged at 17 000 x g for 1 min. The remainder of the supernatant

was removed, and the pellets were washed 3x in 200µl of PBS. The washed pellet is resuspended in 250 µl of 0.2% Triton X-100 prior to the addition of 5 µl of Phalloidin 488 (ThermoFisher Scientific; Cat # A123779) and overnight incubation at 4°C in the dark. Following the overnight incubation 1 µl of DAPI was added and incubated for 1 hour in the dark at room temperature. Stained cells were then centrifuged at 17 000 x g for 2 min the supernatant was removed, and pellets were washed 3x in 200 µl PBS. Washed pellets were then suspended in 5-10 µl of Vectashield (Vector Laboratories; Cat # H-1000), dependent on pellet size. 1µl of cell suspension in Vectashield was spotted onto a glass slide, covered with a round #1.5 glass coverslip, sealed with Revlon nail polish, and allowed to dry in the dark for 15 minutes prior to imaging using an EVOS FL Auto at 100x magnification. The 100x oil objective lens had a numerical aperture of 1.28. Micrographs were collected and analysis of yeast budding was performed as previously described using FIJI v.2.3.0 (60–62). Large-budded cells were defined as having a bud length equal to, or greater than, 1/3 of the mother cell. Analysis was performed by a person blinded to the protein expression plasmids but familiar with fluorescent microscopy acquisition methods.

### **2.1.6 Statistical Analysis**

All statistical comparisons were performed using Graphpad Prism 9.5.1. Data is presented as the mean with error bars representing SEM. Growth Reduction Co-efficient (GRC) for comparison of yeast growth in liquid media was calculated as described in Lauman and Dennis. (228) Statistical analyses were determined through one-way ANOVA with Tukey's multiple comparison test. Statistical significance is indicated as follows:  $P > 0.05 = \text{ns}$ ,  $P < 0.05 = *$ ,  $P < 0.01 = **$ ,  $P < 0.001 = ***$ ,  $P < 0.0001 = ****$ .

## **Chapter 2.2: Assessing SspH1 activity *in vitro***

### **2.2.1 Structure Preparation Using Homology Modelling**

Swissmodel, a homology protein modelling program, was used to create protein models for SspH1, Ubv A06, and Ubv D09. (229) Available structures of highly similar proteins, as determined by basic local alignment search tool (BLAST), were used as templates onto which the amino acid sequence of the proteins of interest were modelled. To identify highly homologous proteins for SspH1, the LRR and NEL domains were separated to increase fidelity. Since structure of the LRR domain of SspH1 has been previously determined it was not

generated by homology modelling, instead the previously determined structure was used (Uniprot ID: D0ZVG2; PDB Entry: 4NKH). Although there is no previously determined structure of the SspH1 NEL domain, the NEL domain of IpaH 9.8, a *Shigella* NEL, was identified as having a high sequence similarity (56.3%). Therefore, the NEL domain was modelled through Swissmodel individually using IpaH 9.8 (Uniprot ID: Q8VSC3; PDB Entry: 6LOL) as a template. In a similar manner, Ubv A06 and UbvD09, were modelled using human ubiquitin (Uniprot ID: P0CG48; PDB Entry: 1UBQ) as the template. Molecular graphics and analyses were performed with UCSF Chimera V1.14, developed by the Resource for Biocomputing, Visualization, and Informatics at the University of California, San Francisco, with support from NIH P41-GM103311. (230)

### **2.2.2 *In silico* Protein-Protein Interaction Predictions**

The interaction between SspH1 and the ubiquitin variants was predicted using the protein-protein docking algorithms, HDOCK and LZERD. (231–235) In short, given the structure of SspH1, as the receptor, and human ubiquitin (PDB Entry: 1UBQ), Ubv A06, or Ubv D09, as the ligand, a fast, Fourier transform (FFT) based strategy was used to sample for possible binding modes which were then evaluated through an iterative knowledge-based approach. The binding modes were then ranked based on their binding energy score and the structures of the 10 highest scoring binding modes were generated and visualized in Chimera V1.14.

### **2.2.3 Cloning**

Bacterial protein expression clones were generated using the Gateway® recombinational cloning system (Invitrogen, ThermoFisher Scientific). (236,237) In short, pDONR::Ubv D09 and pDONR::ΔDiGly served as entry clones, which were introduced into the destination vector pDEST 527 (Addgene; Plasmid #11518, Kindly donated by Dominic Esposito) through the LR reaction (LR Clonase II Enzyme Mix, ThermoFisher Scientific) and transformed into DH5α *E. coli* for propagation and storage. pDEST527::Ubv D09, and pDEST527::ΔDiGly were then propagated into BL21(DE3) *E. coli* for protein expression by standard methods.

**Table 3.3.1 Strains Used for Cloning for Protein Purification Studies**

| <b>Stock Name</b>                 | <b>Organism</b> | <b>Strain #</b> | <b>Description</b>  |
|-----------------------------------|-----------------|-----------------|---|
| pDONR::Ubv D09                    | DH5 $\alpha$    | <b>APB 2</b>    | (174,176)   |
| pDONR:: $\Delta$ DiGly            | DH5 $\alpha$    | <b>APB 3</b>    | (174,176)   |
| pDEST527                          | CB3.1           | <b>APB 293</b>  | pDest-527 was a gift from Dominic Esposito (Addgene plasmid #11518) |
| pDEST527::Ubv D09                 | DH5 $\alpha$    | <b>APB 295</b>  | This Work - Bradley Dubrule   |
| pDEST527:: $\Delta$ DiGly         | DH5 $\alpha$    | <b>APB 296</b>  | This Work - Bradley Dubrule   |
| pDEST527:: $\Delta$ DiGly         | BL21(DE3)       | <b>APB 300</b>  | This Work - Bradley Dubrule   |
| pDEST527::Ubv D09                 | BL21(DE3)       | <b>APB 302</b>  | This Work - Bradley Dubrule   |
| <i>Escherichia coli</i> BL21(DE3) | BL21(DE3)       | <b>APB 125</b>  | NEB (Cat # C2527)   |
| pGEX-PP-3xHA::SspH1               | DH10B           | <b>AB 286</b>   | This Work - Amit Bhavsar  |
| pGEX-PP-3xHA::SspH1               | BL21(DE3)       | <b>AB 287</b>   | This Work - Amit Bhavsar  |

### 2.2.4 Protein Purification

A 100 mL culture of BL21 DE3 *E. coli* containing either pDEST527 + Ubv  $\Delta$ DiGly or pDEST527 + Ubv D09 was grown overnight with shaking at 200 rpm at 37°C in lysogeny broth (LB) containing 10 g/L NaCl, 5 g/L yeast extract, 10 g/L tryptone, 15 g/L agar and 0.1 mg/mL ampicillin (Amp). The overnight culture was then diluted in 900 mL of fresh LB for a total volume of 1 L and incubated for 1 hour at 37°C. Protein expression was induced by the addition of 400  $\mu$ M of isopropyl  $\beta$ -D-1-thiogalactopyranoside (IPTG) and incubation for 4 hours at 37°C. The culture was centrifuged for 15 min at 4°C at 7 000 x g in a JLA 10.5 rotor. Pellets were pooled and resuspended in 20 mL of cold lysis buffer (200 mM NaPO<sub>4</sub> pH 7.4, 500 mM NaCl, 25 mM Imidazole, 10  $\mu$ g/mL DNase A, 1  $\mu$ g/mL RNase, 2x Pierce Protease Inhibitor Tablets (ThermoFisher Scientific; Cat #A32953)) prior to being lysed by three passages through a French pressure cell (Thermofisher Scientific; Cat #FA-032) at 1100 PSI. Lysates were then centrifuged for 15 min at 4°C at 8000 x g to remove cellular debris followed by a second centrifugation of the previous supernatant 15 min at 4°C at 30 000 x g to remove inclusion bodies. The supernatant was then filtered through a 0.45  $\mu$ m filter. Nickel-NTA affinity chromatography was performed using an AKTA GO and HisTrapFF 1 mL columns (Cytiva Life Sciences; Cat # 17525501). Elution was performed using a 20 mL gradient of imidazole from 25 mM to 500 mM that also contained 500mM NaCl, and 20 mM NaPO<sub>4</sub> pH 7.4 with 0.5 mL fractions being collected. 1 mL Fractions were collected over 20 column volumes (CV) containing Ubv D09 or  $\Delta$ DiGly were identified by SDS-PAGE and pooled. Size exclusion chromatography was performed on a Superdex 200 Increase 10/300 GL column (Cytiva Life Sciences; Cat # 28990944) using a buffer which contained 50 mM Tris pH 8.0, 100 mM NaCl, 1mM EDTA, and 1mM DTT over an elution length of 2 CV while 2 mL fractions were collected. 2 mL Fractions were collected over 1.2 CV containing His-D09 or His-DiGly were identified by SDS-PAGE and pooled. Pooled fractions were concentrated using a 5 kDa molecular weight cut off (MWCO) concentrator (Amicon Ultra; Cat #UFC900308) through centrifugation at 4 000 x g for 45 min. Higher molecular weight species were then removed using a 30 kDa MWCO concentrator (Amicon Ultra; Cat #UFC803002) by centrifugation at 4 000 x g for 45 min and the flow-through was kept. The presence of concentrated Ubv D09 and  $\Delta$ DiGly was confirmed by

SDS-PAGE and western blot. Protein concentration was determined by Pierce BCA protein assay. (ThermoFisher Scientific; Cat # 23225)

Recombinant SspH1 with tandem N-terminal GST and HA epitope tags was purified according to the procedure outlined in (238) before precision protease digestion to remove the GST tag. Briefly, 50 µg of purified GST-HA-SspH1 was mixed with 2 µg in-house purified GST-tagged precision protease and pre-equilibrated Glutathione Sepharose 4B beads (GE Healthcare) in precision protease buffer (50 mM Tris pH 7.5, 300 mM NaCl, 1 mM EDTA, 1 mM DTT). Reactions were incubated overnight to allow for protease cleavage between the GST and HA tags of SspH1 before beads were precipitated. Cleaved HA-SspH1 was recovered from the supernatant.

### **2.2.5 Mass Spectrometry**

Mass spectrometry work was performed by the Alberta Proteomics and Mass Spectrometry Facility in the Faculty of Medicine and Dentistry at the University of Alberta. Purified protein was separated on 4-20% polyacrylamide gradient gels (Bio-Rad; Cat #4561094) by electrophoresis at 175 V for 45 min. The gel was washed 3x with ddH<sub>2</sub>O and subsequently stained with Imperial protein stain (ThermoFisher Scientific; Cat #24615) for 2 hours at room temperature with shaking at 70 rpm. Staining solution was then removed and replaced with ddH<sub>2</sub>O and the gel was destained overnight at room temperature with shaking at 70 rpm. Protein bands of interest were identified and excised for further processing. Samples were reduced (10 mM β-mercaptoethanol in 100 mM ammonium bicarbonate) and alkylated (55 mM iodoacetamide in 100 mM ammonium bicarbonate). After dehydration, enough trypsin (6ng/µL, Promega Sequencing grade) was added to just cover the gel pieces and the digestion was allowed to proceed overnight (~16 hrs.) at 37°C. Tryptic peptides were first extracted from the gel using 97% H<sub>2</sub>O, 2% acetonitrile, 1% formic acid followed by a second extraction using 50% of the first extraction buffer and 50% acetonitrile.

The tryptic peptides were resolved using nano flow HPLC (Easy-nLC 1000, Thermo Scientific) coupled to an Orbitrap Q Exactive mass spectrometer (Thermo Scientific) with an EASY-Spray capillary HPLC column (ES902A, 75 µm x 25 cm, 100 Å, 2 µm, Thermo Scientific). The mass spectrometer was operated in data-dependent acquisition mode with a resolution of 35,000 and

m/z range of 300–1700. The twelve most intense multiply charged ions were sequentially fragmented by using HCD dissociation, and spectra of their fragments were recorded in the orbitrap at a resolution of 17,500. After fragmentation all precursors selected for dissociation were dynamically excluded for 30 s. Data was processed using Proteome Discoverer 1.4 (Thermo Scientific) and the database was searched using SEQUEST (Thermo Scientific). Search parameters included a strict false discovery rate (FDR) of .01, a relaxed FDR of .05, a precursor mass tolerance of 10 ppm and a fragment mass tolerance of 0.01 Da. Peptides were searched with carbamidomethyl cysteine as a static modification and oxidized methionine and deamidated glutamine and asparagine as dynamic modifications.

### **2.2.6 SspH1 Ubiquitination Assays**

0.15 µg of purified HA-SspH1 was incubated with 0.22 µg of recombinant human UBE1 (R&D Systems; Cat #E-305-025), 4.0 µg of human UBE2D2 (R&D Systems; Cat #E2-622-100 ), 1.8 µg of HA-ubiquitin (R&D Systems; Cat #U-110-01M), His-ΔDiGly, His-Ubv D09, and/or 0.41 µg GST-PKN1 (ThermoFischer Scientific; Cat #PV3790) in ubiquitination reaction buffer (80 mM Tris-HCl, 50 mM NaCl, 10 mM MgCl<sub>2</sub>, 0.1 mM DTT) before 2 mM ATP was added to initiate *in vitro* SspH1 activity. All samples were incubated for 3 hours at 37°C prior to being quenched by addition of SDS-PAGE sample buffer and boiling at 100°C for 5 minutes.

### **2.2.7 Immunoprecipitation**

Recombinant GST-PKN1 was co-incubated with purified HA-SspH1, human UBE1, human UBE2D2, and HA-ubiquitin in ubiquitination reaction buffer (80 mM Tris-HCl, 50 mM NaCl, 10 mM MgCl<sub>2</sub>, 0.1 mM DTT) and 2 mM ATP to initiate *in vitro* SspH1 ubiquitination activity. All samples were incubated for 3 hours at 37°C prior to immunoprecipitation. Immunoprecipitation was carried out using protein G-conjugated magnetic beads (New England Biolabs). Beads were prepared by washing three times with IP wash buffer (PBS + 0.1% Tween-20 (Sigma-Aldrich; Cat #P1379)), then incubated with 2 µg Rabbit α-GST polyclonal antibody (Santa Cruz Biotechnology; Cat #sc-459) for 20 minutes at room temperature with agitation. Washing steps were repeated to remove unbound antibody, then beads were blocked with 3% milk powder solution for 1 hour at 4°C. After blocking, beads were washed again, and purified protein samples were incubated with the beads for 1 hour at 4°C with agitation. Washing steps were

performed a final time followed by elution from the beads by addition of SDS-PAGE sample buffer and boiling at 100°C for 5 minutes.

### **2.2.8 Immunoblotting**

Proteins were separated on 4-20% polyacrylamide gradient gels (Bio-Rad; Cat #4561094) by electrophoresis and transferred to nitrocellulose membranes (Bio-Rad; Cat #1620115). Transfer was performed using a Trans-Blot Turbo (Biorad; Cat #1704150) set to a limit of 25 volts and a constant 2.5 amps for 14 min, in a buffer containing 48 mM Tris base (Invitrogen; Cat #15504-020), 39 mM Glycine (ThermoFisher Scientific; Cat #G7126), and 20% methanol. Membranes blocked with TBS blocking buffer (Li-Cor; Cat #927-60001) before overnight incubation with primary antibody diluted in TBS blocking buffer. Membranes were washed and incubated with secondary antibodies diluted in TBS blocking buffer for 1 hour. The antibodies used in this study are: mouse  $\alpha$ -Actin (sc-8433; Santa Cruz Biotechnology) 1: 2000; Mouse  $\alpha$ -UBE2D2 (OTI2C2; ThermoFisher Scientific) 1:2 000; mouse  $\alpha$ -Myc (9E10; Provided by Dr. Rob Ingham, University of Alberta) 1:2 500; mouse  $\alpha$ -His (27E8; Cell Signaling Technology) 1: 2 500; rabbit  $\alpha$ -K48-linkage specific polyubiquitin (D9D5; Cell Signaling Technology) 1:2 000; rabbit  $\alpha$ -63-linkage specific polyubiquitin (D7A11; Cell Signaling Technology) 1:2 000; mouse  $\alpha$ -Ubiquitin (P4D1; Cell Signaling Technology) 1:2 000; rat  $\alpha$ -HA (3F10; Roche Diagnostics) 1:2 500; rabbit  $\alpha$ -GST (sc-459; Santa Cruz Biotechnology) 1:2 500; goat  $\alpha$ -mouse (926-68020; Licor) 1:5 000; goat  $\alpha$ -rabbit (925-32211; Licor) 1:5 000; goat  $\alpha$ -rat (926-32219; Licor) 1:5 000. Blots were imaged with a Li-Cor Odyssey and analyzed using Image Studio Lite V5.2.

### **2.2.9 Coomassie Brilliant Blue Protein Staining**

Proteins were separated on polyacrylamide gels by electrophoresis and subsequently stained with 1x Coomassie Brilliant Blue R-250 solution (0.1% Coomassie brilliant blue R-250, 10% Acetic acid, 40% ddH<sub>2</sub>O, 50% MeOH) (Bio-Rad; Cat #1610400) in the dark for 45 min at room temperature with shaking at 70rpm. Stained gels were then rinsed 2x with destain solution (10% Acetic acid, 40% ddH<sub>2</sub>O, 50% MeOH) prior to being covered in destain solution and allowed to destain overnight in the dark at room temperature with shaking at 70rpm. The destaining solution was then discarded and gels were imaged using a Bio-Rad Gel Doc XR+ Gel Imager (Bio-Rad).

### **2.2.10 Statistical Analysis**

All statistical comparisons were performed using Graphpad Prims 9.5.1. Data is presented as the mean with error bars representing SEM. Statistical analyses were determined through one-way ANOVA with Tukey's multiple comparison test or unpaired t-test. Statistical significance is indicated as follows:  $P > 0.05 = \text{ns}$ ,  $P < 0.05 = *$ ,  $P < 0.01 = **$ ,  $P < 0.001 = ***$ ,  $P < 0.0001 = ****$ .

## Chapter 3: Results

### 3.1 Identifying Ubiquitin Variant Inhibitors of SspH1

The ubiquitin variant library described by Ernst et al. was screened for high-affinity binders of SspH1 in collaboration with Dr. Wei Zhang. (174) This library contains over  $6.8 \times 10^{10}$  unique ubiquitin variants that were generated using a soft-randomization strategy which diversified 24 positions within ubiquitin while also ensuring protein stability. GST-SspH1 was immobilized and subjected to multiple rounds of phage display selection. Through this process, Dr. Zhang identified Two Ubvs that bound to SspH1 with an increased affinity relative to wildtype ubiquitin (Fig. 3.1.1A) (176,179). *In silico* protein-protein interaction predictions indicated that either Ubv was likely to have a higher binding affinity to SspH1 than human ubiquitin (Fig. 3.1.2). Sequence alignment revealed 12 amino acid differences between human ubiquitin and either ubiquitin variants, but only 2 amino acid differences between Ubv A06 and Ubv D09 (Fig. 3.1.1B, C). I used homology modelling to predict protein structures for Ubv A06 and D09, which were then visualized using UCSF Chimera to compare the spatial positioning of the altered amino acids between human ubiquitin and the ubiquitin variants (Fig 3.1.2C). (229,230) The selected UbVs had mutations mainly found in the Isoleucine 44 recognition patch of ubiquitin, which is a known interface in E2-E3 ubiquitin transfer, as well as in the C-terminal tail. (34,121) Predictive and comparative structural modeling done with Alphafold Multimer revealed two predicted wildtype ubiquitin binding sites on SspH1, one within the active site and a second along the C-terminal thumb domain which is known to be the E2 interacting motif (Fig. 3.1.1D). (239) Ubv A06 and D09 were also predicted to bind within these pockets suggesting the mutations do not vastly change the structural relationship between the Ubv and SspH1, which is notable since the Ile 44 patch is predicted to be the primary interaction face between the Ubv and SspH1. Collectively, these results suggest that Ubv A06 and Ubv D09 may have improved binding to SspH1 binding compared to human ubiquitin.

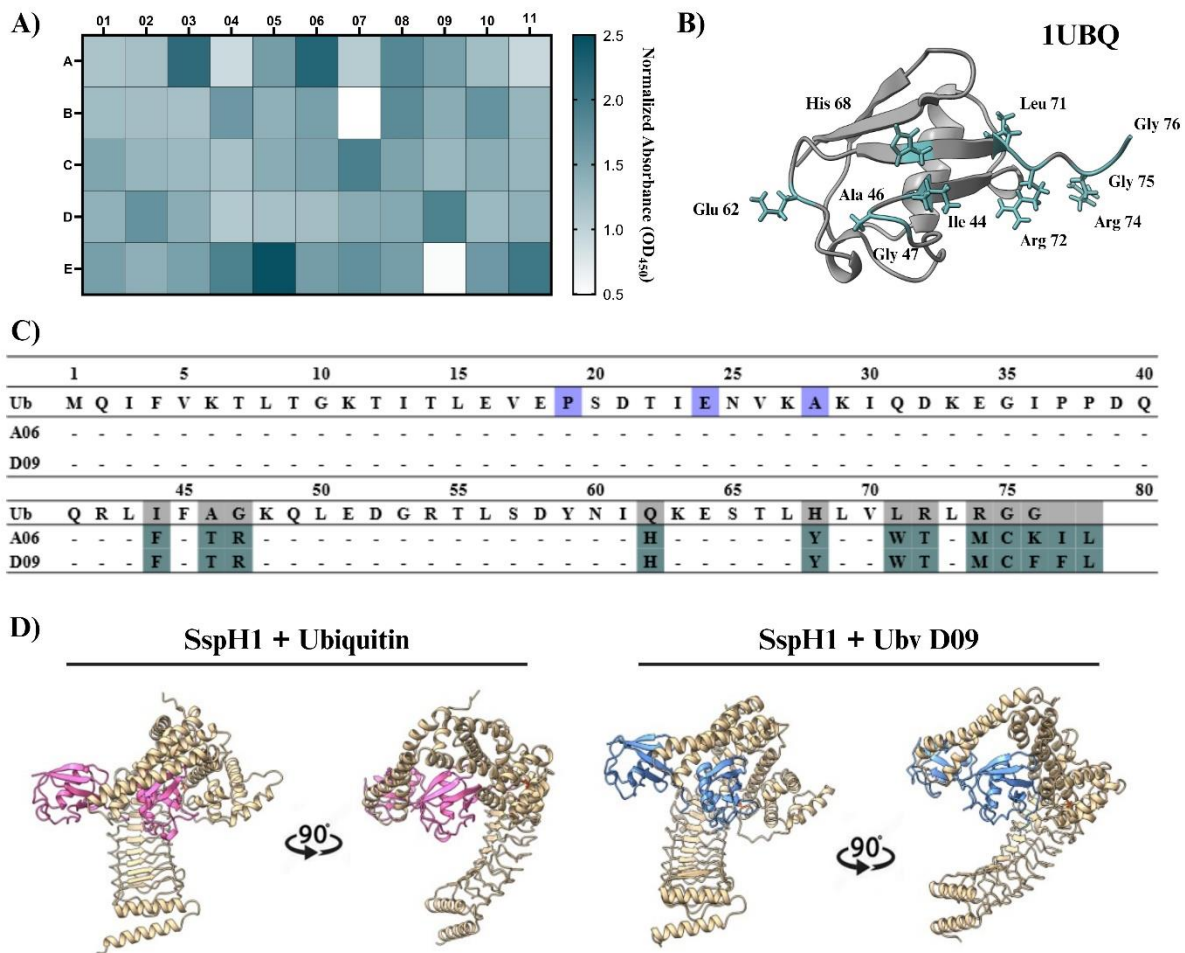


**Fig. 3.1.1 Ubiquitin Variants may act as Enhanced Binders of SspH1**

(A) The binding specificities of phage displayed Ubvs as assessed by phage ELISA.

Subsaturating concentrations of phage were added to immobilized proteins as indicated. Bound phages were detected by the addition of anti-M13-HRP and colorimetric development of TMB peroxidase substrate. The mean value of the absorbance at 450 nm is indicated by color. Variant labels were based on the letter and number indicated along the y- and x-axis, respectively. (B) Structural depiction of human ubiquitin (1UBQ) with the mutated residues highlighted and the wildtype side chains shown. (C) Sequences of Ubvs that bind with a high affinity to SspH1. Amino acids differences between human ubiquitin, ubiquitin variant A06 and ubiquitin variant D09 are highlighted in green. Amino acid differences between human ubiquitin and *S. cerevisiae* ubiquitin are highlighted in purple. (D) AlphaFold multimer predictions of SspH1 interacting

with human ubiquitin, in pink, or ubiquitin variant D09, in blue. The catalytic residue of SspH1, Cys 492, is highlighted in orange. The thumb region is located at C-terminus of NEL domain.

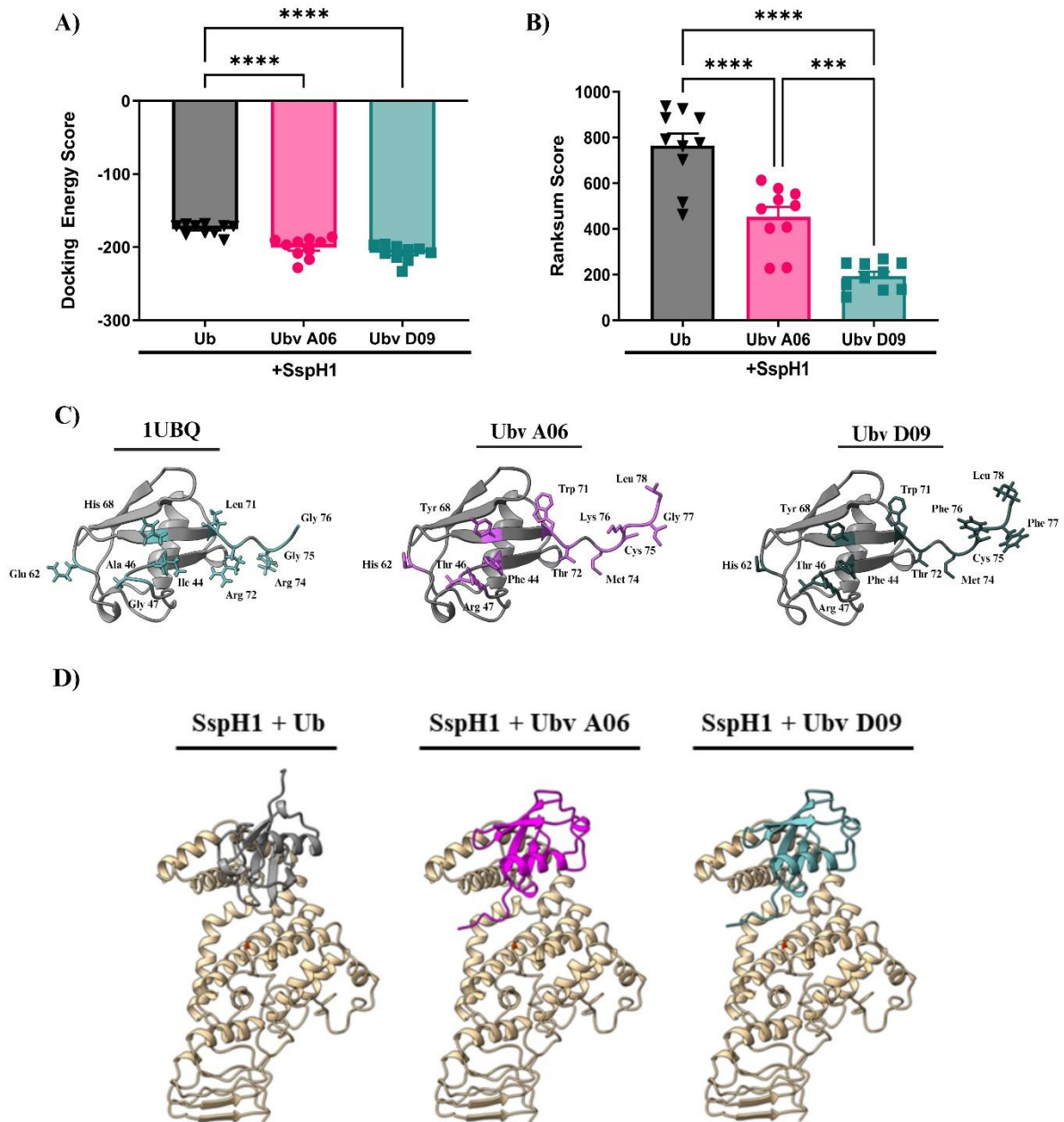


**Fig. 3.1.2 Ubiquitin Variants have a Higher Predicted Binding Affinity for SspH1**

(A) Predicted docking energy score of SspH1 binding to human ubiquitin (Ub), Ubv A06 and Ubv D09 generated with the HDock protein-protein docking server ([hdock.phys.hust.edu.cn](http://hdock.phys.hust.edu.cn)). (231,235) Docking energy score indicates the likelihood of the binding model occurring, with a

more negative score indicating a more favorable interaction. Quantification of the 10 most favorable conformations for each pair of bound proteins are depicted with error bars representing the standard error of the mean. Data was analyzed by one-way ANOVA using Tukey's multiple comparisons test. **(B)** Predicted Ranksum score of SspH1 binding to human ubiquitin (Ub), Ubv A06 and Ubv D09 generated with the LZERD protein docking web server ([lzerd.kiharalab.org](http://lzerd.kiharalab.org)). (232–234) Ranksum score is an aggregate of previously described statistical descriptors of binding (GOAP, DFIRE, ITScore) with a lower score indicating a more likely binding interaction. Quantification of the 10 most favorable conformations for each pair of bound proteins are depicted with error bars representing the standard error of the mean. Data was analyzed by one-way ANOVA using Tukey's multiple comparisons test. **(C)** Structural comparison of human ubiquitin (1UBQ) with Ubiquitin variant A06 and Ubiquitin variant D09. Ubiquitin variants were generated through homology modelling with Swissmodel, mutated amino acids have been highlighted and side chains have been shown. **(D)** Graphical depiction of lowest docking energy score SspH1-Ub, SspH1-Ubv A06 and SspH1-Ubv D09 binding conformation visualized with ChimeraX (V1.2.5) Data was analyzed using Tukey's multiple comparisons test.

### 3.2 Ubv A06 & Ubv D09 Suppress SspH1-Mediated Toxicity in Yeast

Yeast are a robust eukaryotic model, have well-developed genetic tools to enable heterologous expression studies, *e.g.* inducible GAL promoter system for controlled gene expression, and contain all the necessary components of the ubiquitin system. (214,240) I took advantage of the GAL expression system to heterologously express SspH1, its catalytic variant and 3 ubiquitin variants- Ubv A06, D09 and a human ubiquitin construct lacking the final diglycine motif at the C-terminus ( $\Delta$ DiGly). I chose to study the functional interaction of SspH1 and Ubvs in a yeast model system because it has been previously shown that catalytically active SspH1 is toxic to yeast. (120) Yeast ubiquitin differs from human ubiquitin at three locations, S19, D24 and S28, none of which are mutated in either Ubv (Fig. 3.1.1B). (241) I confirmed that all proteins were expressed under our assay conditions (Fig. 3.2.1A). To first determine if expression of either Ubv A06 or D09 was detrimental to yeast growth, I expressed each Ubv individually and monitored yeast growth in both liquid and solid media over a 48 hour period. Growth in liquid media was quantified using the relative growth equation described in Lauman and Dennis. (228) I observed similar growth of yeast expressing Ubv A06 and Ubv D09 compared to the non-inducing condition in both solid and liquid media, indicating that Ubv expression alone does not confer toxicity by interfering with the endogenous ubiquitin-proteasome-system (Fig. 3.2.1B-E).

Having determined that the ubiquitin variants have no detrimental effect on yeast growth when expressed alone, I next sought to determine if Ubv co-expression would have any functional consequences on SspH1. To accomplish this I monitored if co-expression of Ubv A06 or Ubv D09 altered, SspH1-mediated toxicity in yeast. (119) As expected, in the presence of SspH1<sup>C492A</sup> +  $\Delta$ DiGly there is no observable difference in relative growth of yeast in liquid media since SspH1 toxicity in yeast requires its E3 ubiquitin ligase activity (Fig. 3.2.2A,B). (118,119,129) Following the expression of SspH1 + Ev or SspH1 + Ubv  $\Delta$ DiGly in liquid media I observed a significant decrease, ~20% and ~40% respectively, relative to yeast grown in the presence of SspH1<sup>C492A</sup> (Fig. 3.2.2A,B). This is consistent with the previously reported effect of SspH1 expression in yeast. (119) By contrast, co-expression of SspH1 with Ubv A06 or Ubv D09 led to no significant difference in relative growth when compared to yeast grown in the presence of SspH1<sup>C492A</sup> (Fig. 3.2.2A,B).

Interestingly, similar assays on solid media showed that Ubv A06 and D09 only partially suppressed SspH1 toxicity. As expected, I observed a lack of yeast toxicity in the presence of SspH1<sup>C492A</sup> + ΔDiGly, as well as, a robust level (~1000-fold) of toxicity in the presence of SspH1 + ΔDiGly (Fig. 3.2.2C,D). (119) This toxicity was decreased 20-fold when SspH1 was expressed alongside Ubv A06 or alongside Ubv D09 in comparison to SspH1 + ΔDiGly. However, unlike in liquid medium, co-expression of SspH1 + Ubv A06 or D09 showed ~50 fold higher toxicity than yeast co-expressing SspH1<sup>C492A</sup> + ΔDiGly on solid medium (Fig. 3.2.2C,D) Taken together, these results indicate that the presence of Ubv A06 and Ubv D09 is sufficient to suppress the SspH1-mediated toxicity of yeast growth.

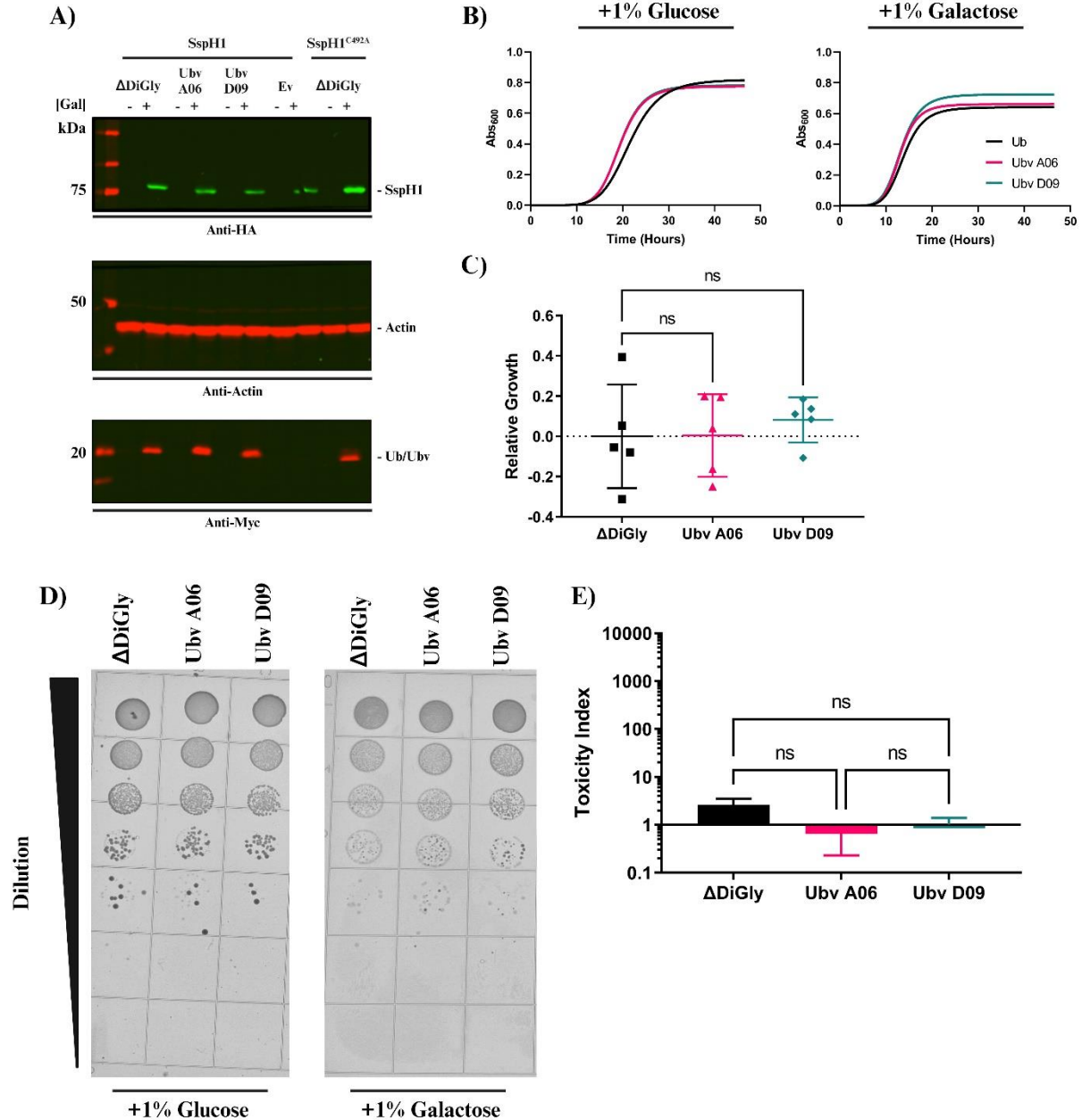


**Fig. 3.2.1. Ubv A06 & D09 are not Toxic to Yeast when Expressed Alone**

**(A)** Expression of SspH1 or SspH1<sup>C492A</sup> and Ubv ΔDiGly, Ubv A06 or Ubv D09 in BY4742α yeast strain co-transformed with galactose-inducible vectors (pGREG515). SspH1 was detected through the use of anti-HA staining whereas Ubvs were detected through anti-Myc staining **(B)** Growth of BY4742α yeast strain transformed with galactose-inducible Ubv ΔDiGly, Ubv A06 or

Ubv D09. Strains were grown overnight in 1% glucose then washed and diluted in 1% galactose or 1% glucose, as indicated, for 48 hours at 30°C in a 96-well plate. Growth was monitored by measuring the Abs<sub>600</sub> every 10 mins for the duration of the 48-hour growth period. **(C)**

Quantification of strain growth using relative growth, where the area under the curve (AUC) for each strain was calculated and compared to the control (Ubv ΔDiGly) in both the inducing and non-inducing conditions. Errors bars represent the standard error of the mean across 5 independent replicates. Relative growth calculated as described in methods. Data was analyzed by one-way ANOVA using Tukey's multiple comparisons test. **(D)** Viability of BY4742α yeast strain transformed with galactose-inducible Ubv ΔDiGly, Ubv A06 or Ubv D09. Strains were spotted as a serial dilution series on 1% galactose or 1% glucose, as indicated, and imaged after 48 hours. **(E)** Quantification of survival on solid media by toxicity index. Errors bars represent the standard error of the mean across 3 independent replicates. Toxicity Index calculated as described in methods. Data was analyzed by one-way ANOVA using Tukey's multiple comparisons test.

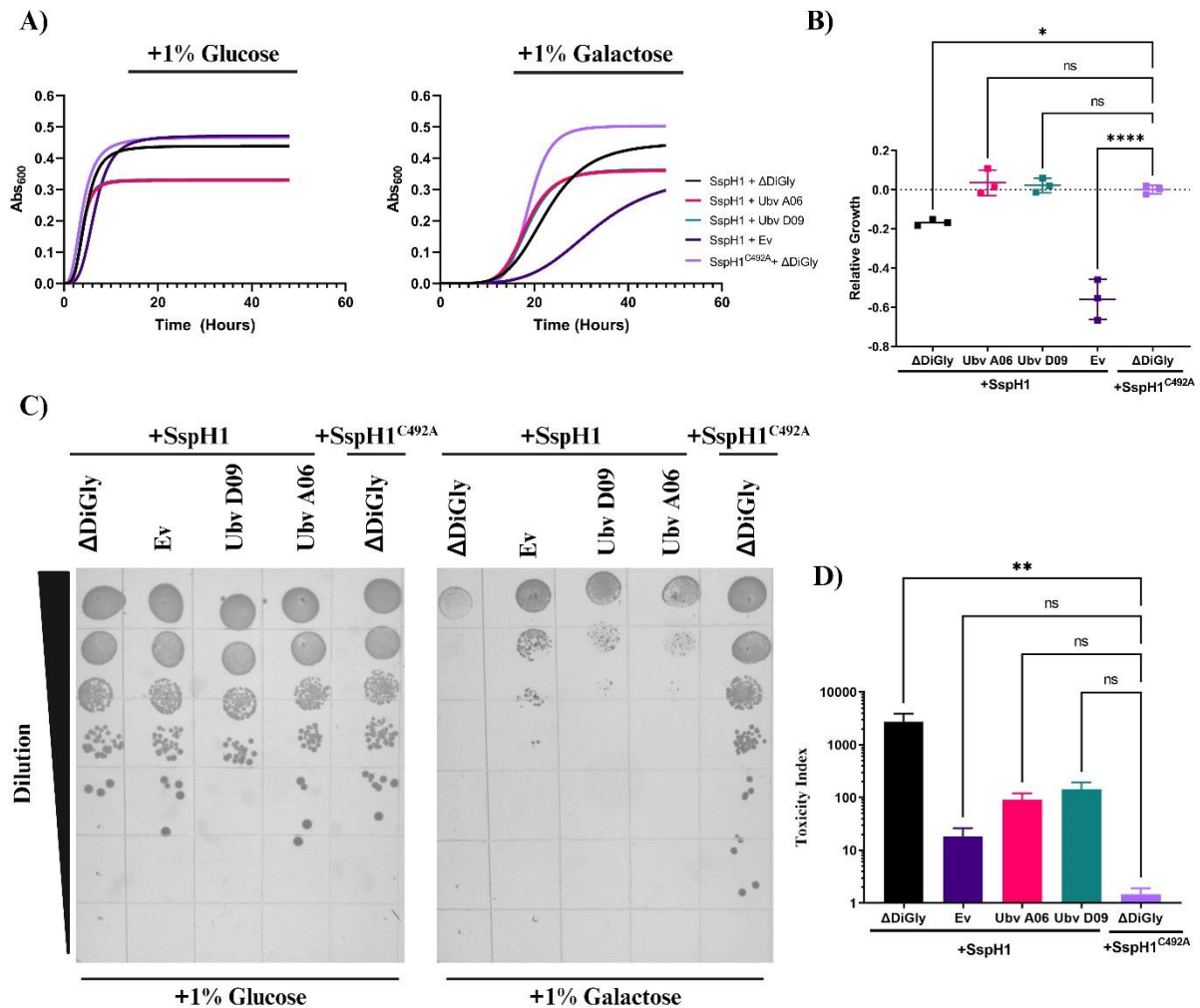


**Fig. 3.2.2. Ubv A06 & D09 Suppress SspH1-Mediated Toxicity in Yeast**

(A) Growth of BY4742 $\alpha$  yeast strain co-transformed with galactose-inducible SspH1 or SspH1<sup>C492A</sup> and Ubv  $\Delta$ DiGly, Ubv A06 or Ubv D09. Strains were grown overnight in 1% glucose then washed and diluted in 1% galactose or 1% glucose, as indicated, for 48 hours at 30°C in a 96-well plate. Growth was monitored by measuring the Abs<sub>600</sub> every 10 mins for the duration of the 48-hour growth period. (B) Quantification of strain growth using relative growth, where the area under the curve (AUC) for each strain was calculated and compared to the control (SspH1<sup>C492A</sup> + Ubv  $\Delta$ DiGly) in both the inducing and non-inducing conditions. Errors bars represent the standard error of the mean across 5 independent replicates. Relative growth

calculated as described in methods. Data was analyzed by one-way ANOVA using Tukey's multiple comparisons test. **(C)** Viability of BY4742 $\alpha$  yeast strain transformed with galactose-inducible SspH1 or SspH1<sup>C492A</sup> and Ubv  $\Delta$ DiGly, Ubv A06 or Ubv D09. Strains were spotted as a serial dilution series on 1% galactose or 1% glucose, as indicated, and imaged after 48 hours. **(D)** Quantification of survival on solid media by toxicity index. Errors bars represent the standard error of the mean across 3 independent replicates. Toxicity Index calculated as described in methods. Data was analyzed by one-way ANOVA using Tukey's multiple comparisons test.

### 3.3 Ubv A06 & D09 Suppress SspH1 Mediated Cell Cycle Arrest in Yeast

To further elucidate the effect of ubiquitin variants on SspH1, I used flow cytometry and microscopy to examine perturbations in the yeast cell cycle caused by SspH1 expression. (209,214,242) Yeast had their nuclei stained with DAPI and both brightfield and fluorescent images were acquired. Direct observation of yeast co-expressing SspH1 +  $\Delta$ DiGly revealed a high proportion of large-budded cells within the population that was significantly reduced in yeast co-expressing SspH1<sup>C492A</sup> +  $\Delta$ DiGly (Fig. 3.3.1). A similarly high proportion of large-budded cells was also observed in yeast co-expressing SspH1 + Ev (Fig. 3.3.1 A,B). This large-budded phenotype suggested that yeast toxicity may be caused by cell cycle interference leading to issues progressing through the G2/M phase. (243) Notably, the proportion of large-budded yeast was significantly reduced when SspH1 was expressed alongside Ubv A06 or Ubv D09 relative to when SspH1 was expressed alongside  $\Delta$ DiGly or alone (Fig. 3.3.1).

Since cell cycle dysregulation was implicated in SspH1-mediated toxicity in yeast, I further interrogated cell cycle dynamics through flow cytometric analyses of cellular DNA content (sFig 2.1, sTable 2). (244) Yeast were arrested in the G2/M phase of the cell cycle through treatment with nocodazole then released by being placed in fresh media. Escape from this arrest was measured by quantifying the proportion of yeast with 2N DNA content. (245,246) Consistent with our previous observation in the growth assays, I observed a substantial decrease (~10-20%) in the proportion of yeast with 2N DNA content after 8 hours in yeast expressing  $\Delta$ DiGly, Ubv A06, or Ubv D09 (Fig. 3.3.2A,B). This suggests that the ubiquitin variants alone are not contributing to the cell cycle interference phenotype. Similarly, in yeast expressing SspH1<sup>C492A</sup> +  $\Delta$ DiGly, I also observed a ~20% decrease in yeast with 2N DNA content after 8 hour, suggesting progression through the cell cycle had resumed (Fig. 3.3.2C,D). In yeast expressing SspH1 + Ev, I only observed a ~5% decrease in the proportion of yeast with 2N DNA content while in yeast expressing SspH1 +  $\Delta$ DiGly I observed a ~5% increase in the proportion of yeast with 2N DNA content relative to the proportion of yeast with 2N DNA that were detected immediately after nocodazole treatment (Fig. 3.3.2C,D). ). These results suggest that the presence of SspH1 prevents progression through the G2/M phase of the cell cycle. By contrast, co-expression of either Ubv suppressed SspH1-mediated interference, allowing for progression through the cell cycle (Fig. 3.3.2C,D).

Together these results suggest that SspH1-mediated toxicity may be caused by cell cycle interference, specifically the inability to progress through the G2/M phase of yeast budding. These results also suggest that ubiquitin variants A06 or D09 are sufficient to suppress the SspH1-mediated interference of cell cycle progression.

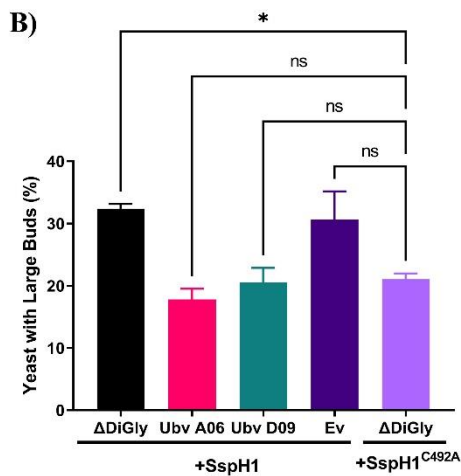
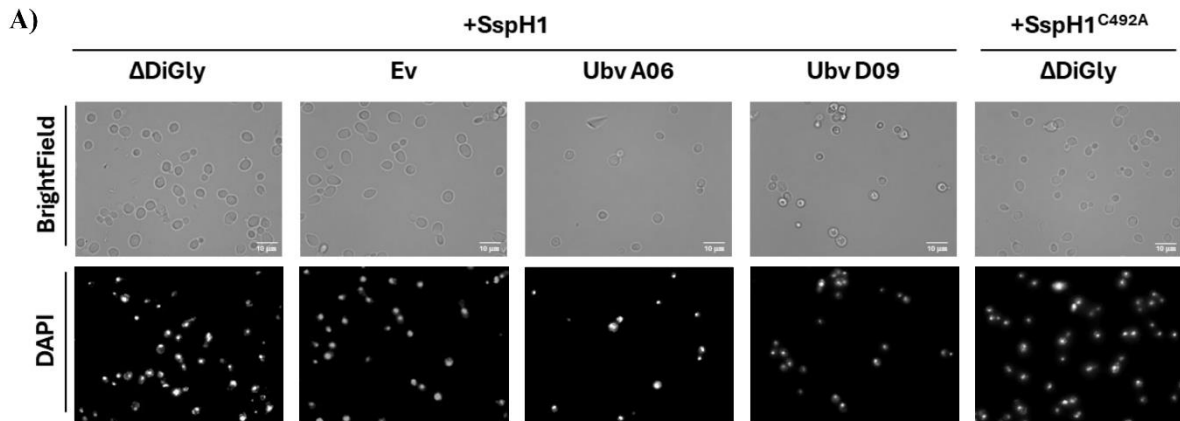


**Fig. 3.3.1 Ubv A06 & D09 Suppress SspH1-Mediated Arrest at the Large Budded Stage in Yeast**

(A) Representative micrographs of yeast co-expressing SspH1 + ΔDiGly, Ubv A06, Ubv D09 or Ev, as well as SspH1<sup>C492A</sup> + ΔDiGly are shown after 8 hours of incubation at 30°C in fresh 1% galactose. Images were collected on an EVOS FL Auto at 100x magnification. DNA was stained in blue using 4',6-diamidino-2-phenylindole (DAPI). (B) Quantification of large, budded yeast was performed as previously described using FIJI v.2.3.0 (<https://fiji.sc/>). (60–62) (Ex. Large budded = >1/3 mother cell size). Data was analyzed by one-way ANOVA using Dunnett's multiple comparisons test.

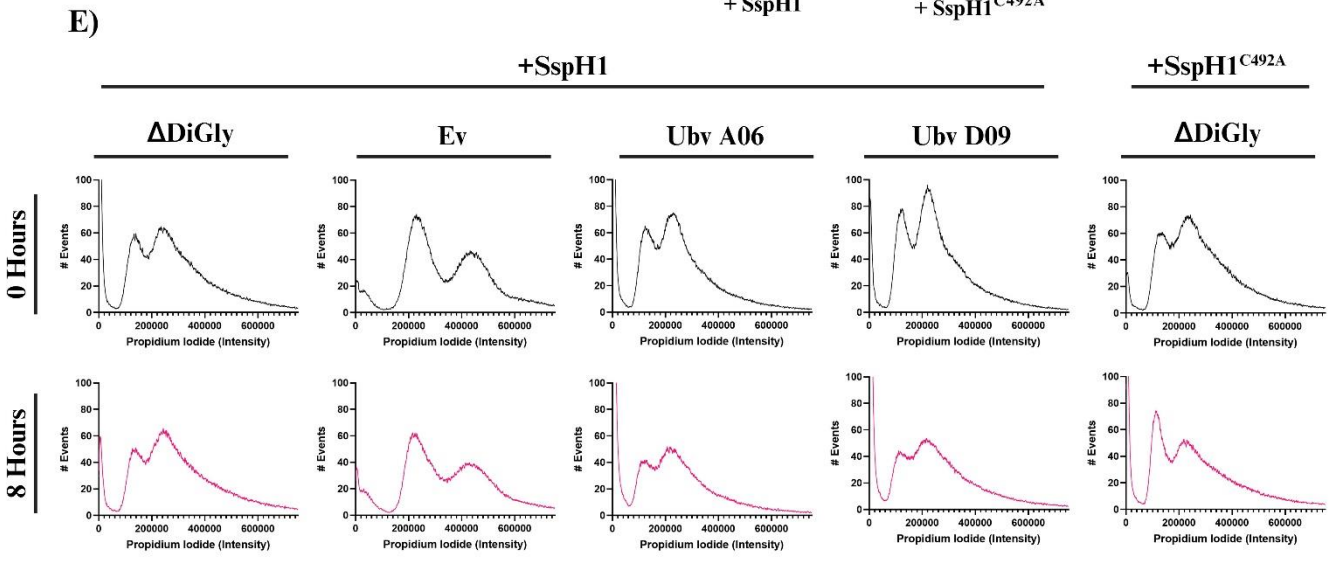
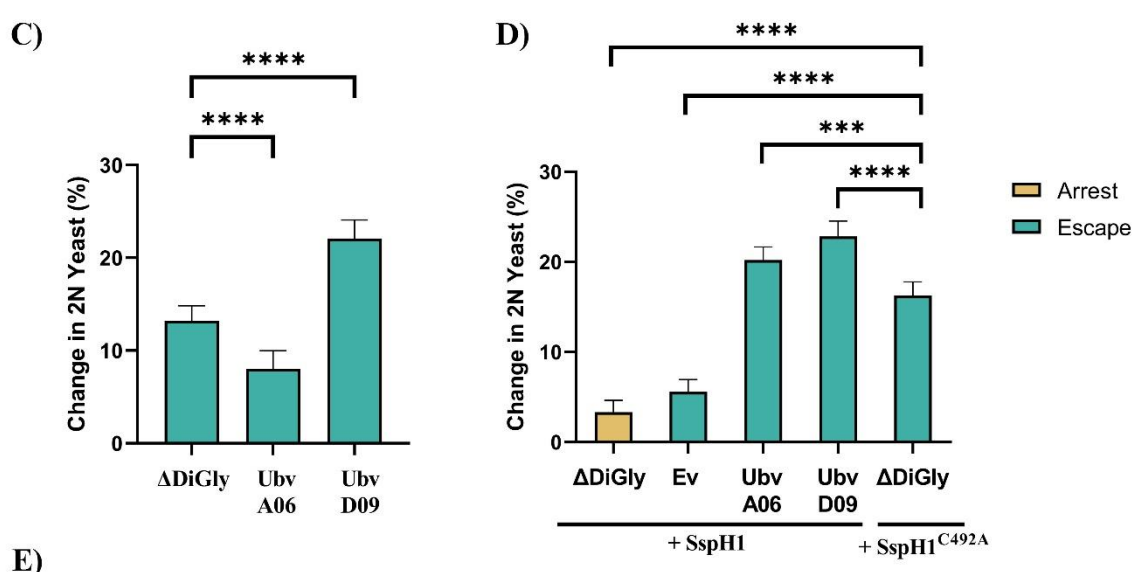
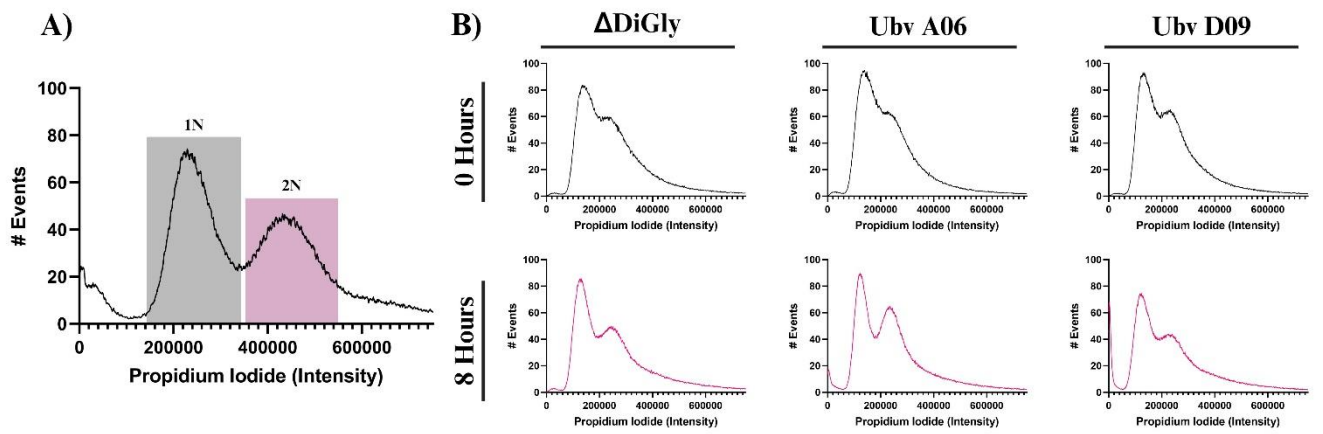


### **Fig. 3.3.2 Ubv A06 & D09 Suppress SspH1-Mediated Cell Cycle Arrest in Yeast**

**(A)** Example of regions used to calculate AUC for yeast with 1N (G1) and 2N (G2/M) DNA content **(B)** Cell cycle analysis of BY4742 $\alpha$  yeast strain transformed with galactose-inducible Ubv  $\Delta$ DiGly, Ubv A06, or Ubv D09. Cell cycles were synchronized at the G2/M phase through treatment with 20  $\mu$ M nocodazole for 3 hours at 30°C than washed multiple times to allow yeast to progress through cell cycle. Yeast were placed into fresh 1% galactose and incubated at 30°C for 8 hours prior to being fixed and having their DNA content stained with propidium iodide (PI). A 0 hour sample was also obtained immediately following the removal of nocodazole. **(C, D)** Quantification of the relative change of yeast arrested with 2N DNA content was calculated as the area under the curve (AUC) of the 2N peak at 8 hours relative to the AUC of the 2N peak 0 hours after nocodazole release as described in the methods. Data are shown as mean  $\pm$  SEM of N=11 replicates **(C)** or N=5 replicates **(D)**. Data was analyzed by one-way ANOVA using Dunnett's multiple comparisons test. **(E)** Cell cycle analysis as described above of BY4742 $\alpha$  yeast strain co-transformed with galactose-inducible SspH1 or SspH1<sup>C492A</sup> and Ubv  $\Delta$ DiGly, Ubv A06, Ubv D09 or Empty Vector (Ev).

### 3.4 Ubiquitin variants alter SspH1's E3 ubiquitin ligase activity *in vitro*

Since SspH1 toxicity phenotypes in yeast were not observed with a catalytic mutant, its E3 ubiquitin ligase activity is likely involved. Accordingly, I next investigated the effect of Ubv D09 on SspH1 E3 ubiquitin ligase activity. I performed *in vitro* ubiquitination assays with recombinant purified proteins as previously described, except with the addition of purified Ubv D09 or Ubv  $\Delta$ DiGly (Fig. 3.4.1). (113,119,121) In this assay, SspH1 activity is assessed by the presence and intensity of high molecular weight ubiquitin chains which form in the presence of E1 and E2 enzymes, as well as ATP. As expected, I did not observe any high molecular weight His-ubiquitin chains when SspH1 was provided Ubv D09 as the sole ubiquitin source, since it lacks the Diglycine motif at the C-terminus (Fig. 3.4.2A). (4) Additionally, I did not observe any high molecular weight His-ubiquitin chains when SspH1 was provided both HA-ubiquitin and Ubv D09, indicating that Ubv D09 is not incorporated into any ubiquitin chains (Fig. 3.4.2A). However, high molecular weight HA-ubiquitinated species were readily observed, suggesting that the presence of Ubv D09 does not abrogate SspH1's ability to form ubiquitin chains *in vitro* (Fig. 3.4.2B). When SspH1 activity was assessed in the presence of  $\Delta$ DiGly I observed a slight, non-significant decrease in the amount of high molecular weight HA-ubiquitinated species when compared to SspH1 activity in the presence of only HA-ubiquitin (Fig. 3.4.2C,D). Surprisingly, in the presence of Ubv D09, I observe a significant, ~2.5 fold increase in the amount high molecular weight HA-ubiquitinated species relative to HA-ubiquitin alone (Fig. 3.4.2C,D). To ensure that the change in SspH1 activity I observed was due to the presence of Ubv D09 and not an unidentified contaminant, I performed mass spectrometry on the purified Ubv D09. This analysis indicates that the primary protein present in our recombinant purification were ubiquitin species, which is most likely Ubv D09, suggesting the changes we see in SspH1 activity are not due to the presence of an unidentified contaminant (sFig 1.1). However, this does not eliminate the possibility that the impurities in the purification are due to Ubv D09 aggregate formation or dimerization mediated by the C75 residue. To fully address this possibility a technique such as differential light scattering would need to be employed to ensure a consistent particle size is observed. Together, these results indicate that while Ubv D09 is not used as a substrate by SspH1, it can potentiate SspH1-mediated formation of HA-ubiquitin chains.

Given that Ubv D09 appeared to potentiate SspH1 activity, I tested if the presence of Ubv D09 alters the ubiquitination pattern of PKN1, a known SspH1 substrate. (120,138) To do this, I conducted *in vitro* ubiquitination assays, as outlined above, in the presence of PKN1 and isolated PKN1 by immunoprecipitation. As expected, in the absence of SspH1, I did not observe an upwards shift in molecular weight for PKN1, indicating a lack of PKN1 ubiquitination (Fig. 3.4.3A,B). In the presence of SspH1, I observed the formation of high molecular weight species which correspond to ubiquitinated PKN1, confirming that SspH1 was capable of ubiquitinated PKN1 *in vitro* (Fig. 3.4.3A, B). (113) I observed no significant change in the relative amount of ubiquitinated PKN1 upon addition of Ubv  $\Delta$ DiGly (Fig. 3.4.3A,B). It is interesting to note the decrease in SspH1 activity I observed when  $\Delta$ DiGly was added in the absence of PKN1 was not observed when the substrate was present. Again surprisingly, but consistent with our previous results, the addition of Ubv D09 led to a significant  $\sim$ 2-fold increase in the amount of ubiquitinated PKN1. (Fig. 3.4.3A,B) Together these results suggest that Ubv D09 has a potentiating effect on the ability of SspH1 to ubiquitinate a known substrate, PKN1, *in vitro*.

The suppressive effect of Ubv D09 on SspH1 toxicity in yeast led us to hypothesize that SspH1 E3 ubiquitin ligase activity was compromised, but our recombinant protein studies suggested this was not the case. To reconcile these observations, I assessed any potential differences in ubiquitin linkage which could impact substrate fate in the cell. Accordingly, I performed the previously described ubiquitination reactions followed by an immunoprecipitation to isolate PKN1 then probed with antibodies specific for K48- and K63-linked ubiquitin chains, as well as global ubiquitin antibody, to uncover the relative amount of K48- and K63-linked ubiquitin chains that were present on PKN1. (247) In the absence of SspH1 or PKN1 there was no observable K48-, K63- or non-lysine specific ubiquitin chain formation. (Fig. 3.4.3C) (120) When both SspH1 and PKN1 were present I observed PKN1-specific ubiquitin chain formation with  $\sim$ 75% of the total ubiquitin chains being K48-linked. (Fig. 3.4.3C,D). (42) The addition of Ubv D09 led to an increase in the overall amount of ubiquitination I detected, which was consistent with our previous experiments (Fig. 3.4.3C,D). Interestingly, I also observed a small but significant decrease in the amount of K48 specific ubiquitin chains in the presence of Ubv D09, which accounted for only  $\sim$ 65% of the total ubiquitin chains, representing a 13% decrease in the relative amount of PKN1-specific K48 ubiquitin chains in the presence of HA-ubiquitin alone. (Fig. 3.4.3C,D) I did not observe the formation of K63-linked ubiquitin chains in the

presence of HA-ubiquitin or HA-ubiquitin + Ubv D09. (Fig. 3.4.4) Taken together these results suggest that, although the presence of Ubv D09 leads to an overall increase in PKN1 ubiquitination, it may interfere with SspH1 ability to form K48-linked ubiquitin chains.

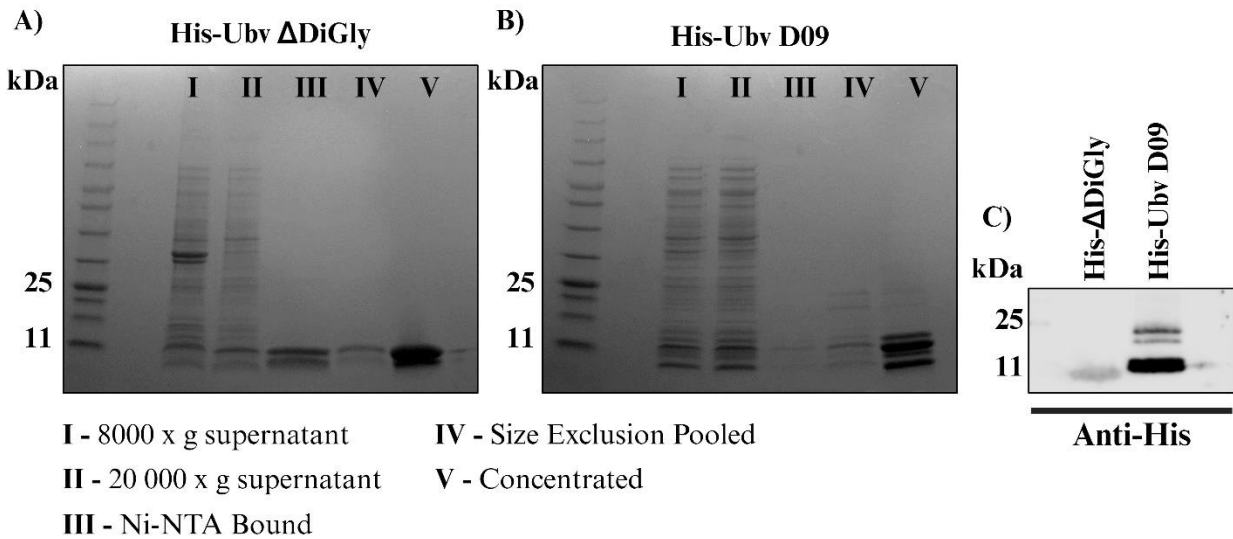


**Fig. 3.4.1 Purification of  $\Delta$ DiGly and Ubv D09**

**(A)** Purification of  $\Delta$ DiGly ubiquitin. Lanes are as indicated: A-8 000 x g Supernatant; B-20 000 x g Supernatant; C-Ni-NTA Bound; D-Pooled Size Exclusion Fractions; E-Concentrated Purified Protein. **(B)** Purification of Ubv D09. Lanes are as indicated: A-8 000 x g Supernatant; B-20 000 x g Supernatant; C-Ni-NTA Bound; D-Pooled Size Exclusion Fractions; E-Concentrated Purified Protein. **(C)** Purified  $\Delta$ DiGly ubiquitin and Ubv D09 were assessed through western blot using an anti-His antibody

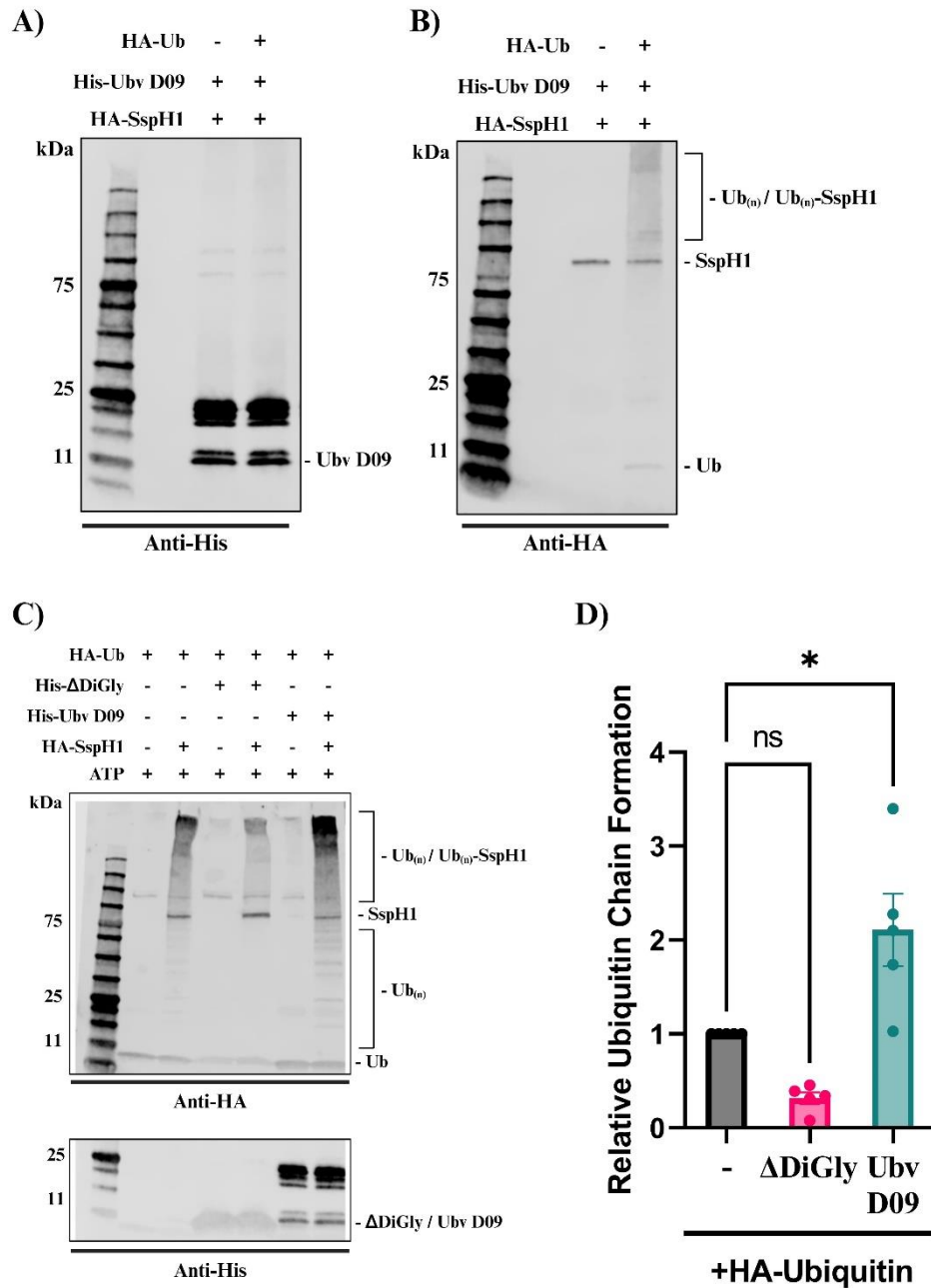


**Fig. 3.4.2. Ubvs modulate the ubiquitination activity of SspH1 *in vitro***

(A) The ability of Ubv D09 to be incorporated into SspH1-mediated ubiquitination was determined by *in vitro* ubiquitination assays containing recombinant E1, E2, SspH1, Ubv and ATP with or without HA-Ub as indicated (-/+). SspH1 activity was analyzed with incorporation of Ubv D09 being monitored by anti-

His immunoblot. **(B)** Ubv D09 impact on polyubiquitin chain formation under the same conditions was monitored by anti-HA immunoblot. Species of interest are indicated on the right. **(C)** The effect of Ubv D09 on the ubiquitination activity of SspH1 was assessed by *in vitro* ubiquitination assays containing recombinant E1, E2, SspH1, HA-Ub, Ubv  $\Delta$ DiGly, or Ubv D09 as indicated (-/+). SspH1 activity was analyzed with Ubv detected by anti-His immunoblot (Bottom) and polyubiquitin chain formation as well as SspH1 detected by anti-HA immunoblot (Top). Species of interest are indicated on the right. **(D)** HA-ubiquitin chain amount was determined through the addition of HA signal in the indicated areas of the immunoblot ( $Ub_{(n)} + Ub_{(n)}\text{-SspH1}$ ) and is presented as a ratio of SspH1 + HA-Ub signal. Errors bars represent the standard error of the mean across 4 independent experiments. Data was analyzed by one-way ANOVA using Tukey's multiple comparisons test.

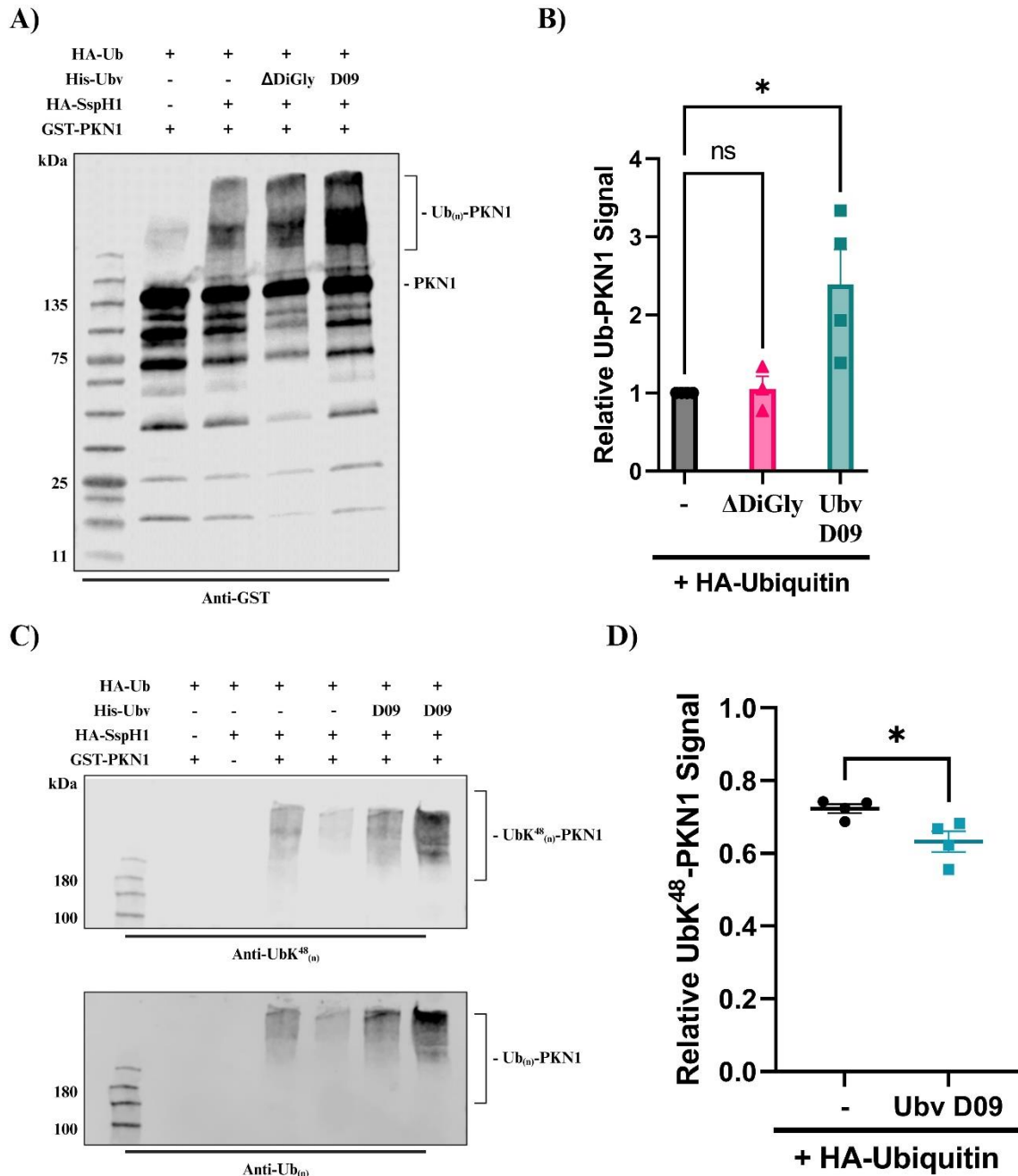
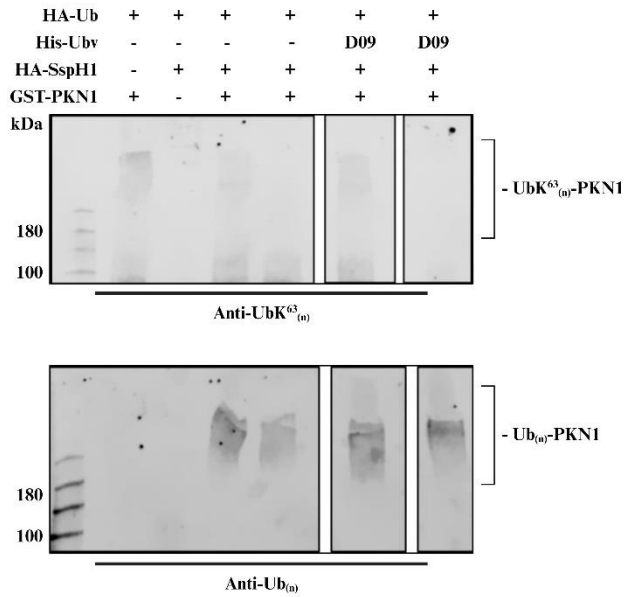


**Fig. 3.4.3. Ubvs modulate SspH1-mediated ubiquitination of PKN1 *in vitro***

(A) SspH1-mediated ubiquitination of PKN1 was determined by *in vitro* ubiquitination assays containing recombinant E1, E2, SspH1, PKN1, HA-Ub, Ubv  $\Delta$ DiGly, or Ubv D09 as indicated. Formation of Ub<sub>(n)</sub>-PKN1 was monitored using anti-GST immunoblot (PKN1 has GST fusion).

Species of interest are indicated on the right. **(B)** Formation of Ub<sub>(n)</sub>-PKN1 is expressed as ratio relative to SspH1 + HA-Ub. Error bars represent the standard error of the mean across 4 independent experiments. Data was analyzed by one-way ANOVA using Dunnett's multiple comparisons test. **(C)** Lysine-specific ubiquitin chain conformation of PKN1-specific, SspH1-mediated ubiquitination was determined by *in vitro* ubiquitination assays containing recombinant E1, E2, SspH1, PKN1, HA-Ub, or Ubv D09 as indicated and analyzed by immunoblot. Two independent reactions are shown. Total ubiquitination was determined by anti-Ub<sub>(n)</sub> [P4D1], K48-specific ubiquitin chains was determined by anti-Ub<sup>K48</sup><sub>(n)</sub> [D9D5]. These immunoblots are representative of a single membrane reprobed in two different fluorescent channels. **(D)** Formation of Ub<sup>K48</sup><sub>(n)</sub>-PKN1 and Ub<sub>(n)</sub>-PKN1 is expressed as ratio relative to the signal of Ub<sub>(n)</sub>-PKN1. Error bars represent the standard error of the mean across 4 independent experiments. Data was analyzed using an unpaired T-test.

A)



B)

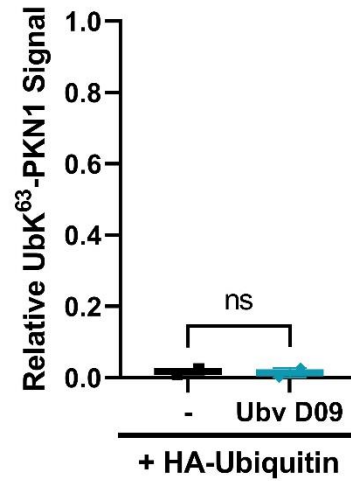


**Fig. 3.4.4 Ubvs modulate SspH1-mediated ubiquitination of PKN1 *in vitro***

(A) Lysine-specific ubiquitin chain conformation of PKN1-specific, SspH1-mediated ubiquitination was determined by *in vitro* ubiquitination assays containing recombinant E1, E2, SspH1, PKN1, HA-Ub, or His-Ubv D09 as indicated and analyzed by immunoblot. Two independent reactions are shown. Total ubiquitination was determined by anti-Ub<sub>(n)</sub> [P4D1], K63-specific ubiquitin chains was determined by anti-Ub<sup>K63</sup><sub>(n)</sub> [D7A11] (B) Formation of UbK<sup>63</sup><sub>(n)</sub>-PKN1 and Ub<sub>(n)</sub>-PKN1 is expressed as ratio relative to the signal of Ub<sub>(n)</sub>-PKN1. Error bars represent the standard error of the mean across 4 independent experiments. Data was analyzed using an unpaired T-test.

## Chapter 4: Discussion

### 4.1 Summary

Throughout my studies I have provided evidence that Ubvs are capable of modulating the activity of a bacterially encoded NEL, both in a eukaryotic model system and *in vitro* activity assays. First, I investigated two Ubvs which were previously identified in a binding screen from a phage-displayed ubiquitin variant library as high-affinity binders for SspH1, a *Salmonella*-encoded NEL, using *in silico* protein prediction software. Using *S. cerevisiae* as a eukaryotic model organism, I was able to demonstrate that the presence of Ubv A06 and Ubv D09 was sufficient to reduce SspH1 toxicity. I also observed that SspH1 expression in *S. cerevisiae* induced cell cycle interference which was alleviated in the presence of Ubv A06 or Ubv D09. Having determined that Ubv were able to inhibit the functional consequences of SspH1 expression in yeast, I next interrogated the direct effect of Ubvs on the ubiquitination activity of SspH1 *in vitro*. Through this process I revealed that Ubv D09, surprisingly, had a potentiating effect on SspH1-mediated ubiquitin chain formation. However, I also observed that the presence of Ubv D09 led to a relative decrease in K48-linked ubiquitination, providing a possible mechanism to reconcile the inhibitory effect in *S. cerevisiae* and the potentiating effect *in vitro*.

### 4.2 Identification of High-Affinity Ubv Binders to SspH1

Prior to my studies, a collaborative effort between the Bhavsar (University of Alberta) and Sidhu (University of Toronto) labs identified, for the first time, that modulators for bacterially-encoded E3 ligases with a unique architecture can be found within a phage-displayed ubiquitin variants library that was designed to target human ubiquitin-interacting proteins. (174) I identified two high-affinity Ubv binders of SspH1, a *Salmonella* encoded NEL, which I refer to as Ubv A06 and Ubv D09. Both Ubvs contained 12 mutations that are not conserved in human or yeast ubiquitin and differed from each other by only 2 amino acids. (Fig. 3.1.1) The mutated residues reside exclusively in diversified regions 2 and 3 of the ubiquitin variant library. (176) *In silico* protein-protein interaction prediction suggests that the Ubvs interact with both the active site and E2~Ub binding site of SspH1. This is consistent with the observed binding interactions between Ubvs and other HECT-like E3 ligases. (169)

### 4.3 Ubv A06 and Ubv D09 suppress SspH1 dependent toxicity in *S. cerevisiae*

Expression of either Ubv in *S. cerevisiae* did not lead to a detectable growth defect on solid media or in liquid media. Although it has been previously shown that expression of ubiquitin containing a mutation at the R74 residue has a dominant negative effect on yeast growth. (248,249) Our observation that yeast growth is not impacted despite the presence of this mutation may be attributed to the selective nature of Ubvs, as they are known to have high specificity for their cognate protein. (183) However, it has also been reported that an intact C-terminal diglycine motif is required for the dominant negative effect of R74 to be observed, which is lacking in both Ubvs. (248) It is also pertinent to note that yeast ubiquitin differs from human ubiquitin at 3 residues (Ser 19, Asp 24, Ser 28), none of which are found within either Ubv. (3) Consistent with previous findings, I observed SspH1-mediated toxicity in yeast that was dependent on the catalytic activity of SspH1. (120) I also observed that Ubv co-expression alongside SspH1 was able to suppress SspH1-mediated toxicity when yeast were grown in liquid media. Conversely, Ubv co-expression on solid media only partially rescued yeast growth. These observations may be attributed to the different environmental pressures experienced by yeast growing in liquid or on solid media as well as the previously observed effects of ubiquitin overexpression. (250)

Despite yeast toxicity being a known consequence of SspH1 expression in *S. cerevisiae* for over a decade, the mechanism behind this phenomenon is not understood. Here I report an increase in cell cycle perturbations, notably the inability for yeast to progress through the G2/M phase of the cell cycle, by both microscopic and cytometric assays in the presence of SspH1. This cell cycle interference phenotype was dependent on the catalytic activity of SspH1 and was suppressed in the presence of either Ubv. Interestingly, the interaction between SspH1 and PKN1 was initially identified through a yeast two-hybrid screen suggesting the presence of a preferred substrate is sufficient to suppress SspH1-mediated toxicity. (138,251) I also observed no detrimental effect of on yeast cell cycle progression when Ubv were expressed alone, consistent with previous observations of yeast growth in the presence of mutated ubiquitin.

#### 4.4 Ubv D09 modulates SspH1 activity *in vitro*.

Intriguingly, despite our hypothesis that Ubvs would interfere with SspH1 E3 ubiquitin ligase activity, which was supported by our yeast studies, I report an increase in *in vitro* SspH1 E3 ubiquitin ligase activity in the presence of Ubv D09 and human ubiquitin. I was unable to purify Ubv A06 for use in these assays despite multiple purification approaches and I speculate that Ubv A06 expression may be toxic to the BL21DE3 *E. coli* that was used for protein production. Nevertheless, our studies with Ubv D09 revealed it could not be polymerized into polyubiquitin chains, as expected given that Ubv D09 lacks the C-terminal diglycine motif necessary for the formation of a thioester linkage (4,252) The slight reduction of SspH1 activity observed in the presence of  $\Delta$ DiGly may also be owed to the lack of a C-terminal diglycine motif. (252) Interestingly,  $\Delta$ DiGly did not reduce SspH1 activity in the presence of PKN1, which may be attributed to the increase in activity NELs are known to undergo in the presence of their cognate substrate. (118) By contrast, Ubv D09 enhanced SspH1 activity in the presence and absence of PKN1, although the linkage pattern of PKN1 ubiquitination was altered by Ubv D09. K48-linked chains are typically associated with proteasomal degradation and have recently been shown to be the primary polyubiquitin linkage formed by SspH1, which is consistent with its described role in mediating PKN1 degradation.(137,251) Our observations confirm that SspH1-mediated ubiquitination primarily consists of K48-linked ubiquitin chains but that this composition can be modulated by the presence of a Ubv. Our experiments were limited to assessing K48- and K63-Ub linkages and I cannot rule out that Ubv D09 had an impact on other linkage types. I was also unable to include a positive control for K63-linked ubiquitination. Moreover, It has been previously observed that the presence of Ubv can affect the natural bias of ubiquitin distribution of an E3 ligase, altering the ratio of processive and distributive ubiquitination of the substrate. (179) Nevertheless, it is tempting to speculate that the basis of SspH1 toxicity in yeast is the formation of K48-linked ubiquitination, and subsequent degradation, of a yeast ortholog of PKN1. Expression of Ubv D09 in yeast may reduce K48-linked ubiquitination on this unknown substrate, to an extent that mitigates yeast toxicity.

#### 4.5 Additional Considerations

Given my use of *S. cerevisiae* rather than mammalian cell culture as a model system, I was not able to assess what effect the presence of Ubvs may have on the previously described

anti-inflammatory role of SspH1. (138,139) Accordingly, I was also unable to determine if Ubv expression would have detrimental effects on the homeostatic function of ubiquitination within complex eukaryotes. This also precluded me from assessing SspH1-mediated PKN1 degradation in the presence of Ubvs within a cellular environment, which could have provided more insight into the functional consequences of the SspH1-Ubv interaction. Additionally, since my work was completed in a BY472a *S. cerevisiae* strain I was unable to utilize a proteasome inhibitor as there are no commercially available small molecules capable of accomplishing this goal. (253,254)

Despite my efforts, many questions remain to be answered regarding the interplay between Ubvs and SspH1. For example, elucidating the biochemical interaction between the Ubvs and SspH1 by crystallizing these proteins in complex could provide valuable information on the unique biology of NEL effectors as well as further clarify the potential mechanism behind Ubv modulation. Similarly, the determination of binding affinities of either Ubv to SspH1 would allow for comparison between the strengths of these interactions. This could be determined by multiple approaches such as microscale thermophoresis (MST), isothermal calorimetry (ITC), or bio-layer interferometry (BLI). (255–257) BLI has been previously implemented to determine the binding affinity of Ubv with a ubiquitin-interacting protein successfully. (184)

The identification of additional Ubvs which are high-affinity binders to other NELs would allow for the discernment of the selectivity of a Ubv approach within the NEL effector family. The exact nature of SspH1 ubiquitination is also yet to be described, although recent work has confirmed that the K48-linked ubiquitin chains are the primary conformation generated by SspH1, its nature as a processive or distributive ligase has yet to be established. The interrogation of the extent to which these discoveries can be generalized to the larger family of NELs would also prove valuable.

#### **4.6 Conclusion and Future Applications**

To our knowledge, this is the first report that demonstrates an Ubv approach can be employed to identify modulators of a bacterial-encoded novel E3 ubiquitin ligase. Despite the presence of NELs amongst several well-studied gram-negative bacterial species their unique structure has limited the available tools to probe their molecular mechanisms. (116) Given that Ubvs have been previously demonstrated to be highly selective between enzymes of the same family, this approach may also be employed to probe the level of redundancy that exists between

the closely related NEL family of effectors. (116,183) Considering the ever-present threat of anti-microbial resistance (AMR), the ability to specifically target bacterial effectors, thereby limiting bacterial pathogenesis, may prove useful as an alternative to traditional antibiotics. (258,259) The approach of limiting bacterial pathogenesis would be advantageous as it places less selective pressure on the bacteria to develop resistance in comparison to approaches which directly target bacterial survival. (260)

Furthermore, Ubv can facilitate the identification of allosteric modulatory sites which can provide a framework to develop small molecule or peptide-based inhibitors to previously undruggable targets. (183,261) Direct use of Ubv as a therapeutic has also been explored but various challenges exist regarding the delivery of a protein-based molecule and the identification of a suitable *in vivo* model to test their effectiveness. (261) Recent work has found some success using virus-based approaches to introduce the genetic material encoding Ubv into cellular system, however these methods carry their own set of safety concerns when applied *in vivo*. (262–264)

In conclusion, throughout the work presented here, I indicate that a Ubv approach, initially intended to target human proteins containing ubiquitin-interacting motifs, can be successfully repurposed to target bacterial effectors with a unique, convergently evolved mechanism of action which provides an additional tool to probe the functional and mechanistic attributes of these effectors.

## References

1. Aitken A. 14-3-3 proteins: a historic overview. *Semin Cancer Biol.* 2006 Jun;16(3):162–72.
2. Xie J, Weiskirchen R. What Does the “AKT” Stand for in the Name “AKT Kinase”? Some Historical Comments. *Front Oncol.* 2020 Aug 11;10:1329.
3. Vijay-Kumar S, Bugg CE, Wilkinson KD, Vierstra RD, Hatfield PM, Cook WJ. Comparison of the three-dimensional structures of human, yeast, and oat ubiquitin. *J Biol Chem.* 1987 May 5;262(13):6396–9.
4. Zhao B, Bhuripanyo K, Schneider J, Zhang K, Schindelin H, Boone D, et al. Specificity of the E1-E2-E3 Enzymatic Cascade for Ubiquitin C-Terminal Sequences Identified by Phage Display. *ACS Chem Biol.* 2012 Dec 21;7(12):2027–35.
5. Hodgins RR, Ellison KS, Ellison MJ. Expression of a ubiquitin derivative that conjugates to protein irreversibly produces phenotypes consistent with a ubiquitin deficiency. *J Biol Chem.* 1992 May 5;267(13):8807–12.
6. Mevissen TET, Komander D. Mechanisms of Deubiquitinase Specificity and Regulation. *Annu Rev Biochem.* 2017 Jun 20;86:159–92.
7. Roscoe BP, Bolon DNA. Systematic Exploration of Ubiquitin Sequence, E1 Activation Efficiency, and Experimental Fitness in Yeast. *J Mol Biol.* 2014 Jul 29;426(15):2854–70.
8. Burch TJ, Haas AL. Site-Directed Mutagenesis of Ubiquitin. Differential Roles for Arginine in the Interaction with Ubiquitin-Activating Enzyme. *Biochemistry.* 1994 Jun 1;33(23):7300–8.
9. Schäfer A, Kuhn M, Schindelin H. Structure of the ubiquitin-activating enzyme loaded with two ubiquitin molecules. *Acta Crystallogr Sect D.* 2014 May 1;70.
10. Hann ZS, Ji C, Olsen SK, Lu X, Lux MC, Tan DS, et al. Structural basis for adenylation and thioester bond formation in the ubiquitin E1. *Proc Natl Acad Sci.* 2019 Jul 30;116(31):15475–84.
11. Olsen SK, Lima CD. Structure of a ubiquitin E1-E2 complex: insights to E1-E2 thioester transfer. *Mol Cell.* 2013 Mar 7;49(5):884–96.
12. Kamadurai HB, Souphron J, Scott DC, Duda DM, Miller DJ, Stringer D, et al. Insights into Ubiquitin Transfer Cascades from a Structure of a UbcH5B~Ubiquitin-HECTNEDD4L Complex. *Mol Cell.* 2009 Dec 24;36(6):1095–102.
13. Page RC, Pruneda JN, Amick J, Klevit RE, Misra S. Structural Insights into the Conformation and Oligomerization of E2~Ubiquitin Conjugates. *Biochemistry.* 2012 May 22;51(20):4175–87.
14. Sakata E, Satoh T, Yamamoto S, Yamaguchi Y, Yagi-Utsumi M, Kurimoto E, et al. Crystal Structure of UbcH5b~Ubiquitin Intermediate: Insight into the Formation of the Self-Assembled E2~Ub Conjugates. *Structure.* 2010;1(18):138–47.
15. Dikic I, Schulman BA. An expanded lexicon for the ubiquitin code. *Nat Rev Mol Cell Biol.* 2023 Apr;24(4):273–87.

16. Kolla S, Ye M, Mark KG, Rapé M. Assembly and function of branched ubiquitin chains. *Trends Biochem Sci.* 2022 Sep 1;47(9):759–71.
17. Mendes ML, Fougeras MR, Dittmar G. Analysis of ubiquitin signaling and chain topology cross-talk. *J Proteomics.* 2020 Mar 20;215:103634.
18. Kliza K, Husnjak K. Resolving the Complexity of Ubiquitin Networks. *Front Mol Biosci* [Internet]. 2020 [cited 2023 Aug 21];7. Available from: <https://www.frontiersin.org/articles/10.3389/fmolb.2020.00021>
19. Deshaies RJ, Joazeiro CAP. RING domain E3 ubiquitin ligases. *Annu Rev Biochem.* 2009;78:399–434.
20. French ME, Klosowiak JL, Aslanian A, Reed SI, Yates JR, Hunter T. Mechanism of ubiquitin chain synthesis employed by a HECT domain ubiquitin ligase. *J Biol Chem.* 2017 Jun 23;292(25):10398–413.
21. Walden H, Rittinger K. RBR ligase-mediated ubiquitin transfer: a tale with many twists and turns. *Nat Struct Mol Biol.* 2018 Jun;25(6):440–5.
22. Chen ZJ, Sun LJ. Nonproteolytic Functions of Ubiquitin in Cell Signaling. *Mol Cell.* 2009 Feb 13;33(3):275–86.
23. Ikeda F, Dikic I. Atypical ubiquitin chains: new molecular signals. ‘Protein Modifications: Beyond the Usual Suspects’ Review Series. *EMBO Rep.* 2008 Jun;9(6):536–42.
24. Akutsu M, Dikic I, Bremm A. Ubiquitin chain diversity at a glance. *J Cell Sci.* 2016 Mar 1;129(5):875–80.
25. Komander D, Rape M. The ubiquitin code. *Annu Rev Biochem.* 2012;81:203–29.
26. Tracz M, Bialek W. Beyond K48 and K63: non-canonical protein ubiquitination. *Cell Mol Biol Lett.* 2021 Jan 5;26(1):1.
27. Lu Y, Lee B hoon, King RW, Finley D, Kirschner MW. Substrate degradation by the proteasome: a single-molecule kinetic analysis. *Science.* 2015 Apr 10;348(6231):1250834.
28. Swatek KN, Komander D. Ubiquitin modifications. *Cell Res.* 2016 Apr;26(4):399–422.
29. Erpapazoglou Z, Walker O, Haguenaer-Tsapis R. Versatile Roles of K63-Linked Ubiquitin Chains in Trafficking. *Cells.* 2014 Nov 12;3(4):1027–88.
30. Cappadocia L, Lima CD. Ubiquitin-like Protein Conjugation: Structures, Chemistry, and Mechanism. *Chem Rev.* 2018 Feb 14;118(3):889–918.
31. Salas-Lloret D, González-Prieto R. Insights in Post-Translational Modifications: Ubiquitin and SUMO. *Int J Mol Sci.* 2022 Mar 18;23(6):3281.
32. Hurley JH, Lee S, Prag G. Ubiquitin-binding domains. *Biochem J.* 2006 Nov 1;399(Pt 3):361–72.
33. Trempe JF. Reading the ubiquitin postal code. *Curr Opin Struct Biol.* 2011 Dec 1;21(6):792–801.

34. Pickart CM, Eddins MJ. Ubiquitin: structures, functions, mechanisms. *Biochim Biophys Acta BBA - Mol Cell Res.* 2004 Nov 29;1695(1):55–72.
35. Randles L, Walters KJ. Ubiquitin and its binding domains. *Front Biosci Landmark Ed.* 2012 Jun 1;17:2140–57.
36. Komander D, Clague MJ, Urbé S. Breaking the chains: structure and function of the deubiquitinases. *Nat Rev Mol Cell Biol.* 2009 Aug;10(8):550–63.
37. Abdul Rehman SA, Kristariyanto YA, Choi SY, Nkosi PJ, Weidlich S, Labib K, et al. MINDY-1 Is a Member of an Evolutionarily Conserved and Structurally Distinct New Family of Deubiquitinating Enzymes. *Mol Cell.* 2016 Jul 7;63(1):146–55.
38. Kwasna D, Abdul Rehman SA, Natarajan J, Matthews S, Madden R, De Cesare V, et al. Discovery and Characterization of ZUFSP/ZUP1, a Distinct Deubiquitinase Class Important for Genome Stability. *Mol Cell.* 2018 Apr 5;70(1):150-164.e6.
39. Schauer NJ, Magin RS, Liu X, Doherty LM, Buhrlage SJ. Advances in Discovering Deubiquitinating Enzyme (DUB) Inhibitors. *J Med Chem.* 2020 Mar 26;63(6):2731–50.
40. Li Y, Reverter D. Molecular Mechanisms of DUBs Regulation in Signaling and Disease. *Int J Mol Sci.* 2021 Jan 20;22(3):986.
41. He M, Zhou Z, Shah AA, Zou H, Tao J, Chen Q, et al. The emerging role of deubiquitinating enzymes in genomic integrity, diseases, and therapeutics. *Cell Biosci.* 2016;6:62.
42. Franklin TG, Pruneda JN. Bacteria make surgical strikes on host ubiquitin signaling. *PLOS Pathog.* 2021 Mar 18;17(3):e1009341.
43. Swatek KN, Komander D. Ubiquitin modifications. *Cell Res.* 2016 Apr;26(4):399–422.
44. Salmon D, Smith T. The bacterium of swine plague. *Am Mon Microsc J.* 1886;7:204–5.
45. Tindall BJ, Grimont P a. D, Garrity GM, Euzéby JP. Nomenclature and taxonomy of the genus *Salmonella*. *Int J Syst Evol Microbiol.* 2005 Jan;55(Pt 1):521–4.
46. Giammanco GM, Pignato S, Mammina C, Grimont F, Grimont PAD, Nastasi A, et al. Persistent endemicity of *Salmonella bongori* 48:z(35):--in Southern Italy: molecular characterization of human, animal, and environmental isolates. *J Clin Microbiol.* 2002 Sep;40(9):3502–5.
47. Fookes M, Schroeder GN, Langridge GC, Blondel CJ, Mammina C, Connor TR, et al. *Salmonella bongori* provides insights into the evolution of the *Salmonellae*. *PLoS Pathog.* 2011 Aug;7(8):e1002191.
48. Pearce ME, Langridge GC, Lauer AC, Grant K, Maiden MCJ, Chattaway MA. An evaluation of the species and subspecies of the genus *Salmonella* with whole genome sequence data: Proposal of type strains and epithets for novel *S. enterica* subspecies VII, VIII, IX, X and XI. *Genomics.* 2021 Sep 1;113(5):3152–62.
49. Cobo-Simón M, Hart R, Ochman H. Gene flow and species boundaries of the genus *Salmonella*. *mSystems.* 2023 Jul 24;8(4):e00292-23.

50. Park CJ, Andam CP. Distinct but Intertwined Evolutionary Histories of Multiple *Salmonella enterica* Subspecies. *mSystems*. 2020 Jan 14;5(1):10.1128/msystems.00515-19.
51. Jajere SM. A review of *Salmonella enterica* with particular focus on the pathogenicity and virulence factors, host specificity and antimicrobial resistance including multidrug resistance. *Vet World*. 2019;12(4):504–21.
52. Gal-Mor O, Boyle EC, Grassl GA. Same species, different diseases: how and why typhoidal and non-typhoidal *Salmonella enterica* serovars differ. *Front Microbiol*. 2014 Aug 4;5:102622.
53. Galán JE. Typhoid toxin provides a window into typhoid fever and the biology of *Salmonella Typhi*. *Proc Natl Acad Sci*. 2016 Jun 7;113(23):6338–44.
54. Raffatellu M, Wilson RP, Winter SE, Bäumlner AJ. Clinical pathogenesis of typhoid fever. *J Infect Dev Ctries*. 2008 Aug 30;2(4):260–6.
55. Institute for Health Metrics and Evaluation, Global Burden of Diseases Collaborative Network. Typhoid and paratyphoid — Level 3 cause | Institute for Health Metrics and Evaluation [Internet]. 2023 [cited 2024 Feb 14]. Available from: [https://www.healthdata.org/results/gbd\\_summaries/2019/typhoid-and-paratyphoid-level-3-cause](https://www.healthdata.org/results/gbd_summaries/2019/typhoid-and-paratyphoid-level-3-cause)
56. Majowicz SE, Musto J, Scallan E, Angulo FJ, Kirk M, O’Brien SJ, et al. The Global Burden of Nontyphoidal *Salmonella* Gastroenteritis. *Clin Infect Dis*. 2010 Mar 15;50(6):882–9.
57. Arya G, Holtslander R, Robertson J, Yoshida C, Harris J, Parmley J, et al. Epidemiology, Pathogenesis, Genosero-typing, Antimicrobial Resistance, and Prevention and Control of Non-Typhoidal *Salmonella* Serovars. *Curr Clin Microbiol Rep*. 2017 Mar 1;4(1):43–53.
58. Hoelzer K, Moreno Switt AI, Wiedmann M. Animal contact as a source of human non-typhoidal salmonellosis. *Vet Res*. 2011 Feb 14;42(1):34.
59. Hilbert F, Smulders FJM, Chopra-Dewasthaly R, Paulsen P. *Salmonella* in the wildlife-human interface. *Food Res Int*. 2012 Mar 1;45(2):603–8.
60. Park SE, Pak GD, Aaby P, Adu-Sarkodie Y, Ali M, Aseffa A, et al. The Relationship Between Invasive Nontyphoidal *Salmonella* Disease, Other Bacterial Bloodstream Infections, and Malaria in Sub-Saharan Africa. *Clin Infect Dis*. 2016 Mar 15;62(suppl\_1):S23–31.
61. Crump JA, Sjölund-Karlsson M, Gordon MA, Parry CM. Epidemiology, Clinical Presentation, Laboratory Diagnosis, Antimicrobial Resistance, and Antimicrobial Management of Invasive *Salmonella* Infections. *Clin Microbiol Rev*. 2015 Oct;28(4):901–37.
62. Stanaway JD, Parisi A, Sarkar K, Blacker BF, Reiner RC, Hay SI, et al. The global burden of non-typhoidal salmonella invasive disease: a systematic analysis for the Global Burden of Disease Study 2017. *Lancet Infect Dis*. 2019 Dec 1;19(12):1312–24.
63. Balasubramanian R, Im J, Lee JS, Jeon HJ, Mogeni OD, Kim JH, et al. The global burden and epidemiology of invasive non-typhoidal *Salmonella* infections. *Hum Vaccines Immunother*. 2019 Jun 3;15(6):1421–6.

64. Marchello CS, Fiorino F, Pettini E, Crump JA, Martin LB, Breggi G, et al. Incidence of nontyphoidal *Salmonella* invasive disease: A systematic review and meta-analysis. *J Infect.* 2021 Nov 1;83(5):523–32.
65. Ao TT, Feasey NA, Gordon MA, Keddy KH, Angulo FJ, Crump JA. Global Burden of Invasive Nontyphoidal *Salmonella* Disease, 2010. *Emerg Infect Dis.* 2015 Jun;21(6):941–9.
66. Hume PJ, Singh V, Davidson AC, Koronakis V. Swiss Army Pathogen: The *Salmonella* Entry Toolkit. *Front Cell Infect Microbiol* [Internet]. 2017 [cited 2024 Feb 15];7. Available from: <https://www.frontiersin.org/articles/10.3389/fcimb.2017.00348>
67. Santos RL, Bäumlér AJ. Cell tropism of *Salmonella enterica*. *Int J Med Microbiol.* 2004 Oct 8;294(4):225–33.
68. Galán JE, Curtiss R. Cloning and molecular characterization of genes whose products allow *Salmonella typhimurium* to penetrate tissue culture cells. *Proc Natl Acad Sci.* 1989 Aug;86(16):6383–7.
69. Santos RL. Pathobiology of *Salmonella*, Intestinal Microbiota, and the Host Innate Immune Response. *Front Immunol* [Internet]. 2014 [cited 2024 Feb 18];5. Available from: <https://www.frontiersin.org/journals/immunology/articles/10.3389/fimmu.2014.00252>
70. Gebert A. The role of M cells in the protection of mucosal membranes. *Histochem Cell Biol.* 1997 Dec;108(6):455–70.
71. Neutra MR, Mantis NJ, Frey A, Giannasca PJ. The composition and function of M cell apical membranes: implications for microbial pathogenesis. *Semin Immunol.* 1999 Jun;11(3):171–81.
72. Lahiri A, Lahiri A, Iyer N, Das P, Chakravorty D. Visiting the cell biology of *Salmonella* infection. *Microbes Infect.* 2010 Oct 1;12(11):809–18.
73. Martínez-Argudo I, Jepson MA. *Salmonella* translocates across an in vitro M cell model independently of SPI-1 and SPI-2. *Microbiol Read Engl.* 2008 Dec;154(Pt 12):3887–94.
74. Niess JH, Brand S, Gu X, Landsman L, Jung S, McCormick BA, et al. CX3CR1-mediated dendritic cell access to the intestinal lumen and bacterial clearance. *Science.* 2005 Jan 14;307(5707):254–8.
75. Nieto PA, Pardo-Roa C, Salazar-Echegarai FJ, Tobar HE, Coronado-Arrázola I, Riedel CA, et al. New insights about excisable pathogenicity islands in *Salmonella* and their contribution to virulence. *Microbes Infect.* 2016 May 1;18(5):302–9.
76. Liu X, Jiang Z, Liu Z, Li D, Liu Z, Dong X, et al. Research Progress of *Salmonella* Pathogenicity Island. *Int J Biol Life Sci.* 2023 May 22;2(3):7–11.
77. Galán JE. Molecular genetic bases of *Salmonella* entry into host cells. *Mol Microbiol.* 1996;20(2):263–71.
78. Shea JE, Hensel M, Gleeson C, Holden DW. Identification of a virulence locus encoding a second type III secretion system in *Salmonella typhimurium*. *Proc Natl Acad Sci U S A.* 1996 Mar 19;93(6):2593–7.

79. Ly KT, Casanova JE. Mechanisms of Salmonella entry into host cells. *Cell Microbiol.* 2007;9(9):2103–11.
80. dos Santos AMP, Ferrari RG, Conte-Junior CA. Virulence Factors in Salmonella Typhimurium: The Sagacity of a Bacterium. *Curr Microbiol.* 2019 Jun 1;76(6):762–73.
81. Francis CL, Ryan TA, Jones BD, Smith SJ, Falkow S. Ruffles induced by Salmonella and other stimuli direct macropinocytosis of bacteria. *Nature.* 1993 Aug;364(6438):639–42.
82. López FE, de las Mercedes Pescaretti M, Morero R, Delgado MA. *Salmonella* Typhimurium general virulence factors: A battle of David against Goliath? *Food Res Int.* 2012 Mar 1;45(2):842–51.
83. Figueira R, Holden DW. Functions of the Salmonella pathogenicity island 2 (SPI-2) type III secretion system effectors. *Microbiol Soc Gen Microbiol.* 2012;158(5):1147–61.
84. Fabrega A, Vila J. Salmonella enterica Serovar Typhimurium Skills To Succeed in the Host: Virulence and Regulation. *Clin Microbiol Rev.* 2013;26(2):308–41.
85. Alpuche-Aranda CM, Racoosin EL, Swanson JA, Miller SI. Salmonella stimulate macrophage macropinocytosis and persist within spacious phagosomes. *J Exp Med.* 1994 Feb 1;179(2):601–8.
86. Hensel M. Salmonella Pathogenicity Island 2. *Mol Microbiol.* 2000;36(5):1015–23.
87. Haraga A, Ohlson MB, Miller SI. Salmonellae interplay with host cells. *Nat Rev Microbiol.* 2008 Jan;6(1):53–66.
88. Herrero-Fresno A, Olsen JE. *Salmonella* Typhimurium metabolism affects virulence in the host – A mini-review. *Food Microbiol.* 2018 May 1;71:98–110.
89. Pillay TD, Hettiarachchi SU, Gan J, Diaz-Del-Olmo I, Yu XJ, Muench JH, et al. Speaking the host language: how Salmonella effector proteins manipulate the host. *Microbiology.* 2023;169(6):001342.
90. Galán JE. Salmonella Typhimurium and inflammation: a pathogen-centric affair. *Nat Rev Microbiol.* 2021 Nov;19(11):716–25.
91. Azimi T, Zamirnasta M, Sani MA, Soltan Dallal MM, Nasser A. Molecular Mechanisms of Salmonella Effector Proteins: A Comprehensive Review. *Infect Drug Resist.* 2020 Jan 6;13:11–26.
92. dos Santos AMP, Ferrari RG, Conte-Junior CA. Type three secretion system in Salmonella Typhimurium: the key to infection. *Genes Genomics.* 2020 May 1;42(5):495–506.
93. Hurley D, McCusker MP, Fanning S, Martins M. Salmonella–Host Interactions – Modulation of the Host Innate Immune System. *Front Immunol [Internet].* 2014 [cited 2024 Feb 16];5. Available from: <https://www.frontiersin.org/journals/immunology/articles/10.3389/fimmu.2014.00481>
94. Raffatellu M, Wilson RP, Chessa D, Andrews-Polymeris H, Tran QT, Lawhon S, et al. SipA, SopA, SopB, SopD, and SopE2 Contribute to Salmonella enterica Serotype Typhimurium Invasion of Epithelial Cells. *Infect Immun.* 2005 Jan;73(1):146–54.
95. McGhie EJ, Brawn LC, Hume PJ, Humphreys D, Koronakis V. *Salmonella* takes control: effector-driven manipulation of the host. *Curr Opin Microbiol.* 2009 Feb 1;12(1):117–24.

96. Miroid S, Ehrbar K, Weissmüller A, Prager R, Tschäpe H, Rüssmann H, et al. Salmonella Host Cell Invasion Emerged by Acquisition of a Mosaic of Separate Genetic Elements, Including Salmonella Pathogenicity Island 1 (SPI1), SPI5, and sopE2. *J Bacteriol.* 2001 Apr;183(7):2348–58.
97. Jennings E, Thurston TLM, Holden DW. Salmonella SPI-2 Type III Secretion System Effectors: Molecular Mechanisms And Physiological Consequences. *Cell Host Microbe.* 2017;22(2):217–31.
98. Walch P, Selkrig J, Knodler LA, Rettel M, Stein F, Fernandez K, et al. Global mapping of Salmonella enterica-host protein-protein interactions during infection. *Cell Host Microbe.* 2021 Aug 11;29(8):1316-1332.e12.
99. Baisón-Olmo F, Cardenal-Muñoz E, Ramos-Morales F. PipB2 is a substrate of the *Salmonella* pathogenicity island 1-encoded type III secretion system. *Biochem Biophys Res Commun.* 2012 Jun 29;423(2):240–6.
100. Freeman JA, Ohl ME, Miller SI. The Salmonella enterica Serovar Typhimurium Translocated Effectors SseJ and SifB Are Targeted to the Salmonella-Containing Vacuole. *Infect Immun.* 2003 Jan;71(1):418–27.
101. Liao J, Orsi RH, Carroll LM, Wiedmann M. Comparative genomics reveals different population structures associated with host and geographic origin in antimicrobial-resistant Salmonella enterica. *Environ Microbiol.* 2020;22(7):2811–28.
102. Delyea C, Luo SY, Dubrule BE, Julien O, Bhavsar AP. NOD1 is super-activated through spatially-selective ubiquitination by the Salmonella effector SspH2 [Internet]. *bioRxiv*; 2021 [cited 2023 Aug 22]. p. 2021.10.08.463692. Available from: <https://www.biorxiv.org/content/10.1101/2021.10.08.463692v2>
103. Büttner D. Protein Export According to Schedule: Architecture, Assembly, and Regulation of Type III Secretion Systems from Plant- and Animal-Pathogenic Bacteria. *Microbiol Mol Biol Rev.* 2012 Jun 11;76(2):262–310.
104. Wagner S, Grin I, Malmsheimer S, Singh N, Torres-Vargas CE, Westerhausen S. Bacterial type III secretion systems: a complex device for the delivery of bacterial effector proteins into eukaryotic host cells. *FEMS Microbiol Lett.* 2018 Aug 9;365(19):fny201.
105. Deng W, Marshall NC, Rowland JL, McCoy JM, Worrall LJ, Santos AS, et al. Assembly, structure, function and regulation of type III secretion systems. *Nat Rev Microbiol.* 2017 Jun;15(6):323–37.
106. Akeda Y, Galán JE. Chaperone release and unfolding of substrates in type III secretion. *Nature.* 2005 Oct 6;437(7060):911–5.
107. Galán JE, Wolf-Watz H. Protein delivery into eukaryotic cells by type III secretion machines. *Nature.* 2006 Nov 30;444(7119):567–73.
108. Bhavsar AP, Guttman JA, Finlay BB. Manipulation of host-cell pathways by bacterial pathogens. *Nat Lond.* 2007;449(7164):827–34.
109. Park D, Lara-Tejero M, Waxham MN, Li W, Hu B, Galán JE, et al. Visualization of the type III secretion mediated Salmonella–host cell interface using cryo-electron tomography. *Musacchio A, Orth K, editors. eLife.* 2018 Oct 3;7:e39514.

110. Diepold A, Armitage JP. Type III secretion systems: the bacterial flagellum and the injectisome. *Philos Trans R Soc B Biol Sci.* 2015 Oct 5;370(1679):20150020.
111. Abby SS, Rocha EPC. The Non-Flagellar Type III Secretion System Evolved from the Bacterial Flagellum and Diversified into Host-Cell Adapted Systems. *PLOS Genet.* 2012 Sep 27;8(9):e1002983.
112. Moest TP, Méresse S. Salmonella T3SSs: successful mission of the secret(ion) agents. *Curr Opin Microbiol.* 2013;16(1):38–44.
113. Rohde JR, Breitskreutz A, Chenal A, Sansonetti PJ, Parsot C. Type III Secretion Effectors of the IpaH Family Are E3 Ubiquitin Ligases. *Cell Host Microbe.* 2007;1(1):77–83.
114. Singer AU, Schulze S, Skarina T, Xu X, Cui H, Eschen-Lippold L, et al. A Pathogen Type III Effector with a Novel E3 Ubiquitin Ligase Architecture. *PLOS Pathog.* 2013 Jan 24;9(1):e1003121.
115. Iyer LM, Burroughs AM, Aravind L. The prokaryotic antecedents of the ubiquitin-signaling system and the early evolution of ubiquitin-like  $\beta$ -grasp domains. *Genome Biol.* 2006 Jul 19;7(7):R60.
116. Bullones-Bolaños A, Bernal-Bayard J, Ramos-Morales F. The NEL Family of Bacterial E3 Ubiquitin Ligases. *Int J Mol Sci.* 2022 Jan;23(14):7725.
117. Norkowski S, Schmidt MA, Rüter C. The species-spanning family of LPX-motif harbouring effector proteins. *Cell Microbiol.* 2018;20(11):e12945.
118. Quezada CM, Hicks SW, Galán JE, Stebbins CE, Bassler BL. A Family of Salmonella Virulence Factors Functions as a Distinct Class of Autoregulated E3 Ubiquitin Ligases. *Proc Natl Acad Sci - PNAS.* 2009;106(12):4864–9.
119. Chou YC, Keszei AFA, Rohde JR, Tyers M, Sicheri F. Conserved Structural Mechanisms for Autoinhibition in IpaH Ubiquitin Ligases. *J Biol Chem.* 2012 Jan 2;287(1):268–75.
120. Keszei AFA, Tang X, McCormick C, Zeqiraj E, Rohde JR, Tyers M, et al. Structure of an SspH1-PKN1 Complex Reveals the Basis for Host Substrate Recognition and Mechanism of Activation for a Bacterial E3 Ubiquitin Ligase. *Mol Cell Biol.* 2013;34(3):362–73.
121. Cook M, Delbecq SP, Schweppe TP, Guttman M, Klevit RE, Brzovic PS. The ubiquitin ligase SspH1 from Salmonella uses a modular and dynamic E3 domain to catalyze substrate ubiquitylation. *J Biol Chem.* 2018 Nov 20;294(3):783–93.
122. Keszei AFA, Sicheri F. Mechanism of catalysis, E2 recognition, and autoinhibition for the IpaH family of bacterial E3 ubiquitin ligases. *Proc Natl Acad Sci U S A.* 2017 Feb 7;114(6):1311–6.
123. Ye Y, Rape M. Building ubiquitin chains: E2 enzymes at work. *Nat Rev Mol Cell Biol.* 2009 Nov;10(11):755–64.
124. Levin I, Eakin C, Blanc MP, Klevit RE, Miller SI, Brzovic PS, et al. Identification of an Unconventional E3 Binding Surface on the UbcH5 ~ Ub Conjugate Recognized by a Pathogenic Bacterial E3 Ligase. *Proc Natl Acad Sci - PNAS.* 2010;107(7):2848–53.

125. Bernal-Bayard J, Ramos-Morales F. Salmonella Type III Secretion Effector SlrP Is an E3 Ubiquitin Ligase for Mammalian Thioredoxin. *J Biol Chem.* 2009 Oct 2;284(40):27587–95.
126. Zouhir S, Bernal-Bayard J, Cordero-Alba M, Cardenal-Muñoz E, Guimaraes B, Lazar N, et al. The structure of the SlrP–Trx1 complex sheds light on the autoinhibition mechanism of the type III secretion system effectors of the NEL family. *Biochem J.* 2014 Oct 23;464(1):135–44.
127. Miao EA, Scherer CA, Tsolis RM, Kingsley RA, Adams LG, Bäumlér AJ, et al. Salmonella typhimurium leucine-rich repeat proteins are targeted to the SPI1 and SPI2 type III secretion systems. *Mol Microbiol.* 1999;34(4):850–64.
128. Herod A, Emond-Rheault JG, Tamber S, Goodridge L, Lévesque RC, Rohde J. Genomic and phenotypic analysis of SspH1 identifies a new Salmonella effector, SspH3. *Mol Microbiol.* 2022;117(4):770–89.
129. Singer AU, Rohde JR, Lam R, Skarina T, Kagan O, DiLeo R, et al. Structure of the Shigella T3SS effector IpaH defines a new class of E3 ubiquitin ligases. *Nat Struct Mol Biol.* 2008 Dec;15(12):1293–301.
130. de Jong MF, Liu Z, Chen D, Alto NM. Shigella flexneri suppresses NF-κB activation by inhibiting linear ubiquitin chain ligation. *Nat Microbiol.* 2016 May 27;1(7):16084.
131. Xin DW, Liao S, Xie ZP, Hann DR, Steinle L, Boller T, et al. Functional Analysis of NopM, a Novel E3 Ubiquitin Ligase (NEL) Domain Effector of Rhizobium sp. Strain NGR234. *PLOS Pathog.* 2012 May 17;8(5):e1002707.
132. Nakano M, Oda K, Mukaihara T. Ralstonia solanacearum novel E3 ubiquitin ligase (NEL) effectors RipAW and RipAR suppress pattern-triggered immunity in plants. *Microbiology.* 2017;163(7):992–1002.
133. Cheng D, Zhou D, Wang Y, Wang B, He Q, Song B, et al. Ralstonia solanacearum type III effector RipV2 encoding a novel E3 ubiquitin ligase (NEL) is required for full virulence by suppressing plant PAMP-triggered immunity. *Biochem Biophys Res Commun.* 2021 Apr 23;550:120–6.
134. Blum M, Chang HY, Chuguransky S, Grego T, Kandasamy S, Mitchell A, et al. The InterPro protein families and domains database: 20 years on. *Nucleic Acids Res.* 2021 Jan 8;49(D1):D344–54.
135. Paysan-Lafosse T, Blum M, Chuguransky S, Grego T, Pinto BL, Salazar GA, et al. InterPro in 2022. *Nucleic Acids Res.* 2023 Jan 6;51(D1):D418–27.
136. Figueroa-Bossi N, Uzzau S, Maloriol D, Bossi L. Variable assortment of prophages provides a transferable repertoire of pathogenic determinants in Salmonella. *Mol Microbiol.* 2001;39(2):260–72.
137. Herod A, Emond-Rheault JG, Tamber S, Goodridge L, Lévesque RC, Rohde J. Genomic and phenotypic analysis of SspH1 identifies a new Salmonella effector, SspH3. *Mol Microbiol* [Internet]. 2021 [cited 2022 Jan 5]; Available from: <http://onlinelibrary.wiley.com/doi/abs/10.1111/mmi.14871>

138. Haraga A, Miller SI. A Salmonella type III secretion effector interacts with the mammalian serine/threonine protein kinase PKN1. *Cell Microbiol.* 2006;8(5):837–46.
139. Haraga A, Miller SI. A Salmonella enterica Serovar Typhimurium Translocated Leucine-Rich Repeat Effector Protein Inhibits NF- $\kappa$ B-Dependent Gene Expression. *Infect Immun.* 2003 Jul;71(7):4052–8.
140. Bierne H, Pourpre R. Bacterial Factors Targeting the Nucleus: The Growing Family of Nucleomodulins. *Toxins.* 2020 Apr;12(4):220.
141. Metzger E, Müller JM, Ferrari S, Buettner R, Schüle R. A novel inducible transactivation domain in the androgen receptor: implications for PRK in prostate cancer. *EMBO J.* 2003 Jan 15;22(2):270–80.
142. Gül E, Huuskonen J, Abi Younes A, Maurer L, Enz U, Zimmermann J, et al. Salmonella T3SS-2 virulence enhances gut-luminal colonization by enabling chemotaxis-dependent exploitation of intestinal inflammation. *Cell Rep.* 2024 Mar 7;43(3):113925.
143. Mukai H. The Structure and Function of PKN, a Protein Kinase Having a Catalytic Domain Homologous to That of PKC. *J Biochem (Tokyo).* 2003;133(1):17–27.
144. Sophocleous G, Owen D, Mott HR. The structure and function of protein kinase C-related kinases (PRKs). *Biochem Soc Trans.* 2021 Feb 1;49(1):217–35.
145. Kazanietz MG, Lemmon MA. Protein Kinase C Regulation: C1 Meets C-tail. *Structure.* 2011 Feb 9;19(2):144–6.
146. Mosaddeghzadeh N, Ahmadian MR. The RHO Family GTPases: Mechanisms of Regulation and Signaling. *Cells.* 2021 Jul;10(7):1831.
147. Kitagawa M, Shibata H, Toshimori M, Mukai H, Ono Y. The Role of the Unique Motifs in the Amino-Terminal Region of PKN on Its Enzymatic Activity. *Biochem Biophys Res Commun.* 1996 Mar 27;220(3):963–8.
148. Yang CS, Melhuish TA, Spencer A, Ni L, Hao Y, Jividen K, et al. The protein kinase C super-family member PKN is regulated by mTOR and influences differentiation during prostate cancer progression. *The Prostate.* 2017;77(15):1452–67.
149. Palmer RH, Dekker LV, Woscholski R, Le Good JA, Gigg R, Parker PJ. Activation of PRK1 by phosphatidylinositol 4,5-bisphosphate and phosphatidylinositol 3,4,5-trisphosphate. A comparison with protein kinase C isoforms. *J Biol Chem.* 1995 Sep 22;270(38):22412–6.
150. Yoshinaga C, Mukai H, Toshimori M, Miyamoto M, Ono Y. Mutational analysis of the regulatory mechanism of PKN: the regulatory region of PKN contains an arachidonic acid-sensitive autoinhibitory domain. *J Biochem (Tokyo).* 1999 Sep;126(3):475–84.
151. Collazos A, Michael N, Whelan RDH, Kelly G, Mellor H, Pang LCH, et al. Site recognition and substrate screens for PKN family proteins. *Biochem J.* 2011 Sep 15;438(3):535–43.

152. Flynn P, Mellor H, Casamassima A, Parker PJ. Rho GTPase control of protein kinase C-related protein kinase activation by 3-phosphoinositide-dependent protein kinase. *J Biol Chem.* 2000 Apr 14;275(15):11064–70.
153. Takahashi M, Mukai H, Toshimori M, Miyamoto M, Ono Y. Proteolytic activation of PKN by caspase-3 or related protease during apoptosis. *Proc Natl Acad Sci U S A.* 1998 Sep 29;95(20):11566–71.
154. Park YH, Wood G, Kastner DL, Chae JJ. Pyrin inflammasome activation and RhoA signaling in the autoinflammatory diseases FMF and HIDS. *Nat Immunol.* 2016 Aug;17(8):914–21.
155. Schnappauf O, Chae JJ, Kastner DL, Aksenitjevich I. The Pyrin Inflammasome in Health and Disease. *Front Immunol.* 2019 Aug 7;10:465008.
156. Davey RA, Grossmann M. Androgen Receptor Structure, Function and Biology: From Bench to Bedside. *Clin Biochem Rev.* 2016 Feb;37(1):3–15.
157. Metzger E, Yin N, Wissmann M, Kunowska N, Fischer K, Friedrichs N, et al. Phosphorylation of histone H3 at threonine 11 establishes a novel chromatin mark for transcriptional regulation. *Nat Cell Biol.* 2008 Jan;10(1):53–60.
158. O’Sullivan AG, Mulvaney EP, Kinsella BT. Regulation of protein kinase C-related kinase (PRK) signalling by the TP $\alpha$  and TP $\beta$  isoforms of the human thromboxane A2 receptor: Implications for thromboxane- and androgen- dependent neoplastic and epigenetic responses in prostate cancer. *Biochim Biophys Acta Mol Basis Dis.* 2017 Apr;1863(4):838–56.
159. Harrison JC, Bardes ESG, Ohya Y, Lew DJ. A role for the Pkc1p/Mpk1p kinase cascade in the morphogenesis checkpoint. *Nat Cell Biol.* 2001 Apr;3(4):417–20.
160. Levin DE, Fields FO, Kunisawa R, Bishop JM, Thorner J. A candidate protein kinase C gene, PKC1, is required for the *S. cerevisiae* cell cycle. *Cell.* 1990 Jul;62(2):213–24.
161. Zhang W, Sidhu SS. Development of inhibitors in the ubiquitination cascade. *FEBS Lett.* 2014 Jan 21;588(2):356–67.
162. Nalepa G, Rolfe M, Harper JW. Drug discovery in the ubiquitin–proteasome system. *Nat Rev Drug Discov.* 2006 Jul;5(7):596–613.
163. Wu HQ, Baker D, Ovaia H. Small molecules that target the ubiquitin system. *Biochem Soc Trans.* 2020 Mar 20;48(2):479–97.
164. Li X, Elmira E, Rohondia S, Wang J, Liu J, Dou QP. A patent review of the ubiquitin ligase system: 2015–2018. *Expert Opin Ther Pat.* 2018 Dec 2;28(12):919–37.
165. Barghout SH, Schimmer AD. E1 Enzymes as Therapeutic Targets in Cancer. Barker E, editor. *Pharmacol Rev.* 2021 Jan 1;73(1):1–58.
166. Osborne HC, Irving E, Forment JV, Schmidt CK. E2 enzymes in genome stability: pulling the strings behind the scenes. *Trends Cell Biol.* 2021 Aug 1;31(8):628–43.

167. Middleton AJ, Teyra J, Zhu J, Sidhu SS, Day CL. Identification of Ubiquitin Variants That Inhibit the E2 Ubiquitin Conjugating Enzyme, Ube2k. *ACS Chem Biol*. 2021 Sep 17;16(9):1745–56.
168. Stewart MD, Ritterhoff T, Klevit RE, Brzovic PS. E2 enzymes: more than just middle men. *Cell Res*. 2016 Apr;26(4):423–40.
169. LeBlanc N, Mallette E, Zhang W. Targeted modulation of E3 ligases using engineered ubiquitin variants. *FEBS J*. 2021;288(7):2143–65.
170. Chen D, Gehringer M, Lorenz S. Developing Small-Molecule Inhibitors of HECT-Type Ubiquitin Ligases for Therapeutic Applications: Challenges and Opportunities. *Chembiochem*. 2018 Oct 18;19(20):2123–35.
171. Hicke L, Schubert HL, Hill CP. Ubiquitin-binding domains. *Nat Rev Mol Cell Biol*. 2005;6(8):610–21.
172. Husnjak K, Dikic I. Ubiquitin-Binding Proteins: Decoders of Ubiquitin-Mediated Cellular Functions. *Annu Rev Biochem*. 2012;81(1):291–322.
173. Zhang W, Sidhu SS. Generating Intracellular Modulators of E3 Ligases and Deubiquitinases from Phage-Displayed Ubiquitin Variant Libraries. In: Mayor T, Kleiger G, editors. *The Ubiquitin Proteasome System: Methods and Protocols* [Internet]. New York, NY: Springer; 2018 [cited 2022 Oct 22]. p. 101–19. (Methods in Molecular Biology). Available from: [https://doi.org/10.1007/978-1-4939-8706-1\\_8](https://doi.org/10.1007/978-1-4939-8706-1_8)
174. Ernst A, Avvakumov G, Tong J, Fan Y, Zhao Y, Alberts P, et al. A Strategy for Modulation of Enzymes in the Ubiquitin System. *Science*. 2013 Feb;339(6119):590–5.
175. Sidhu SS. Phage display in pharmaceutical biotechnology. *Curr Opin Biotechnol*. 2000 Dec 1;11(6):610–6.
176. Leung I, Jarvik N, Sidhu SS. A Highly Diverse and Functional Naïve Ubiquitin Variant Library for Generation of Intracellular Affinity Reagents. *J Mol Biol*. 2017;429(1):115–27.
177. McCafferty J, Griffiths AD, Winter G, Chiswell DJ. Phage antibodies: filamentous phage displaying antibody variable domains. *Nature*. 1990 Dec 6;348(6301):552–4.
178. Jaroszewicz W, Morcinek-Orłowska J, Pierzynowska K, Gaffke L, Węgrzyn G. Phage display and other peptide display technologies. *FEMS Microbiol Rev*. 2022 Mar 1;46(2):fuab052.
179. Zhang W, Wu KP, Sartori MA, Kamadurai HB, Ordureau A, Jiang C, et al. System-Wide Modulation of HECT E3 Ligases with Selective Ubiquitin Variant Probes. *Mol Cell*. 2016 Apr 7;62(1):121–36.
180. Garg P, Ceccarelli DF, Keszei AFA, Kurinov I, Sicheri F, Sidhu SS. Structural and Functional Analysis of Ubiquitin-based Inhibitors That Target the Backsides of E2 Enzymes. *J Mol Biol*. 2020 Feb 14;432(4):952–66.
181. Middleton AJ, Wright JD, Day CL. Regulation of E2s: A Role for Additional Ubiquitin Binding Sites? *J Mol Biol*. 2017 Nov 10;429(22):3430–40.

182. Manczyk N, Yates BP, Veggiani G, Ernst A, Sicheri F, Sidhu SS. Structural and functional characterization of a ubiquitin variant engineered for tight and specific binding to an alpha-helical ubiquitin interacting motif. *Protein Sci.* 2017;26(5):1060–9.
183. Veggiani G, Yates BP, Martyn GD, Manczyk N, Singer AU, Kurinov I, et al. Panel of Engineered Ubiquitin Variants Targeting the Family of Human Ubiquitin Interacting Motifs. *ACS Chem Biol.* 2022 Apr 15;17(4):941–56.
184. Zhang W, Bailey-Elkin BA, Knaap RCM, Khare B, Dalebout TJ, Johnson GG, et al. Potent and selective inhibition of pathogenic viruses by engineered ubiquitin variants. *PLoS Pathog.* 2017;13(5):e1006372.
185. Zhang Q, Jia Q, Gao W, Zhang W. The Role of Deubiquitinases in Virus Replication and Host Innate Immune Response. *Front Microbiol* [Internet]. 2022 [cited 2024 Feb 24];13. Available from: <https://www.frontiersin.org/journals/microbiology/articles/10.3389/fmicb.2022.839624>
186. Proulx J, Borgmann K, Park IW. Role of Virally-Encoded Deubiquitinating Enzymes in Regulation of the Virus Life Cycle. *Int J Mol Sci.* 2021 Jan;22(9):4438.
187. D’Astolfo DS, Pagliero RJ, Pras A, Karthaus WR, Clevers H, Prasad V, et al. Efficient Intracellular Delivery of Native Proteins. *Cell.* 2015 Apr 23;161(3):674–90.
188. Auger A, Park M, Nitschke F, Minassian LM, Beilhartz GL, Minassian BA, et al. Efficient Delivery of Structurally Diverse Protein Cargo into Mammalian Cells by a Bacterial Toxin. *Mol Pharm.* 2015 Aug 3;12(8):2962–71.
189. Richardson PG, Hideshima T, Anderson KC. Bortezomib (PS-341): A Novel, First-in-Class Proteasome Inhibitor for the Treatment of Multiple Myeloma and Other Cancers. *Cancer Control.* 2003 Sep 1;10(5):361–9.
190. Demo SD, Kirk CJ, Aujay MA, Buchholz TJ, Dajee M, Ho MN, et al. Antitumor Activity of PR-171, a Novel Irreversible Inhibitor of the Proteasome. *Cancer Res.* 2007 Jul 6;67(13):6383–91.
191. Kupperman E, Lee EC, Cao Y, Bannerman B, Fitzgerald M, Berger A, et al. Evaluation of the Proteasome Inhibitor MLN9708 in Preclinical Models of Human Cancer. *Cancer Res.* 2010 Feb 28;70(5):1970–80.
192. Yang Y, Kitagaki J, Dai RM, Tsai YC, Lorick KL, Ludwig RL, et al. Inhibitors of ubiquitin-activating enzyme (E1), a new class of potential cancer therapeutics. *Cancer Res.* 2007 Oct 1;67(19):9472–81.
193. Majeed S, Aparnathi MK, Nixon KCJ, Venkatasubramanian V, Rahman F, Song L, et al. Targeting the Ubiquitin–Proteasome System Using the UBA1 Inhibitor TAK-243 is a Potential Therapeutic Strategy for Small-Cell Lung Cancer. *Clin Cancer Res.* 2022 May 2;28(9):1966–78.
194. Hyer ML, Milhollen MA, Ciavarri J, Fleming P, Traore T, Sappal D, et al. A small-molecule inhibitor of the ubiquitin activating enzyme for cancer treatment. *Nat Med.* 2018 Feb;24(2):186–93.
195. Chen JJ, Tsu CA, Gavin JM, Milhollen MA, Bruzzese FJ, Mallender WD, et al. Mechanistic studies of substrate-assisted inhibition of ubiquitin-activating enzyme by adenosine sulfamate analogues. *J Biol Chem.* 2011 Nov 25;286(47):40867–77.

196. Ceccarelli DF, Tang X, Pelletier B, Orlicky S, Xie W, Plantevin V, et al. An Allosteric Inhibitor of the Human Cdc34 Ubiquitin-Conjugating Enzyme. *Cell*. 2011 Jun 24;145(7):1075–87.
197. Pulvino M, Liang Y, Oleksyn D, DeRan M, Van Pelt E, Shapiro J, et al. Inhibition of proliferation and survival of diffuse large B-cell lymphoma cells by a small-molecule inhibitor of the ubiquitin-conjugating enzyme Ubc13-Uev1A. *Blood*. 2012 Aug 23;120(8):1668–77.
198. Tsukamoto S, Takeuchi T, Rotinsulu H, Mangindaan REP, van Soest RWM, Ukai K, et al. Leucettamol A: a new inhibitor of Ubc13-Uev1A interaction isolated from a marine sponge, *Leucetta aff. microrhaphis*. *Bioorg Med Chem Lett*. 2008 Dec 15;18(24):6319–20.
199. Su J, Zhou X, Wang L, Yin X, Wang Z. Curcumin inhibits cell growth and invasion and induces apoptosis through down-regulation of Skp2 in pancreatic cancer cells. *Am J Cancer Res*. 2016;6(9):1949–62.
200. Cai Q, Sun H, Peng Y, Lu J, Nikolovska-Coleska Z, McEachern D, et al. A Potent and Orally Active Antagonist (SM-406/AT-406) of Multiple Inhibitor of Apoptosis Proteins (IAPs) in Clinical Development for Cancer Treatment. *J Med Chem*. 2011 Apr 28;54(8):2714–26.
201. Strickson S, Campbell DG, Emmerich CH, Knebel A, Plater L, Ritorto MS, et al. The anti-inflammatory drug BAY 11-7082 suppresses the MyD88-dependent signalling network by targeting the ubiquitin system. *Biochem J*. 2013 Apr 12;451(3):427–37.
202. Keating MJ, Bach C, Yasothan U, Kirkpatrick P. Bendamustine. *Nat Rev Drug Discov*. 2008 Jun;7(6):473–4.
203. Tian M, Zeng T, Liu M, Han S, Lin H, Lin Q, et al. A cell-based high-throughput screening method based on a ubiquitin-reference technique for identifying modulators of E3 ligases. *J Biol Chem*. 2019 Feb 1;294(8):2880–5770.
204. Mund T, Lewis MJ, Maslen S, Pelham HR. Peptide and small molecule inhibitors of HECT-type ubiquitin ligases. *Proc Natl Acad Sci*. 2014 Nov 25;111(47):16736–41.
205. Weinstock J, Wu J, Cao P, Kingsbury WD, McDermott JL, Kodrasov MP, et al. Selective Dual Inhibitors of the Cancer-Related Deubiquitylating Proteases USP7 and USP47. *ACS Med Chem Lett*. 2012 Oct 11;3(10):789–92.
206. Li J, Zhang Y, Da Silva Sil Dos Santos B, Wang F, Ma Y, Perez C, et al. Epidithiodiketopiperazines Inhibit Protein Degradation by Targeting Proteasome Deubiquitinase Rpn11. *Cell Chem Biol*. 2018 Nov 15;25(11):1350-1358.e9.
207. Chen J, Dexheimer TS, Ai Y, Liang Q, Villamil MA, Inglese J, et al. Selective and Cell-Active Inhibitors of the USP1/ UAF1 Deubiquitinase Complex Reverse Cisplatin Resistance in Non-small Cell Lung Cancer Cells. *Chem Biol*. 2011 Nov 23;18(11):1390–400.
208. LaPlante G, Zhang W. Targeting the Ubiquitin-Proteasome System for Cancer Therapeutics by Small-Molecule Inhibitors. *Cancers*. 2021 Jan;13(12):3079.
209. Mager WH, Winderickx J. Yeast as a model for medical and medicinal research. *Trends Pharmacol Sci Regul Ed*. 2005;26(5):265–73.

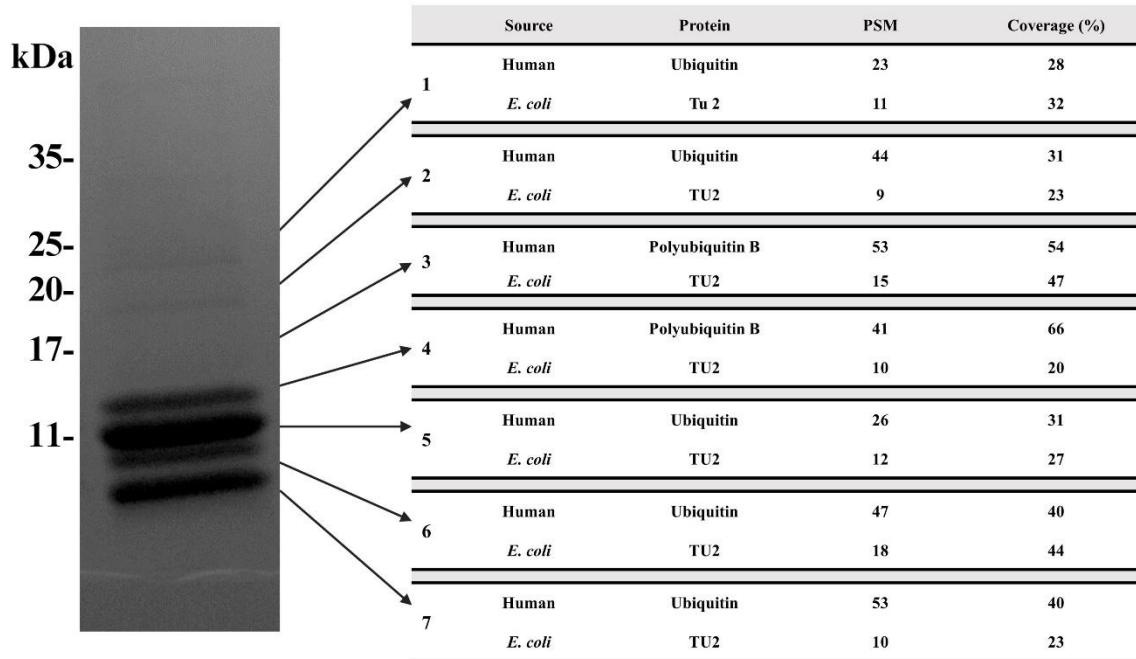
210. Burgess SM, Powers T, Mell JC. Budding Yeast *Saccharomyces Cerevisiae* as a Model Genetic Organism. In: Encyclopedia of Life Sciences [Internet]. John Wiley & Sons, Ltd; 2017 [cited 2024 Feb 13]. p. 1–12. Available from: <https://onlinelibrary.wiley.com/doi/abs/10.1002/9780470015902.a0000821.pub2>
211. Rivera AL, Magaña-Ortiz D, Gómez-Lim M, Fernández F, Loske AM. Physical methods for genetic transformation of fungi and yeast. *Phys Life Rev.* 2014 Jun 1;11(2):184–203.
212. Johnston M. A model fungal gene regulatory mechanism: the GAL genes of *Saccharomyces cerevisiae*. *Microbiol Rev.* 1987 Dec;51(4):458–76.
213. Elison GL, Xue Y, Song R, Acar M. Insights into Bidirectional Gene Expression Control Using the Canonical GAL1/GAL10 Promoter. *Cell Rep.* 2018 Oct 16;25(3):737-748.e4.
214. Popa C, Coll NS, Valls M, Sessa G. Yeast as a Heterologous Model System to Uncover Type III Effector Function. *PLoS Pathog.* 2016 Feb 25;12(2):e1005360.
215. Curak J, Rohde J, Stagljar I. Yeast as a tool to study bacterial effectors. *Curr Opin Microbiol.* 2009 Feb 1;12(1):18–23.
216. Juanes MA, Piatti S. The final cut: cell polarity meets cytokinesis at the bud neck in *S. cerevisiae*. *Cell Mol Life Sci.* 2016 Aug 1;73(16):3115–36.
217. Howell AS, Lew DJ. Morphogenesis and the Cell Cycle. *Genetics.* 2012 Jan 1;190(1):51–77.
218. Cid VJ, Durán A, del Rey F, Snyder MP, Nombela C, Sánchez M. Molecular basis of cell integrity and morphogenesis in *Saccharomyces cerevisiae*. *Microbiol Rev.* 1995 Sep;59(3):345–86.
219. Kamada Y, Jung US, Piotrowski J, Levin DE. The protein kinase C-activated MAP kinase pathway of *Saccharomyces cerevisiae* mediates a novel aspect of the heat shock response. *Genes Dev.* 1995 Jul 1;9(13):1559–71.
220. Mellor H, Parker PJ. The extended protein kinase C superfamily. *Biochem J.* 1998 Jun 1;332 ( Pt 2)(Pt 2):281–92.
221. Denis V, Cyert MS. Molecular Analysis Reveals Localization of *Saccharomyces cerevisiae* Protein Kinase C to Sites of Polarized Growth and Pkc1p Targeting to the Nucleus and Mitotic Spindle. *Eukaryot Cell.* 2005 Jan;4(1):36–45.
222. Heinisch JJ. Baker's yeast as a tool for the development of antifungal kinase inhibitors—targeting protein kinase C and the cell integrity pathway. *Biochim Biophys Acta BBA - Proteins Proteomics.* 2005 Dec 30;1754(1):171–82.
223. Levin DE. Cell Wall Integrity Signaling in *Saccharomyces cerevisiae*. *Microbiol Mol Biol Rev.* 2005 Jun;69(2):262–91.
224. Madden K, Sheu YJ, Baetz K, Andrews B, Snyder M. SBF cell cycle regulator as a target of the yeast PKC-MAP kinase pathway. *Science.* 1997 Mar 21;275(5307):1781–4.
225. Jung US, Levin DE. Genome-wide analysis of gene expression regulated by the yeast cell wall integrity signalling pathway. *Mol Microbiol.* 1999 Dec;34(5):1049–57.

226. Jansen G, Wu C, Schade B, Thomas DY, Whiteway M. Drag&Drop cloning in yeast. *Gene*. 2005 Jan 3;344:43–51.
227. Auweter SD, Bhavsar AP, de Hoog CL, Li Y, Chan YA, van der Heijden J, et al. Quantitative Mass Spectrometry Catalogues Salmonella Pathogenicity Island-2 Effectors and Identifies Their Cognate Host Binding Partners. *J Biol Chem*. 2011 Jul 8;286(27):24023–35.
228. Lauman P, Dennis JJ. Synergistic Interactions among Burkholderia cepacia Complex-Targeting Phages Reveal a Novel Therapeutic Role for Lysogenization-Capable Phages. *Microbiol Spectr* [Internet]. 2023 Jun [cited 2023 Sep 18];11(3). Available from: <https://www.ncbi.nlm.nih.gov/pmc/articles/PMC10269493/>
229. Waterhouse A, Bertoni M, Bienert S, Studer G, Tauriello G, Gumienny R, et al. SWISS-MODEL: homology modelling of protein structures and complexes. *Nucleic Acids Res*. 2018;46(Journal Article):W296–303.
230. Pettersen EF, Goddard TD, Huang CC, Couch GS, Greenblatt DM, Meng EC, et al. UCSF Chimera—a visualization system for exploratory research and analysis. *J Comput Chem*. 2004 Oct;25(13):1605–12.
231. Yan Y, Zhang D, Zhou P, Li B, Huang SY. HDock: a web server for protein-protein and protein-DNA/RNA docking based on a hybrid strategy. *Nucleic Acids Res*. 2017;45(W1):W365–73.
232. Christoffer C, Bharadwaj V, Luu R, Kihara D. LZerD Protein-Protein Docking Webserver Enhanced With de novo Structure Prediction. *Front Mol Biosci*. 2021;8:724947.
233. Christoffer C, Chen S, Bharadwaj V, Aderinwale T, Kumar V, Hormati M, et al. LZerD webserver for pairwise and multiple protein-protein docking. *Nucleic Acids Res*. 2021 Jul 2;49(W1):W359–65.
234. Esquivel-Rodriguez J, Filos-Gonzalez V, Li B, Kihara D. Pairwise and multimeric protein-protein docking using the LZerD program suite. *Methods Mol Biol Clifton NJ*. 2014;1137:209–34.
235. Yan Y, Tao H, He J, Huang SY. The HDock server for integrated protein–protein docking. *Nat Protoc*. 2020 May;15(5):1829–52.
236. Hartley JL, Temple GF, Brasch MA. DNA cloning using in vitro site-specific recombination. *Genome Res*. 2000 Nov;10(11):1788–95.
237. Raran-Kurussi S, Waugh DS. Expression and Purification of Recombinant Proteins in Escherichia coli with a His6 or Dual His6-MBP Tag. *Protein Crystallogr*. 2017 Jun 2;1607:1–15.
238. Bhavsar AP, Brown NF, Stoepel J, Wiermer M, Martin DDO, Hsu KJ, et al. The Salmonella Type III Effector SspH2 Specifically Exploits the NLR Co-chaperone Activity of SGT1 to Subvert Immunity. *PLOS Pathog*. 2013;9(7):e1003518.
239. Evans R, O'Neill M, Pritzel A, Antropova N, Senior A, Green T, et al. Protein complex prediction with AlphaFold-Multimer [Internet]. *bioRxiv*; 2022 [cited 2023 Sep 19]. p. 2021.10.04.463034. Available from: <https://www.biorxiv.org/content/10.1101/2021.10.04.463034v2>
240. Slagowski NL, Kramer RW, Morrison MF, LaBaer J, Lesser CF. A Functional Genomic Yeast Screen to Identify Pathogenic Bacterial Proteins. *PLOS Pathog*. 2008 Jan 18;4(1):e9.

241. Sloper-Mould KE, Jemc JC, Pickart CM, Hicke L. Distinct Functional Surface Regions on Ubiquitin \*. *J Biol Chem*. 2001 Aug 10;276(32):30483–9.
242. Calvert MEK, Lannigan JA, Pemberton LF. Optimization of yeast cell cycle analysis and morphological characterization by multispectral imaging flow cytometry. *Cytometry A*. 2008;73A(9):825–33.
243. Chiou J geng, Balasubramanian MK, Lew DJ. Cell Polarity in Yeast. *Annu Rev Cell Dev Biol*. 2017 Oct 6;33(1):77–101.
244. Foltman M, Molist I, Sanchez-Diaz A. Synchronization of the Budding Yeast *Saccharomyces cerevisiae*. In: Sanchez-Diaz A, Perez P, editors. *Yeast Cytokinesis: Methods and Protocols* [Internet]. New York, NY: Springer; 2016 [cited 2021 Jul 16]. p. 279–91. (Methods in Molecular Biology). Available from: [https://doi.org/10.1007/978-1-4939-3145-3\\_19](https://doi.org/10.1007/978-1-4939-3145-3_19)
245. Greenwood BL, Stuart DT. Synchronization of *Saccharomyces cerevisiae* Cells for Analysis of Progression Through the Cell Cycle. In: Wang Z, editor. *Cell-Cycle Synchronization: Methods and Protocols* [Internet]. New York, NY: Springer US; 2022 [cited 2023 Dec 13]. p. 145–68. (Methods in Molecular Biology). Available from: [https://doi.org/10.1007/978-1-0716-2736-5\\_12](https://doi.org/10.1007/978-1-0716-2736-5_12)
246. Künkel W. Effects of the antimicrotubular cancerostatic drug nocodazole on the yeast *Saccharomyces cerevisiae*. *Z Für Allg Mikrobiol*. 1980;20(5):315–24.
247. Newton K, Matsumoto ML, Wertz IE, Kirkpatrick DS, Lill JR, Tan J, et al. Ubiquitin Chain Editing Revealed by Polyubiquitin Linkage-Specific Antibodies. *Cell*. 2008 Aug 22;134(4):668–78.
248. Padhy AA, Mavor D, Sahoo S, Bolon DNA, Mishra P. Systematic profiling of dominant ubiquitin variants reveals key functional nodes contributing to evolutionary selection. *Cell Rep*. 2023 Sep 26;42(9):113064.
249. Duerksen-Hughes PJ, Xu X, Wilkinson KD. Structure and function of ubiquitin: evidence for differential interactions of arginine-74 with the activating enzyme and the proteases of ATP-dependent proteolysis. *Biochemistry*. 1987 Nov 1;26(22):6980–7.
250. Chen Y, Piper PW. Consequences of the overexpression of ubiquitin in yeast: elevated tolerances of osmotic stress, ethanol and canavanine, yet reduced tolerances of cadmium, arsenite and paromomycin. *Biochim Biophys Acta BBA - Mol Cell Res*. 1995 Jul 20;1268(1):59–64.
251. Bullones-Bolaños A, Martín-Muñoz P, Vallejo-Grijalba C, Bernal-Bayard J, Ramos-Morales F. Specificities and redundancies in the NEL family of bacterial E3 ubiquitin ligases of *Salmonella enterica* serovar Typhimurium. *Front Immunol*. 2024 Feb 1;15:1328707.
252. Pickart CM, Kaspersek EM, Beal R, Kim A. Substrate properties of site-specific mutant ubiquitin protein (G76A) reveal unexpected mechanistic features of ubiquitin-activating enzyme (E1). *J Biol Chem*. 1994 Mar 11;269(10):7115–23.
253. Lee DH, Goldberg AL. Selective Inhibitors of the Proteasome-dependent and Vacuolar Pathways of Protein Degradation in *Saccharomyces cerevisiae* \*. *J Biol Chem*. 1996 Nov 1;271(44):27280–4.
254. Liu C, Apodaca J, Davis LE, Rao H. Proteasome inhibition in wild-type yeast *Saccharomyces cerevisiae* cells. *BioTechniques*. 2007 Feb;42(2):158–62.

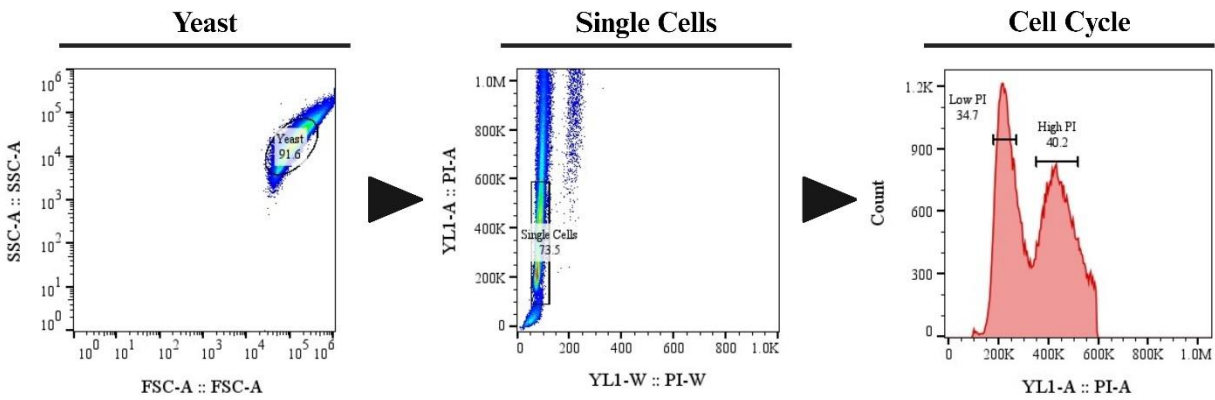
255. Shah NB, Duncan TM. Bio-layer Interferometry for Measuring Kinetics of Protein-protein Interactions and Allosteric Ligand Effects. *JoVE J Vis Exp*. 2014 Feb 18;(84):e51383.
256. Jerabek-Willemsen M, André T, Wanner R, Roth HM, Duhr S, Baaske P, et al. MicroScale Thermophoresis: Interaction analysis and beyond. *J Mol Struct*. 2014 Dec 5;1077:101–13.
257. O’Neill MAA, Gaisford S. Application and use of isothermal calorimetry in pharmaceutical development. *Int J Pharm*. 2011 Sep 30;417(1):83–93.
258. Chow LKM, Ghaly TM, Gillings MR. A survey of sub-inhibitory concentrations of antibiotics in the environment. *J Environ Sci*. 2021 Jan 1;99:21–7.
259. Rahman S, Kesselheim AS, Hollis A. Persistence of resistance: a panel data analysis of the effect of antibiotic usage on the prevalence of resistance. *J Antibiot (Tokyo)*. 2023 May;76(5):270–8.
260. Murugaiyan J, Kumar PA, Rao GS, Iskandar K, Hawser S, Hays JP, et al. Progress in Alternative Strategies to Combat Antimicrobial Resistance: Focus on Antibiotics. *Antibiotics*. 2022 Feb;11(2):200.
261. Tang JQ, Marchand MM, Veggiani G. Ubiquitin Engineering for Interrogating the Ubiquitin–Proteasome System and Novel Therapeutic Strategies. *Cells*. 2023 Jan;12(16):2117.
262. Canny MD, Moatti N, Wan LCK, Fradet-Turcotte A, Krasner D, Mateos-Gomez PA, et al. Inhibition of 53BP1 favors homology-dependent DNA repair and increases CRISPR-Cas9 genome-editing efficiency. *Nat Biotechnol*. 2018 Jan;36(1):95–102.
263. McClary WD, Catala A, Zhang W, Gamboni F, Dzieciatkowska M, Sidhu SS, et al. A Designer Nanoparticle Platform for Controlled Intracellular Delivery of Bioactive Macromolecules: Inhibition of Ubiquitin-Specific Protease 7 in Breast Cancer Cells. *ACS Chem Biol*. 2022 Jul 15;17(7):1853–65.
264. Bulcha JT, Wang Y, Ma H, Tai PWL, Gao G. Viral vector platforms within the gene therapy landscape. *Signal Transduct Target Ther*. 2021 Feb 8;6(1):53.
265. Akram Z, Ahmed I, Mack H, Kaur R, Silva RC, Castilho BA, et al. Yeast as a Model to Understand Actin-Mediated Cellular Functions in Mammals—Illustrated with Four Actin Cytoskeleton Proteins. *Cells*. 2020 Mar;9(3):672.

# Appendix I



**sFig. 1.1 Mass Spectrometry of Purified Ubv D09**

Purified Ubv D09 was analyzed by SDS-PAGE on a 4-20% gradient gel. Bands were excised at the indicated locations and subjected to mass spectrometry using an Orbitrap Q Exactive mass spectrometer. Data was processed using Proteome Discoverer 1.4 and the Human and *E. coli* proteomic databases were searched using SEQUEST. The most abundant protein found in every excised band is shown alongside the most abundant contaminant. Mass spectrometry was performed by the Alberta Proteomics and Mass Spectrometry Facility in the Faculty of Medicine and Dentistry at the University of Alberta. (PSM = Peptide Spectral Matches)



**sFig. 2.1 Gating Strategy for Cell Cycle Flow Cytometry Analysis**

Yeast were identified, and debris was excluded, using a forward scatter area (FSC-A) versus side scatter area (SSC-A) gate. Single cells were then selected on a YL1/PI-W versus YL1/PI-A plot to exclude doublets. Cell cycle analysis was then performed in this cell population by quantifying the ratio of cells with low PI and high PI fluorescent signal.

| Plasmid    | Expression Protein           | Promoter | Amino Acid Marker | Protein Tag |
|------------|------------------------------|----------|-------------------|-------------|
| pAG426GALL | SspH1/SspH1 <sup>C492A</sup> | Gal      | URA2              | HA          |
| pGREG515   | Ub/Ubv/Ev                    | Gal      | LEU3              | 6-Myc       |

**sTable 1. Expression Vectors Summary**

SspH1 or SspH1C492A were co-transformed with Ub, Ubv or Ev into BY4742 $\alpha$  (MAT $\alpha$ , his3 $\Delta$ 1, leu2 $\Delta$ 0, lys2 $\Delta$ 0, ura3 $\Delta$ 0) yeast. Ubiquitin variant constructs were identified by ELISA assay and provided by the Sidhu lab at the University of Toronto. Both expression vectors are under the control of a galactose (Gal) inducible promoter.

|                          |                                    |
|--------------------------|------------------------------------|
| <b>Instrument:</b>       | ThermoFisher Scientific Attune NxT |
| <b>Laser Lines:</b>      | YL1                                |
| <b>Emission Filters:</b> | 585/16                             |
| <b>Fluorochrome:</b>     | Propidium Iodide (PI)              |

**sTable 2. Flow Cytometry Instrument Settings**

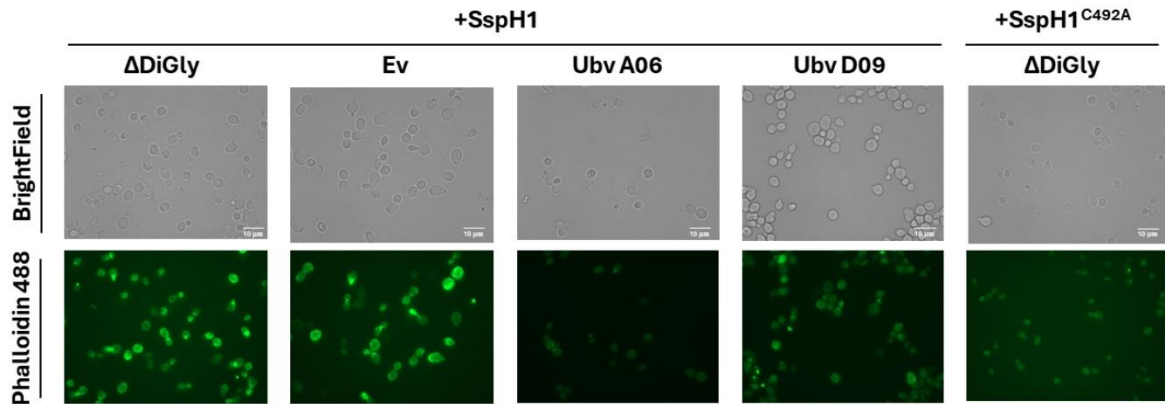
Propidium Iodide was detected on the YL1 laser line with a 585/16 emission filter using an Attune Nxt

## Appendix II

### Yeast Actin Cytoskeleton Was Not Affected by SspH1 Expression

Since I observed SspH1-mediated interference of the *S. cerevisiae* cell cycle, I explored whether this was caused by modification to the yeast actin cytoskeleton because, as with many eukaryotic cells, yeast relies heavily on actin rearrangements to facilitate cell division. Three discrete structures of filamentous actin (F-actin) are observed in yeast: cortical actin patches, cytoplasmic actin cables, and the contractile actomyosin ring. (265) While actin patches and cytoplasmic cables are present during all phases of the cell cycle, the contractile actomyosin ring is only observed during mitosis. In addition to the prominent role actin cytoskeleton rearrangement has in cell division, it has also been previously reported that disruption of the cytoskeleton is the most common strategy used by T3SS to facilitate infections. (214) Taken together, these observations indicated that targeting actin rearrangement could be a possible mechanism underlying SspH1-mediated cell cycle interference.

To probe for any alterations to the actin cytoskeleton, I stained F-actin within yeast expressing SspH1 or SspH1<sup>C492A</sup> alongside  $\Delta$ DiGly, Ubv A06, Ubv D09, or Ev using Alexa Fluor 488 phalloidin. This allowed me to examine the location and number of F-actin structures that were formed in the presence of the various SspH1 and Ubv combinations. I did not observe any significant changes in the F-actin cytoskeleton structures which suggests that SspH1-mediated cell cycle interference is not being mediated through the disruption of actin cytoskeletal rearrangements (sFig. 3.1).



**sFig. 3.1 Analysis of Yeast Actin Cytoskeleton by Fluorescent Microscopy**

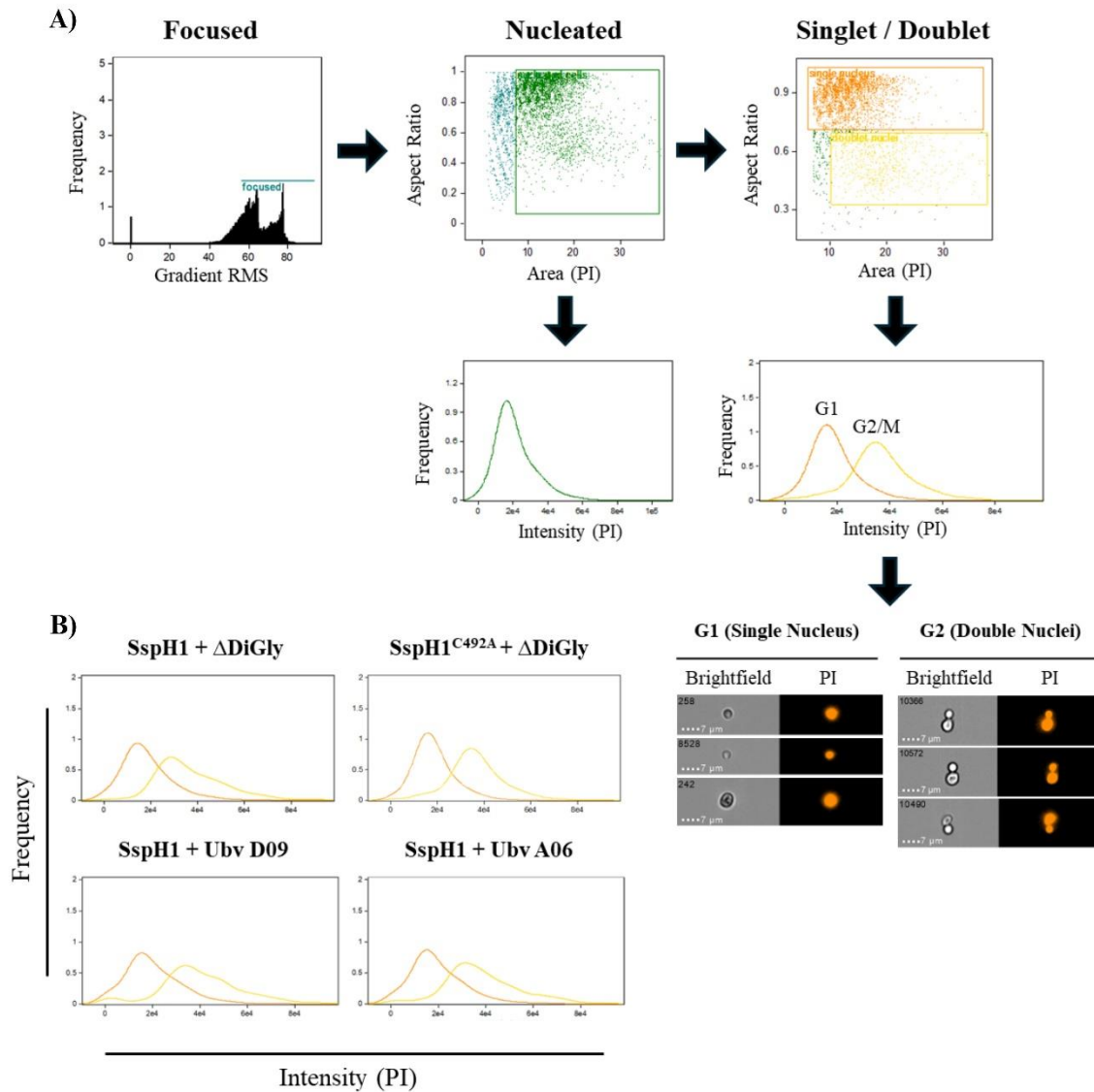
Representative micrographs of yeast co-expressing SspH1 +  $\Delta$ DiGly, Ubv A06, Ubv D09 or Ev as well as SspH1<sup>C492A</sup> +  $\Delta$ DiGly were incubated for 8 hours at 30°C in fresh 1% galactose post-nocodazole wash. Images were collected on an EVOS FL Auto at 100x magnification. The filamentous actin cytoskeleton was stained in green using Alexa Fluor 488 phalloidin.

## Imaging Flow Cytometry

Co-transformed yeast was grown overnight in a shaker at 200rpm and 30°C in CSM-LEU-URA + 1% Glucose liquid media. 2 mL subcultures were made by diluting overnight cultures to  $6 \times 10^6$  cells per mL in CSM-LEU-URA + 1% Glucose liquid media. Subcultures were washed 3x in 500  $\mu$ L sterile ddH<sub>2</sub>O before being resuspended in CSM-LEU-URA + 1% Galactose liquid media with 15 $\mu$ g per mL of nocodazole, which induces G2/M arrest through microtubule depolymerization. Cultures were returned to the incubator and grown in a shaker at 200rpm and at 30°C for 2 hours before being washed 3x in 500  $\mu$ L sterile ddH<sub>2</sub>O to remove nocodazole. Washed pellets were resuspended in 3 mL CSM-LEU-URA + 1% Galactose liquid media. Cultures grown in a shaker at 200 rpm and 30°C for 8 hours post-nocodazole wash. 400  $\mu$ L of sample was collected and fixed with 600  $\mu$ L of cold 70% EtOH. Fixed samples were then processed by the addition 500  $\mu$ L of 50mM sodium citrate followed by centrifugation at 400 x g for 5 mins and 17 000 x g for 2 mins. The supernatant was removed, and the pellet was resuspending in 500  $\mu$ L of 50mM sodium citrate containing 0.1 mg/mL of RNaseA. The resuspended pellet was incubated for 90 mins at 37°C before the addition of 500  $\mu$ L of 50mM sodium citrate containing 10  $\mu$ g/mL PI. Staining was allowed to proceed through a 1-hour incubation in the dark at room temperature. Samples were processed using a Cytex Amnis Mark II which collected 5000 events at a 60x magnification per sample. Data was analyzed with IDEAS V6.2.

## Imaging Flow Cytometry Did Not Reveal SspH1-mediated Cell Cycle Perturbations

In addition to monitoring *S. cerevisiae* cell cycle progression by fluorescent microscopy and flow cytometry, I also employed an imaging flow cytometry workflow. This methodology aimed to combine the high-throughput capabilities of traditional flow cytometry with the specificity of microscopy to provide additional insight into yeast cell cycle progression. Additionally, these methods often rely on a single biological event to determine which stage of the cell cycle a particular yeast is currently undergoing. In the case of microscopy this determination is solely based on bud emergence, and, in the case of flow cytometry, this determination is solely based on DNA replication. (242) Imaging flow cytometry allows for the coupling of these features where I can define cells in the G1 phase as those with 1N DNA content and a round appearance (aspect ratio  $\sim 1$ ) and the cells in the G2/M phase as those with 2N DNA and an elongated appearance (aspect ratio  $< 0.7$ ) (sFig 4.1A). However, cell cycle analysis by imaging flow cytometry did not reveal any significant differences in the proportion of yeast in the G1 or G2/M phases of the cell cycle when SspH1 or SspH1<sup>C492A</sup> were present alongside  $\Delta$ DiGly, Ubv A06 or Ubv D09 (sFig 4.1B). I were able to confirm that most of the large, budded cells had a higher PI staining intensity signaling that they contained 2N DNA content but failed to identify a pattern between SspH1 and SspH1<sup>C492A</sup> expressing yeast. The only notable, albeit non-significant, difference that I observed was a consistent increased intensity of PI signal in yeast meeting the criteria for being in the G2/M phase of the cell cycle and expressing SspH1<sup>C492A</sup> +  $\Delta$ DiGly relative to yeast expressing SspH1 +  $\Delta$ DiGly (sFig 4.1B). This may be due to the use of PI as the DNA stain, which tends to have a more diffuse signal than some alternatives. Other research has suggested that DNA staining with Sytox green allows for better delineation of 1N and 2N DNA content. (242) This allows for consistent identification of yeast in the S phase of the cell cycle, something I was unable to accomplish using PI staining.



**sFig. 4.1 Analysis of Yeast Cell Cycle by Imaging Flow Cytometry**

(A) Gating strategy for cell cycle analysis by imaging flow cytometry. In focus images were identified by gradient RMS. Yeast with stained nuclei were then identified, and debris was excluded, using an aspect ratio versus YL1/PI-A gate. Unbudded and budded cells were discriminated for based on aspect ratio where unbudded/singlet cells had an aspect ratio of between 1.0 and  $\sim$ 0.75 and budded cells had an aspect ratio of between  $\sim$ 0.7 and  $\sim$ 0.35. Cell cycle analysis was then performed in these cell populations by quantifying the relative frequency of specific YL1/PI intensities in each population. (B) Relative frequency and intensity of PI

signal of yeast within the single (Orange) and budded/doublet (Yellow) stages of the cell cycle from BY4742 $\alpha$  yeast strain co-transformed with galactose-inducible vectors (pGREG515) that expressed SspH1 +  $\Delta$ DiGly, SspH1 + Ubv A06, SspH1 + Ubv D09, SspH1 + Empty Vector (Ev) or SspH1<sup>C492A</sup> +  $\Delta$ DiGly.